Using a novel approach to precisely measure the sedimentation velocity of a (bio)chemical sediment: cyanobacteria-ferrihydrite aggregates

By

Yuhao Li

A thesis submitted in partial fulfillment of the requirements for the degree of

Master of Science

Department of Earth and Atmospheric Sciences

University of Alberta

Abstract

Banded iron formations (BIF) are iron-rich (~20-40% Fe), siliceous (~40-50% SiO2), and organic-lean (<0.5 wt.%) sedimentary deposits that precipitated widely during the late Archean (2.7-2.5 Ga) and Paleoproterozoic (2.5-1.8 Ga). As cyanobacteria evolved, the reaction between dissolved Fe(II) and photosynthetically produced O_2 would have became a viable mechanism for Fe(II) oxidation near the surface of the Precambrian oceans. If a biological mechanism was important in the initial process of Fe(II) oxidation in an Archean ocean water column, it is then expected that biomass settled to the seafloor along with the Fe(III) minerals (Konhauser et al., 2005). Yet, BIF contain very little organic carbon (i.e., < 0.5 wt.%; Gole and Klein, 1981), meaning either that biomass was oxidized in the water column or bottom sediment via the combined metabolic processes of fermentation and chemoheterotrophy (e.g., Konhauser et al., 2005) or that the biomass and ferrihydrite did not associate and settle together (Gauger et al., 2016). The presence or absence of a strong association of cells with minerals or encrustation in minerals especially influences the rate and extent of sedimentation of the microbial cells, i.e., the biomass. Sedimentation velocity of such chemical sediments are typically calculated using Stokes's law. However, applying it to chemical sediments that form in situ in the water column is not ideal because the particle properties do not fulfil many of the assumptions underpinning the applicability of Stokes' law. As a consequence, it has been difficult to predict the sedimentation rate of BIF because their primary sediments likely comprised aggregates of ferric hydroxides, such as ferrihydrite [$Fe(OH)_3$], and marine bacterial biomass, including cyanobacteria. In this thesis, I used a novel approach that combined geochemical, geophysical and geomicrobiological methods to comprehensively investigate the sedimentation processes, sedimentation velocity, total Fe content and total biomass content of ferrihydrite-*Synechococcus* aggregates that formed *in situ.* over a wide range of pH and

initial Fe(II) concentrations. My results indicate that: (1) Using Stokes' law to measure the sedimentation velocity of chemical sediments is not suitable nor precise; (2) the sedimentation velocity is positively correlated with both pH and initial Fe(II) concentration; (3) it was unlikely that Archean and Paleoproterozoic oceans were at pH 6 due to the extremely slow sedimentation velocity of Fe-cell aggregates such that there would have been no sufficient Fe minerals deposited to form BIF on a massive scale; and (4) the actual Fe:C_{org} ratio far in the water column must have exceeded the theoretical ratio of 4:1 (as expected from biological oxidation of ferrous iron), thus accounting for the excess Fe(III) deposited to the sediments that later was transformed into hematite with little to no organic carbon preserved.

Preface

This is a paper-based thesis that represents a cumulative work of two papers that focused on cyanobacteria-Fe aggregates, the primary sediments to banded iron formations. As the first author of the following two papers, I was actively involved in all aspects of each paper from developing a new approach, conducting experiments and subsequent analysis, to drafting each paper. This work was conducted under the supervision of Dr. Kurt Konhauser, and with the assistance of Dr. Bruce Sutherland, Dr. George Owttrim, and Dr. Murray Gingras, from the department of Earth and Atmospheric Sciences at the University of Alberta.

Chapter 2 has been submitted to the *Journal Sedimentary Research* as: Li, Y., Sutherland, B.R., Gingras, M.K., Owttrim, G.W., Konhauser K.O., A novel approach to investigate the deposition of (bio)chemical sediments: The sedimentation velocity of cyanobacteria-ferrihydrite aggregates. I was responsible for experiment design with Dr. Bruce Sutherland, growing microbial cultures with Dr. George Owttrim, conducting all sedimentation experiments and data analysis individually, and initial drafting of the manuscript. All authors have contributed greatly to the writing of the manuscript.

Chapter 3 have been prepared for submission as: Li, Y., Sutherland, B.R., Gingras, M.K., Owttrim, G.W., Gao, J.Y., Konhauser K.O. Cyanobacteria-ferrihydrite aggregates as primary sediments to BIF and their implications for Archean-Paleoproterozoic seawater geochemistry. I was responsible for experiment design with Dr. Bruce Sutherland, growing microbial cultures with Dr. George Owttrim, conducting all sedimentation experiments and data analysis, and initial drafting of the

manuscript. Mr. Gao Jueyu has assisted with sedimentation velocity analysis. All authors have contributed greatly to the writing of the manuscript.

For my parents: Mrs. Yanping Jia and Mr. Xueting Li

“Dracarys.”

- Daenerys Targeryen, Game of Thrones.

Acknowledgements

First and foremost, I would like to thank my parents for their unconditional support for me and my pursue of academics. My dad, although with very limited education, has taught me and is still teaching me how to be a decent human being as he is, and I am forever thankful for that. I would like to sincerely thank my mentor and my supervisor Dr. Kurt Konhauser, who gave me a chance to further my education when I was lost, who keeps supporting my research and showing me what it is like to become a scholar. I would like to thank Dr. George Pemberton. I started my career as a geologist solely because of his EAS222 class. His stories inspired me tremendously. I would like to thank my partner Mr. Chris James, who has been nothing but supportive and loving to me. I would like to also thank all my co-authors, colleagues and friends who have generously helped me throughout my master's degree: Dr. Bruce Sutherland, Dr. George Owttrim, Dr. Murray Gingras, Dr. Daniel Alessi, Mr. Gao Jueyu, Dr. Leslie Robbins, Dr. Weiduo Hao, Mr. Karrel Mänd, Mr. Logan Swaren, Dr. Tiffany Playter, Dr. Denise Whitford, Mr. Logan Brand, Mr. Mark Labbe, Dr. Nathan Gerein and Ms. Kate Nicols.

The work presented in this thesis was supported by NSERC Discovery Grants to Dr. Konhauser (RGPIN-165831), Dr. Sutherland (RGPIN- 2015-04758), Dr. Gingras (RGPIN-2020-05138), and Dr. Owttrim (RGPIN-171319).

Table of Contents

List of Figures

List of Tables

References

Gauger, T., Byrne, J.M., Konhauser, K.O., Obst, M., Crowe, S. and Kappler, A., 2016. Influence of organics and silica on Fe (II) oxidation rates and cell–mineral aggregate formation by the green-sulfur Fe (II)-oxidizing bacterium *Chlorobium ferrooxidans* KoFox–Implications for Fe (II) oxidation in ancient oceans. Earth and Planetary Science Letters, 443, pp.81-89.

Gole, M.J. and Klein, C., 1981. Banded iron-formations through much of Precambrian time. The Journal of Geology, 89(2), pp.169-183.

Konhauser, K.O., Newman, D.K. and Kappler, A., 2005. The potential significance of microbial Fe (III) reduction during deposition of Precambrian banded iron formations. Geobiology, 3(3), pp.167-177.

Chapter 1. Introduction

1.1 Banded Iron Formations

Banded Iron Formations (herein BIF), as the world's largest iron ore deposits, are chemical sedimentary rocks that are characteristically iron- (~20-40% Fe) and silica-rich (~40-50% SiO_2). BIF precipitated throughout much of the Archean and Paleoproterozoic eons (2.7-1.8Ga) (James, 1954; Cloud, 1973; Trendall, 2002; Konhauser et al., 2007; Molszewska et al., 2015). Generally, BIF display distinctive interbedded layers of different thickness from mm-scale microbands to m-scale macrobands. Traditionally, BIF are categorized into two groups: Algoma-type and Superior-type. Algoma-type BIF are usually associated with submarine volcanoes that are situated around volcanic arcs and spreading centres with rock compositions including mafic to ultramafic volcanic rocks, volcaniclastic rocks such as greywackes and shales, and common massive sulfide deposits (Bekker et al., 2010). Comparatively, laterally extensive Superior-type BIF are believed to be formed under shallow marine environments in passive margins. With only limited volcanic rock input, Superior-type BIF are usually dominated by interbedded clastic sedimentary rocks with iron-rich bands. Some of the most studied Superior-type BIF include the ca. 2.60 to 2.45 Ga Hamersley Group in Australia, the 2.70 to 2.05 Ga Transvaal Supergroup in South Africa.

What makes BIF different from other chemical sedimentary rocks are their unique mineral assemblages, which consist of fine-grained quartz (SiO_2), magnetite (Fe_3O_4), hematite (Fe_2O_3), stilpnomelane ($K(Fe^{2+},Mg,Fe^{3+})_8(Si,Al)_{12}(O,OH)_{27}\cdot n(H_2O)$), greenalite ($(Fe^{2+},Fe^{3+})_{2\text{-}3}Si_2O_5OH_4$), siderite ($FeCO_3$), ankerite ($Ca(Fe,Mg,Mn)(CO_3)_2$), calcite ($CaCO_3$), dolomite ($CaMg(CO_3)_2$) and locally pyrite ($FeS_2$). Importantly, it is widely accepted that BIF underwent significant post-

depositional alterations during diagenesis and various grades of metamorphism. The primary iron phases during BIF deposition are interpreted to have consisted of either ferrihydrite, $Fe(OH)_3$, or an amorphous Fe(III)-Si gel.

1.2 The composition of Archean oceans

The composition of Archean seawater is fundamentally different from the modern. Iron and silica were extremely enriched in the Archean oceans. It is estimated that the background Fe(II) concentration was at least 30 μM, 4 orders of magnitudes higher than it is today (Holland, 1984). The reason for the high concentrations was enhanced submarine hydrothermal activities at that time in Earth's history (Isley, 1995). In some extreme cases, seawater that was proximal to upwelling currents could have had a Fe(II) concentration as high as 1800 μM (Edmond et al., 1982). Si was also at a high concentration in the Archean, ranging from 0.67 mM to 2.2 mM (Maliva et al., 1989). Two sources of silica have been proposed, hydrothermal fluids and continental runoff (Froelich et al., 1992; Morlock et al 1993). Today, the silica concentration in seawater is less than 180 μM because of the emergence of phytoplanktons that are capable of removing silica from seawater extremely efficiently to form hardened structures such as cell walls of diatoms (Siever, 1992).

1.3 The roles of microorganisms in the formation of Banded Iron Formations

Three biological mechanisms have been invoked for ferrihydrite precipitation (see Posth et al., 2013a; 2015 for reviews). The first, and perhaps most ancient, involves the oxidation of dissolved Fe(II) during anoxygenic photosynthesis, also known as photoferrotrophy (Garrels et al., 1973;

Hartmann, 1984; Ehrenreich and Widdel, 1994; Konhauser et al., 2002; Czaja et al., 2013; Pecoits et al., 2015).

$$[1]\ 4Fe^{2+} + CO_2 + 11H_2O \rightarrow CH_2O + 4Fe(OH)_3 + 8H^+$$

Photoferrotrophic organisms use light energy and Fe(II) as an electron donor for CO_2 reduction and the production of cell biomass (Widdel et al., 1993). This type of metabolism is widespread amongst freshwater and marine phototrophic bacteria, including purple sulfur bacteria (Croal et al., 2004), purple non-sulfur bacteria (Jiao et al., 2005; Poulain and Newman, 2009; Wu et al., 2014) and green sulfur bacteria (Heising et al., 1999; Crowe et al., 2008).

As soon as cyanobacteria evolved and began producing oxygen in the photic zone, the reaction between dissolved Fe(II) and O_2 also became a viable Fe(II) oxidation mechanism:

$$[2]\ CO_2 + H_2O \rightarrow CH_2O + O_2$$

$$[3]\ 4Fe^{2+} + O_2 + 10H_2O \rightarrow 4Fe(OH)_3 + 8H^+$$

Under an anoxic atmosphere, this O_2 could have been confined to localised "oxygen oases" associated with cyanobacterial blooms in coastal settings (Kasting, 1992; Olson et al., 2013). Other bacteria may have played a more direct role in Fe(II) oxidation. For example, Holm (1989) originally speculated that oxidation of Fe(II) by chemolithoautotrophic species such as *Gallionella ferruginea* would have been kinetically favoured in an ocean with limited free oxygen.

$$[4]\ 6Fe^{2+} + 0.5O_2 + CO_2 + 16H_2O \rightarrow CH_2O + 6Fe(OH)_3 + 12H^+$$

Studies have since demonstrated that these organisms can grow across a range of O_2 concentrations, measured as low as 2 μM, though lower concentrations have not been tested (Stolper et al., 2010). Recently, a comparison between biotic and abiotic Fe oxidation kinetics, in the presence of varying levels of O_2, showed that aerobic Fe(II) oxidizers could have oxidized dissolved Fe(II) at rates fast enough to account for BIF deposition (Chan et al., 2017).

If a biological mechanism was important in the initial process of Fe(II) oxidation in an Archean ocean water column, it is then expected that biomass settled to the seafloor along with the Fe(III) minerals (Konhauser et al., 2005). Yet, BIF contain very little organic carbon (i.e., < 0.5 wt.%; Gole and Klein, 1981), meaning either that biomass was oxidized in the water column or bottom sediment via the combined metabolic processes of fermentation and chemoheterotrophy (e.g., Konhauser et al., 2005) or that the biomass and ferrihydrite did not associate and settle together (Gauger et al., 2016). In the first instance, the presence of partially reduced phases, such as magnetite and siderite, suggests the likelihood of dissimilatory iron reduction, DIR (Nealson and Myers, 1990), a chemoheterotropjhic metabolism that couples the oxidation of organic carbon to the reduction of ferric iron:

$$[5]\quad CH_3COO^- + 8Fe(OH)_3 \rightarrow 8Fe^{2+} + 2HCO_3^- + 15OH^- + 5H_2O$$

Evidence of ancient microbial Fe(III) reduction comes from Fe isotopic ratios in Fe-bearing minerals from Archean sedimentary rocks (e.g., Yamaguchi et al., 2005; Steinhofel et al., 2010) that closely mimic those observed during modern dissimilatory Fe(III) reduction (Johnson et al., 2004). More recent studies have also suggested that the oxidation of organic carbon coupled to DIR can occur at temperatures above the thresholds of life, and yet form the same minerals as presently found in BIF (Posth et al., 2013b; Kohler et al., 2013; Li et al., 2013).

In the second instance, several experiments have demonstrated that photoferrotrophic cells can remain in suspension after Fe(II) oxidation relative to the total number of cells produced (Posth et al., 2010; Gauger et al., 2016). This implies that during times of BIF deposition, ferric iron particles would have settled to the seafloor without the entirety of cell biomass that produced them.

1.4 Objectives

The following is a list of objectives of all the work presented in this thesis:

1) Stokes' Law is commonly used to estimate the sedimentation rate of chemical sediments but it was not designed for such particles. Therefore, it is important to create a novel method to precisely measure the sedimentation velocity of chemical sediments, such as cyanobacteria-ferrihydrite aggregates.
2) Although many studies have addressed the interactions between microorganisms and Fe minerals, only a few have focused on cyanobacteria, especially *Synechococcus* sp, which is one of the most abundant planktonic species in modern oceans. Thus, one of the main objectives of this thesis is to conduct a thorough investigation on *Synechococcus*-ferrihydrite aggregates. Specifically, this work investigates whether cyanobacteria co-deposit with Fe minerals, what is the total Fe and biomass content of the deposited aggregates, and what is the sedimentation velocity of the aggregates.
3) The estimated Archean seawater pH ranges from 5.7 to 7.0 (Grotzinger and Kasting, 1993; Halevy and Bachan, 2017; Krissansen-Ton et al., 2018). Most of the constraints come from modelling of the carbon cycle. However, to date, there is no constraint of Archean seawater pH from other perspectives, for example, if the sedimentation velocity of aggregates at pH from 5.7 to 7.0 would be sufficient to deposit BIF within the required time frame of BIF deposition. Thus, the third objective of this work is to further constrain the Archean seawater pH from sedimentation velocity of cyanobacteria-ferrihydrite aggregates.

1.5 References

Bekker, A., Slack, J.F., Planavsky, N., Krapez, B., Hofmann, A., Konhauser, K.O. and Rouxel, O.J., 2010. Iron formation: the sedimentary product of a complex interplay among mantle, tectonic, oceanic, and biospheric processes. Economic Geology, 105(3), pp.467-508.

Bolhar, R., Kamber, B.S., Moorbath, S., Fedo, C.M. and Whitehouse, M.J., 2004. Characterisation of early Archaean chemical sediments by trace element signatures. Earth and Planetary Science Letters, 222(1), pp.43-60.James, H.L., 1954. Sedimentary facies of iron-formation. *Economic Geology*, *49*(3), pp.235-293.

Bruland, K.W. and Lohan, M.C., 2004. Em Treatise on Geochemistry–The Oceans and Marine Geochemistry v. 6.

Cloud, P., 1973. Paleoecological significance of the banded iron-formation. *Economic Geology*, *68*(7), pp.1135-1143.

Chan, C.S., Emerson, D. and Luther III, G.W., 2016. The role of microaerophilic Fe-oxidizing micro-organisms in producing banded iron formations. Geobiology, 14(5), pp.509-528.

Crowe, S.A., Jones, C., Katsev, S., Magen, C., O'Neill, A.H., Sturm, A., Canfield, D.E., Haffner, G.D., Mucci, A., Sundby, B. and Fowle, D.A., 2008. Photoferrotrophs thrive in an Archean Ocean analogue. Proceedings of the National Academy of Sciences, 105(41), pp.15938-15943.

Czaja, A.D., Johnson, C.M., Beard, B.L., Roden, E.E., Li, W. and Moorbath, S., 2013. Biological Fe oxidation controlled deposition of banded iron formation in the ca. 3770 Ma Isua Supracrustal Belt (West Greenland). Earth and Planetary Science Letters, 363, pp.192-203.

Edmond, J.M., Von Damm, K.L., McDuff, R.E., Measures, C. I., 1982, Chemistry of hot springs on the east pacific rise and their effluent dispersal: Nature, v. 297, p. 187-191.

Ehrenreich, A. and Widdel, F., 1994. Anaerobic oxidation of ferrous iron by purple bacteria, a new type of phototrophic metabolism. Applied and environmental microbiology, 60(12), pp.4517-4526.

Froelich, P.N., Blanc, V., Mortlock, R.A., Chillrud, S.N., Dunstan, W., Udomkit, A. and Peng, T.H., 1992. River fluxes of dissolved silica to the ocean were higher during glacials: Ge/Si in diatoms, rivers, and oceans. Paleoceanography, 7(6), pp.739-767.

Garrels, R.M., Perry, E.A. and Mackenzie, F.T., 1973. Genesis of Precambrian iron-formations and the development of atmospheric oxygen. Economic Geology, 68(7), pp.1173-1179.

Gauger, T., Byrne, J.M., Konhauser, K.O., Obst, M., Crowe, S. and Kappler, A., 2016. Influence of organics and silica on Fe (II) oxidation rates and cell–mineral aggregate formation by the green-sulfur Fe (II)-oxidizing bacterium Chlorobium ferrooxidans KoFox–Implications for Fe (II) oxidation in ancient oceans. Earth and Planetary Science Letters, 443, pp.81-89.

Gole, M.J., Klein, C., 1981, Banded iron-formations through much of precambrian time: Journal of Geology, v. 89, p. 169-183.

Grotzinger, J.P. and Kasting, J.F., 1993. New constraints on Precambrian ocean composition. The Journal of Geology, 101(2), pp.235-243.

Halevy, I. and Bachan, A., 2017. The geologic history of seawater pH. Science, 355(6329), pp.1069-1071.

Mortlock, R.A., Froelich, P.N., Feely, R.A., Massoth, G.J., Butterfield, D.A., Lutpon, J.E., 1993. Silica and germanium in Pacific Ocean hydrothermal vents and plumes.Earth and Planetary Science Letters 119:365-378.

Hartman H (1984) The evolution of photosynthesis and microbial mats: A speculation on the banded iron formations. In: Cohen Y, Castenholz RW, Halvorson HO (eds) Microbial Mats: Stromatolites . Alan Liss Inc., New York, pp 449–453.

Heising, S., Richter, L., Ludwig, W. and Schink, B., 1999. Chlorobium ferrooxidans sp. nov., a phototrophic green sulfur bacterium that oxidizes ferrous iron in coculture with a "Geospirillum" sp. strain. Archives of Microbiology, 172(2), pp.116-124.

Holland, H.D., 1984. The chemical evolution of the atmosphere and oceans. Princeton University Press.Jiao, N., Yang, Y., Hong, N., Ma, Y., Harada, S., Koshikawa, H. and Watanabe, M., 2005. Dynamics of autotrophic picoplankton and heterotrophic bacteria in the East China Sea. Continental Shelf Research, 25(10), pp.1265-1279.

Isley, A.E., 1995. Hydrothermal plumes and the delivery of iron to banded iron formation. The Journal of Geology, 103(2), pp.169-185.

Johnson, C.M., Roden, E.E., Welch, S.A. and Beard, B.L., 2005. Experimental constraints on Fe isotope fractionation during magnetite and Fe carbonate formation coupled to dissimilatory hydrous ferric oxide reduction. Geochimica et Cosmochimica Acta, 69(4), pp.963-993.

Jiao, N., Yang, Y., Hong, N., Ma, Y., Harada, S., Koshikawa, H. and Watanabe, M., 2005. Dynamics of autotrophic picoplankton and heterotrophic bacteria in the East China Sea. Continental Shelf Research, 25(10), pp.1265-1279.

Kasting, J.F., Holland, H.D. and Kump, L.R., 1992. Atmospheric evolution: the rise of oxygen. The Proterozoic Biosphere: A Multidisciplinary Study, pp.1185-1188.

Konhauser, K.O., Hamade, T., Raiswell, R., Morris, R.C., Ferris, F.G., Southam, G. and Canfield, D.E., 2002. Could bacteria have formed the Precambrian banded iron formations?. Geology, 30(12), pp.1079-1082.

Konhauser, K.O., Newman, D.K. and Kappler, A., 2005. The potential significance of microbial Fe (III) reduction during deposition of Precambrian banded iron formations. Geobiology, 3(3), pp.167-177.Posth, N.R., Canfield, D.E. and Kappler, A., 2014. Biogenic Fe (III) minerals: from formation to diagenesis and preservation in the rock record. Earth-Science Reviews, 135, pp.103-121.

Konhauser, K.O., Amskold, L., Lalonde, S.V., Posth, N.R., Kappler, A. and Anbar, A., 2007. Decoupling photochemical Fe (II) oxidation from shallow-water BIF deposition. *Earth and Planetary Science Letters*, *258*(1-2), pp.87-100.

Köhler, I., Konhauser, K.O., Papineau, D., Bekker, A. and Kappler, A., 2013. Biological carbon precursor to diagenetic siderite with spherical structures in iron formations. Nature Communications, 4(1), pp.1-7.

Krissansen-Totton, J., Arney, G.N. and Catling, D.C., 2018. Constraining the climate and ocean pH of the early Earth with a geological carbon cycle model. Proceedings of the National Academy of Sciences, 115(16), pp.4105-4110.Widdel, F., Schnell, S.,

Li, W., Czaja, A.D., Van Kranendonk, M.J., Beard, B.L., Roden, E.E. and Johnson, C.M., 2013. An anoxic, Fe (II)-rich, U-poor ocean 3.46 billion years ago. Geochimica et Cosmochimica Acta, 120, pp.65-79.

Maliva, R.G., Knoll, A.H. and Siever, R., 1989. Secular change in chert distribution; a reflection of evolving biological participation in the silica cycle. Palaios, 4(6), pp.519-532.

Mloszewska, A.M., Cole, D.B., Planavsky, N.J., Kappler, A., Whitford, D.S., Owttrim, G.W., Konhauser, K.O., 2018, UV radiation limited the expansion of cyanobacteria in early marine photic environments: Nature Communication, 9, article number 3088

Nealson, K.H. and Myers, C.R., 1990. Iron reduction by bacteria: a potential role in the genesis of banded iron formations. American Journal of Science, 290, pp.35-45.

Olson, S.L., Reinhard, C.T. and Lyons, T.W., 2016. Cyanobacterial diazotrophy and Earth's delayed oxygenation. Frontiers in microbiology, 7, p.1526.

Pecoits, E., Smith, M.L., Catling, D.C., Philippot, P., Kappler, A., and Konhauser, K.O., 2015, Atmospheric hydrogen peroxide and Eoarchean iron formations: Geobiology, v. 13, p. 1–14, https://doi.org/10.1111/ gbi.12116.

Posth, N.R., Huelin, S., Konhauser, K.O. and Kappler, A., 2010. Size, density and composition of cell–mineral aggregates formed during anoxygenic phototrophic Fe (II) oxidation: impact on modern and ancient environments. Geochimica et Cosmochimica Acta, 74(12), pp.3476-3493.

Posth, N.R., Konhauser, K.O. and Kappler, A., 2013. Microbiological processes in banded iron formation deposition. Sedimentology, 60(7), pp.1733-1754.

Poulain, A.J. and Newman, D.K., 2009. Rhodobacter capsulatus catalyzes light-dependent Fe (II) oxidation under anaerobic conditions as a potential detoxification mechanism. Applied and environmental microbiology, 75(21), pp.6639-6646.

Stolper, D.A., Revsbech, N.P. and Canfield, D.E., 2010. Aerobic growth at nanomolar oxygen concentrations. Proceedings of the National Academy of Sciences, 107(44), pp.18755-18760.

Steinhoefel, G., von Blanckenburg, F., Horn, I., Konhauser, K.O., Beukes, N.J. and Gutzmer, J., 2010. Deciphering formation processes of banded iron formations from the Transvaal and the Hamersley successions by combined Si and Fe isotope analysis using UV femtosecond laser ablation. Geochimica et Cosmochimica Acta, 74(9), pp.2677-2696.

Trendall, A.F., 2002. The significance of iron-formation in the Precambrian stratigraphic record. *Precambrian sedimentary environments: A modern approach to ancient depositional systems*, pp.33-66.

Wu, W., Swanner, E.D., Hao, L., Zeitvogel, F., Obst, M., Pan, Y. and Kappler, A., 2014. Characterization of the physiology and cell–mineral interactions of the marine anoxygenic phototrophic Fe (II) oxidizer Rhodovulum iodosum–implications for Precambrian Fe (II) oxidation. FEMS Microbiology Ecology, 88(3), pp.503-515.

Yamaguchi, K.E., Johnson, C.M., Beard, B.L. and Ohmoto, H., 2005. Biogeochemical cycling of iron in the Archean–Paleoproterozoic Earth: constraints from iron isotope variations in sedimentary rocks from the Kaapvaal and Pilbara Cratons. Chemical Geology, 218(1-2), pp.135-169.

Chapter 2. A novel approach to investigate the deposition of (bio)chemical sediments: The sedimentation velocity of cyanobacteria-ferrihydrite aggregates

2.1 Introduction

Sedimentation velocity refers to the speed at which particles fall through a viscous fluid. Understanding grain-fall behavior is a key factor to understand how sediments settle through the water column in different environments, e.g., rivers, lakes, deltas, estuaries, and pelagic marine settings possessing a range of abiotic parameters. Studies used to determine the sedimentation velocity of sediments have typically measured the average size and density of sediments and subsequently applied Stokes' Law, which defines the terminal velocity of a spherical particle descending through a uniform balance of buoyancy and viscous forces (Konhauser et al., 2005; Posth et al., 2010; Thompson et al., 2019). The steady velocity is a function of gravity, particle density, fluid density, fluid viscosity and particle radius (Stokes, 1856; Arnold, 1911). For a sufficiently small and slowly descending spherical particle, the viscous force exerted has a defined magnitude, given by $F\mu = 6\pi\mu r\, U_S$, where μ is the molecular viscosity of the fluid, r is the radius of the spherical particle, and U_S is the sedimentation velocity. Also acting on the particle is the buoyancy force, $F_b = \frac{4}{3}\pi r^3 \left(\rho_P - \rho_f\right)g$, which is the difference between the weight of the particle and of the fluid it displaced. Here, ρ_P is the particle density, ρ_f is the fluid density, and g is the acceleration of gravity. The terminal velocity predicted by Stokes' law results when the viscous force is equal and opposite to the buoyancy force, and is given by

$$U_S = \frac{2}{9} \times \frac{(\rho_P - \rho_f)\cdot g \cdot r^2}{\mu} \qquad \text{Equation 1}$$

There are several assumptions leading to the derivation of the terminal velocity, including the following: (1) the Reynolds number, Re= $\rho_f Us\, r/\mu$, is less than 0.1, which means Stokes' law

only applies to laminar flows surrounding sufficiently small and slow-settling particles; (2) the particles are rigid spheres; and (3) any surrounding particles are sufficiently separated (typically further than 10 particle diameters) from the surrounding convective fluid motion that they have negligible influence on the settling of the particle in question (Arnold 1911; Wray 1977). Obviously, these rigid parameters severely limit accurate analysis of sedimentation velocity in natural habitats.

In the work presented here, we use the example of ferrihydrite-cyanobacteria aggregates to demonstrate whether an established method that measures the sedimentation velocity of clays is also applicable to (bio)chemical sediments (Sutherland et al., 2015; Playter et al., 2017). We chose these components because they provided major contributions to the deposition of BIF, the iron-rich (15-40 wt.% Fe) and siliceous (40-60 wt.% SiO_2) chemical deposits that formed on the continental shelves throughout the Precambrian Eon (Konhauser et al., 2017). The best-preserved successions are composed primarily of fine-grained quartz (SiO_2), magnetite (Fe_3O_4) and hematite (Fe_2O_3), with variable amounts of Fe-rich silicate and carbonate minerals. It is generally agreed that none of the minerals in BIF are primary in origin in the sense that the original seafloor precipitate was likely a hydrous and amorphous precipitate that was transformed post-depositionally during diagenesis and metamorphism. Instead, iron oxides in BIF are interpreted to have formed from an initial ferrihydrite phase which precipitated in the photic zone via bacterial oxidation of dissolved ferrous iron; the bacterial role was either direct through anoxygenic photosynthesis or indirect through reaction with cyanobacteria-generated oxygen (Konhauser et al. 2018).

Although there is general consensus for the composition comprising BIF primary sediment and that the driving mechanism for Fe(II) oxidation was biological, what remains unanswered are:

(1) the physical processes by which ferrihydrite-microbes were sedimented, and (2) the rate of particle flocculation through a marine water column likely <150 meters in depth. Previous studies examining the association between Fe(III) minerals and different anoxygenic, photosynthetic, Fe(II)-oxidizing bacteria, the so-called photoferrotrophs, have consistently shown that the attachment between the Fe minerals and cells is minimal (e.g., Konhauser et al., 2005; Gauger et al., 2016). This is logical since a tight association would lead to a reduction in cell survival resulting from sedimentation out of the photic zone. In the case of the photoferrotrophic bacterium, *Chlorobium phaeoferrooxidans* strain KB01, a photoferrotrophic bacterium that was isolated from the water column of ferruginous Kabuno Bay, a sub-basin of Lake Kivu in East Africa, experiments demonstrated that only 6% of the cells were sedimented in Fe- and Si-rich media used as a modern analogue of Archean seawater composition (Thompson et al. 2019).

Based on a number of photoferrotroph iron oxidation experiments, particle sizes were generally between 10 to 40 μm (Konhauser et al. 2005; Posth et al. 2010; Schad et al. 2019), with sedimentation velocity using Stokes' Law estimated between from 0.01 cm s^{-1} to 0.24 cm s^{-1}. As predicted, the sedimentation velocity increased with particle size and the Fe:C ratio (which influences particle density); the cell component of the biogenic minerals lowers the total particle density resulting in a decreased sedimentation velocity (Posth et al. 2010). Interestingly, despite the experiments using a wide range of Fe(II) starting concentrations (from 200 to 1000 μM), a strong trend between initial Fe(II) concentration and aggregate size was not observed.

By comparison to the photoferrotrophs, the only study to date, that we are aware of, looking at the interaction of cyanobacteria (specifically *Synechococcus* sp. PCC 7002) with ferrihydrite products of Fe(II) oxidation demonstrated a strong cell-mineral association as might be expected because excretion of O_2 during oxygenic photosynthesis reacts rapidly with Fe(II), causing

precipitation of ferrihydrite on the cell surface (Thompson et al. 2019). Moreover, this association was likely facilitated by ferrihydrite binding to organic ligands on the cell's surface (Phoenix et al. 2000). If cyanobacteria, such as *Synechococcus*, were readily encrusted in ferrihydrite, do the mineral-cell aggregates increase sedimentation velocities, and can those velocities be quantified in a more meaningful manner than Stokes' Law? Ultimately, this information is essential for describing the sedimentation velocity of BIF.

2.2 Methods

2.21 Experimental design

The experiment design was followed as per Sutherland et al. (2015) and Playter et al. (2017). The experiments were performed in a 30 cm tall clear acrylic tank with horizontal dimensions of 20 cm × 5.1 cm (Fig. 1). Black construction paper was placed at the back of the water tank from 10 cm above the bottom to the top of the tank. Translucent mylar sheets were affixed to the back of the tank over the bottom 10 cm, while a halogen light was placed behind the water tank to enhance visualization of the particles during the settling process. A Panasonic HDC-HS250 digital camcorder or a Huawei P30 pro mobile phone were used for recording videos that were shorter than or longer than 1.5 hours, respectively. Continuous movies were recorded at 24 frames per second of the backlit portion of the tank. Ambient light variations were blocked by a black cloth that covered the entire set-up between the camera and tank.

2.22 Sedimentation media preparation

Three sedimentation components, consisting of a Si-rich ferrihydrite and cyanobacteria corresponding to the predicted initial composition of BIF sediment, were prepared separately and

mixed *in situ* in the water tank. The Fe(II) stock solution (0.2 M) was produced anaerobically from ferrous chloride tetrahydrate. The silica (Si) stock solution (0.2 M) was made from sodium metasilicate nonahydrate. The microbial cultures were inoculated from the axenically-grown cyanobacterium *Synechococcus* sp. PCC 7002 (referred from herein as *Synechococcus*) grown on agar plates and subsequently incubated in modified liquid A+ marine media at 30ºC (Mloszewska et al. 2018). The original A+ media that was designed for growing marine cyanobacteria species was modified to exclude ethylenediaminetetraacetic acid (EDTA) such that Fe mineral formation was not chelated during the experiments. The optical density of the *Synechococcus* cultures at 750 nm were closely monitored and cultures were harvested for experiments when the optical density reached 0.5 or higher.

As a general background to the Precambrian conditions we aim to mimic, concentrations of dissolved Fe(II) in the bulk oceans may have varied between the range of 30 μM (Holland 1973) to 500 μM (Morris 1993), but in the vicinity of hydrothermal plumes it is possible that dissolved Fe(II) concentrations may have been 1–2 orders of magnitude higher than today (Kump and Seyfried 2005); the concentration of Fe(II) effused from some modern deep sea vents is 1800 μM (Edmond et al., 1982). Recent work also suggests that in the presence of dissolved silica, whose concentration was potentially 2200 μM in Precambrian seawater (Konhauser et al. 2007), the initial water column precipitate may have been a Fe(III)-Si gel (Zheng et al., 2016).

To demonstrate the settling process of aggregates under various chemical conditions, as well as the relationship between sedimentation velocity with different chemical parameters, eleven experiments were conducted over a range of pH values and initial Fe(II) concentrations (Table 1).

Experimental mixtures of chemicals and biomass were created as follows. Ultrapure water was supplemented with NaCl and $NaHCO_3$ to final concentrations of 0.56 M and 70 μM,

respectively. Subsequently, a concentrated liquid cyanobacteria culture (OD 750 nm ~0.2) and Si (2200 μM) were added. The pH of this mixture was rapidly adjusted using either concentrated HCl or NaOH to obtain the indicated pH.

The final mixture was immediately added to the culture tank and the recording started. Simultaneously, an initially anaerobic Fe(II) stock solution was added via a sterile syringe to obtain the indicated final concentrations ranging from 225 μM to 1800 μM. Note that experiments were not conducted at the lower concentration range of dissolved iron predicted for in the Archean (30 μM; Holland 1973) because our focus here was to oxidize sufficient Fe(II) so that flocculation of ferrihydrite would occur over the time course of these experiments. The mixture was stirred vigorously with a sterile plastic pasture pipette to ensure a homogeneous state, and then the mixture was left undisturbed with cyanobacteria-ferrihydrite aggregates forming and settling in the relatively quiescent fluid until the end of the recording process. All of the experiments were left open to atmosphere because we were primarily interested in elucidating the physical settling process after formation of the aggregates, not the oxidation of Fe(II).

2.23 Video processing

The movies were pre-processed using the open source software "ffmpeg" to reduce file size. This was accomplished by cropping the image to include only the 10 cm deep backlit portion of the tank and then constructing a time-lapse movie using one frame every second and catenating those frames to form a new movie. This resulted in a video that ran 24 times faster than the original recording.

After pre-processing, the program MATLAB (https://www.mathworks.com) was used to input and digitize the movies and, from this, construct vertical time series images from which the

aggregates descent could be measured. Specifically, how the time series were constructed depended upon the mechanism by which aggregates settled. Based on our observation of all preliminary experiments, aggregates settled exclusively through one of two mechanisms: (1) a sediment-concentration front developed and descended uniformly across the span of the tank capturing most of the suspended particles with it, or (2) one or more localized plumes developed with cell-mineral aggregates descending in the plumes but also rising in the ambient fluid surrounding the plumes, as occurs in convective cells.

2.24 Calculations for the settling-front mechanism

At pH values above 9, the cell-mineral aggregates grew to form large aggregates that were visible by eye; estimated sizes were measured on Adobe Illustrator from individual frames selected from the video recordings based on the dimension of the water tank. The aggregates then formed a sediment concentration-front that descended quickly in the tank, with settling times ranging from 5 to 30 minutes (Fig. 2). In this case, we used MATLAB to construct vertical time series of the horizontally averaged light intensity. Specifically, from each frame of the time-lapse movie, the horizontal average produced a plot of mean light intensity as a function of height from the bottom of the tank. The successive intensity-versus-height plots were then stacked side-by-side to produce a plot of light intensity as a function of height and time. The descending concentration front was then highlighted by applying a false color scheme (Fig. 3). To quantify the sedimentation velocity of the front, three contours of constant light intensity were plotted on top of the vertical time series. The contours were chosen from 20% to 75% of the maximum light intensity occurring with no particles in suspension. Shortly after the settling front formed, it was found to descend at near-

constant rate. By applying best-fit lines to the three contours using Adobe Illustrator, estimates of the front sedimentation velocity and its error were determined.

2.25 Calculations for the plume mechanism

It was uncommon to observe a well-defined descending concentration front when the pH was lower than 9. Instead, the aggregates grew slowly over several hours. Although individual aggregates were difficult to observe by eye, they interacted collectively to descend as horizontally localized convective cells or plumes, which are horizontally localized buoyancy-driven flows (Turner 1973) (Fig. 4). Corresponding upward circulations were observed on either side of the plume. The sedimentation velocity of aggregates in the descending plumes were measured to be the speed of a single descending plume. Thus, the sedimentation velocity only accounts for the maximum descending velocity of a single plume formed in the solution and not the velocity at which all the aggregates eventually settled. MATLAB was used to extract just a single vertical time slice through each frame located at the horizontal position of the plume where it initially formed. The successive images of light intensity versus height were then stacked to construct a vertical time series, as shown in Figure 5. On each vertical time series, the slope of three lines that depict descending regions of relatively high light intensity were chosen for quantification of sedimentation velocity and their errors.

2.3 Results

From the 11 experiments that were conducted for this study, cell-Fe(III) mineral aggregates settled in the form of a concentration front in 8 experiments, 7 of which were at pH 11 and 1 was at pH

10. In the remaining 3 experiments, aggregates settled in the form of plumes at lower pH values from 7 to 9 (Table 1).

The sedimentation velocity measured in settling-front experiments ranged from 0.0284 cm s^{-1} to 0.0447 cm s^{-1} with increasing initial Fe(II) concentration. At higher initial Fe(II) concentrations from 1800 to 1200 μM, aggregates were densely distributed across the water tank. As a result, these aggregates interacted with each other and collected to produce larger aggregates on the order of 2 cm in diameter (Fig. 6A and 6B). However, at lower Fe(II) concentrations from 900 to 225 μM, aggregates were more sparsely distributed and thus some individual aggregates could be identified and measured. Visible aggregates ranged in scale from 0.2 to 0.5 cm (Fig. 6C and 6D). At pH 11, the 7 settling-front experiments with different initial Fe(II) concentration from 225 μM to 1800 μM showed increasing sedimentation velocity with increasing initial Fe(II) concentrations and corresponding larger aggregate sizes (Fig. 7).

The 3 experiments where aggregates settled in the form of plumes had pH values ranging from 7 to 9 while the initial Fe(II) concentration was fixed at 1800 μM. The calculated sedimentation velocity varied from 0.036 (+/- 0.005) to 0.090 (+/- 0.013) cm s^{-1}, increasing steadily with increasing pH (Fig. 8).

We evaluated the relationship between our measured sedimentation velocities with rates estimated by Stokes' law, using equation (1) with $\mu=1.02 \times 10^{-2}$ g cm^{-1} s^{-1}, $g=981$ cm s^{-2} and ambient fluid density $\rho_f=1.022$g cm^{-3}. The effective radius of the aggregate was taken to be 0.2 cm when the Fe(II) concentration was 225 μM, and 2 cm when the Fe(II) concentration was 1800 μM (Konhauser et al. 2005). Assuming a particle is conservatively composed of 1% ferric oxide (with a density of 3.8 g cm^{-3}) and 99% ambient fluid in its pores, we estimate the effective particle density ρ_P to be 1.05 g cm^{-3}. These parameters predict a wide range of sedimentation velocities

from 30 cm s^{-1} to $3x10^4$ cm s^{-1}, which are several orders of magnitude faster than what was measured using our method. This drastic difference highlights how Stokes' law cannot be applied when calculating the sedimentation velocity of such chemical sediments.

2.4 Discussion

Applying Stokes' Law (equation 1) to calculate the sedimentation velocity of chemical flocculants, such as cyanobacteria-ferrihydrite aggregates, that form in suspension and settle through a water column, provides at best a crude approximation. First, naturally occurring aggregates are irregularly shaped, owing to their porous nature (Schädler et al. 2008). Second, aggregate size constantly changes from their initial formation in the water column to deposition, and it is thus challenging to measure accurately the particle size regardless of the size of the sample pool. Third, we observed complex settling mechanisms in which aggregates interacted with each other to settle collectively through the water column either as convective cells or plumes.

Our results provide four major insights into the chemical and mechanistic mechanisms contributing to BIF formation. First, the settling processes of cyanobacteria-ferrihydrite aggregates are more complicated than previously anticipated from Stokes' law-based calculations. Depending on a combination of pH and initial Fe(II) concentration, the form of aggregates descending through a water column can be classified into three categories: (1) a concentration front that settles at a steady rate; (2) settling as single or multiple plumes; and (3) slow dispersion that takes several hours to even days. We focused on the first two mechanisms because the third mechanism was only observed at pH below 7, and the settling velocity was too slow to be measured and modeled in MATLAB. Aggregates settled in the form of a concentration front over a range of initial Fe(II) concentrations at pH 10 or above. Although pH 10 is higher than the maximum pH value of 8.6

that was predicted in the Archean oceans (Krissansen-Totton et al. 2018), higher pH values could have occurred episodically when high-pH and silica-rich hydrothermal fluids were introduced to shallow marine environments (Sekine et al. 2015). Under these conditions, our results indicate that cyanobacterial-ferrihydrite aggregates could have settled to the continental shelf seafloor in the form of a concentration front. On the other hand, when the pH was below 10 but above 6, our data indicates that aggregates exclusively settled in the form of plumes. In sum, these results imply that plume deposition may have been more predominant in the near-shore Archean water column.

Second, sedimentation velocity of cyanobacteria-ferrihydrite aggregates depended on a combination of pH and initial Fe(II) concentrations (Fig. 7; Fig. 8). Qualitatively, our result from concentration-front experiments is consistent with Stokes' Law equation 1, which predicts that the terminal velocity of a settling sphere is proportional to the density difference of the particle and fluid and increases as the square of the size of the objects. Although the iron precipitate in our experiments is ferrihydrite, with a known density of 3.8 g cm^{-3}, the actual density of an aggregate must take into account the volume fraction of ambient fluid within the aggregate. Assuming this fraction comprises a fixed ratio as the aggregate expands, our results indicated that the primary factor governing the sedimentation velocity was aggregate size that is directly dependent on initial Fe(II) concentration. Meanwhile, our result from plume experiments showed that sedimentation velocity increased not only with increasing initial Fe(II) concentration but also with increasing pH. The increased sedimentation velocity at higher pH is likely related to the rate of Fe(II) oxidation to Fe(III) and the subsequent hydrolysis of dissolved Fe(III) to form solid-phase ferrihydrite (Singer and Stumm 1970). Moreover, the surface charge of the ferrihydrite surface changes with increasing pH, from predominantly $>FeOH_2^+$ below pH 4 to >Fe(OH) between pH 4-12 (Millero 2001). Increased surface exposure of hydroxy groups (-OH) facilitates hydrogen bonding between

ferrihydrite particles, thus leading to greater polymerization and flocculation (Dzombak and Morel 1990).

Third, *Synechococcus* cells were observed to co-deposit with ferrihydrite, contributing to the accumulation of sedimented material under every geochemical condition tested (Fig. 2; Fig. 4). These findings indicate a tight physical association between *Synechococcus* cells with ferrihydrite in vivo, confirming the observations described by Thompson et al. (2019). In contrast, tight associations were not observed between anoxygenic photosynthesis bacteria and Fe(III) minerals (Konhauser et al. 2005; Gauger et al. 2016; Schad et al. 2019). Importantly, if cyanobacteria were the dominant biological mechanism for Fe(II) oxidation (versus photoferrotrophs), then the co-deposition we observed with the cell-mineral aggregates implies that biomass must have been deposited to the ancient seafloor. This biomass, in turn, would subsequently have served as a suitable electron donor to various respiratory processes during diagenesis, such as dissimilatory Fe(III) reduction (Konhauser et al. 2005). This specific biochemical deposition process shown here will contribute to the explanation of the origin of both the common secondary iron minerals in BIF, such as siderite ($FeCO_3$) (Köhler et al. 2013) or magnetite (Li et al. 2013), as well as the low organic carbon contents preserved in BIF (Gole and Klein 1981).

Fourth, the maximum sedimentation velocity of ferrihydrite-cell aggregates at pH 7 with 1800 μM initial Fe(II) concentration is 0.0360 (+/- 0.0050) cm/sec. This value is ~30% lower than the sedimentation velocity predicted by Stokes' Law using similar aggregates (0.05 cm/sec) at pH 6.8 (Kappler and Newman 2004; Konhauser et al, 2005). It should be noted that even considering that we observed increases in the sedimentation velocity with Fe(II) concentration, the low predicted Fe(II) concentration in Archean oceans (30-500 μM; Holland 1973; Morris 1993)

compared to the 1800 μM used here would suggest that the functional sedimentation velocity of aggregates during BIF deposition would have been substantially lower than reported here.

The observations presented here are crucial as they provide new insights into the conditions and mechanisms contributing to BIF deposition. Previous studies have attempted to calculate annual iron fluxes from the water column to the seafloor during BIF deposition as a means of not only determining the time-scale for BIF deposition but also the iron concentration that existed in the paleo-oceans to supply BIF. Our findings suggest that iron fluxes have been significantly overestimated, potentially altering the time scale for BIF deposition compared to estimates calculated from Stokes' Law. In addition, the corresponding Reynolds number of the aggregates size we observed under the concentration-front mechanism ranges between 2 and 4, significantly above the limiting Reynolds number of 0.1, below which Stokes' law is applicable. Thus, in the Archean ocean, utilization of Stokes' Law is not sufficient to accurately describe BIF deposition. Combined, our observations provide informative mechanistic data for incorporation into future BIF deposition modeling, specifically the formation and deposition of ferrihydrite-cyanobacteria aggregates occurs via uniquely independent mechanisms inherently dependent on pH and initial Fe concentration.

2.5 Conclusions

To understand the rate of BIF accumulation, it is crucial to understand the range of sedimentation velocity for Fe-cell aggregates, which are considered as one of the primary sediments contributing to BIF. In this work, we use a new method that allows real-time observation of the settling processes associated with the formation of (bio)chemical sediments. Using a range of pH and Fe(II) concentrations, we determined the sedimentation velocity of ferrihydrite-cyanobacteria aggregates

under a range of chemical conditions. Importantly, our measured sedimentation velocities are significantly lower than previously proposed, based on Stokes' Law. This observation is a significant consideration to incorporate into models that predict the rate of BIF accumulation. Our results substantially refine previous estimates based on Stokes' law, and crucially indicate that both pH and initial Fe(II) concentration combine to determine the mechanism and sedimentation velocity of BIF precursor sediments.

2.6 References

Arnold, H.D., 1911, LXXIV. Limitations imposed by slip and inertia terms upon Stokes' law for the motion of spheres through liquids, The London, Edinburgh, and Dublin Philosophical Magazine and Journal of Science, v. 22, p. 755-775.

Dzombak, D.A., Morel, F.M.M., 1990, Surface Complexation Modeling: Hydrous Ferric Oxide: John Wiley & Sons.

Edmond, J.M., Von Damm, K.L., McDuff, R.E., Measures, C. I., 1982, Chemistry of hot springs on the east pacific rise and their effluent dispersal: Nature, v. 297, p. 187-191.

Gauger, T., Byrne, J.M., Konhauser, K.O., Obst, M., Crowe, S., Kappler, A., 2016, Influence of organics and silica on fe(II) oxidation rates and cell–mineral aggregate formation by the green-sulfur fe(II)-oxidizing bacterium chlorobium ferrooxidans KoFox – implications for fe(II) oxidation in ancient oceans: Earth and Planetary Science Letters, v. 443, p. 81-89.

Gole, M.J., Klein, C., 1981, Banded iron-formations through much of precambrian time: Journal of Geology, v. 89, p. 169-183.

Holland, H.D., 1973, The oceans; A possible source of iron in iron-formations: Economic Geology, v.68, p. 1169-1172.

Kappler, A., Newman, D.K., 2004, Formation of Fe(III)-minerals by Fe(II)-oxidizing photoautotrophic bacteria: Geochimica Et Cosmochimica Acta, v. 68, p. 1217-1226.

Köhler, I., Konhauser, K.O., Papineau, D., Bekker, A., Kappler, A., 2013, Biological carbon precursor to diagenetic siderite with spherical structures in iron formations: Nature Communications, 4, article number 1741.

Konhauser, K.O., Newman, D.K., Kappler, A., 2005, The potential significance of microbial fe(III) reduction during deposition of precambrian banded iron formations: Geobiology, v. 3, p. 167-177.

Konhauser, K.O., Amskold, L., Lalonde, S.V., Posth, N.R., Kappler, A., Anbar, A., 2007, Decoupling photochemical fe(II) oxidation from shallow-water BIF deposition: Earth and Planetary Science Letters, v. 258, p. 87-100.

Konhauser, K.O., Planavsky, N.J., Hardisty, D.S., Robbins, L.J., Warchola, T.J., Haugaard, R., Lalone, S.V., Partin, C.A., Onnk, P.B.H., Tsikos, H., Lyons, T.W., Bekker, A., Johnson, C.M., 2017, Iron formations: A global record of Neoarchaean to Palaeoproterozoic environmental history: Earth-Science Review, v. 172, p. 140-177.

Konhauser, K.O., Robbins, L.J., Alessi, D.S., Flynn, S.L., Gingras, M.K., Martinez, R.E., Kappler, A., Swanner, E.D., Li, Y-L., Crowe, S.A., Planavsky, N.J., Reinhard, C.T., Lalonde, S.V., 2018, Phytoplankton contributions to the trace-element composition of precambrian banded iron formations: GSA Bulletin, v. 130, p. 941-951.

Krissansen-Totton, J., Arney, G.N., & Catling, D.C., 2018, Constraining the climate and ocean pH of the early earth with a geological carbon cycle model: Proceedings of the National Academy of Sciences of the United States of America, v. 115, p. 4105-4110.

Kump, L.R., Seyfried, W.E., 2005, Hydrothermal fe fluxes during the precambrian: Effect of low oceanic sulfate concentrations and low hydrostatic pressure on the composition of black smokers: Earth and Planetary Science Letters, v. 235, p. 654-662.

Li, Y-L., Konhauser, K.O., Kappler, A., and Hao, X-L., 2013, Experimental low-grade alteration of biogenic magnetite indicates microbial involvement in generation of banded iron formations: Earth and Planetary Science Letters, v. 361, p. 229-237.

Millero., F., 2001, Speciation of metals in natural waters: Geochemical Transactions, v. 2, p. 57-65.

Mloszewska, A.M., Cole, D.B., Planavsky, N.J., Kappler, A., Whitford, D.S., Owttrim, G.W., Konhauser, K.O., 2018, UV radiation limited the expansion of cyanobacteria in early marine photic environments: Nature Communication, 9, article number 3088.

Morris, R.C., 1993, Genetic modelling for banded iron-formation of the hamersley group, pilbara craton, western Australia: Precambrian Research, v. 60, p. 243-286.

Phoenix, V.R., Adams, D.G., Konhauser, K.O., 2000, Cyanobacterial viability during hydrothermal biomineralization: Chemical Geology, v. 169, p. 329-338.

Playter, T., Konhauser, K.O., Owttrim, G.W., Hodgson, C., Warchola, T., Mloszewska, A.M., Sutherland, B.R., Bekker, A., Zonneveld, J.-P., Pemberton, S.G., Gingras, M., 2017, Microbe-clay interactions as a mechanism for the preservation of organic matter and trace metal biosignatures in black shales: Chemical Geology, v. 459, p. 75-90.

Posth, N.R., Huelin, S., Konhauser, K.O., Kappler, A., 2010, Size, density and composition of cell–mineral aggregates formed during anoxygenic phototrophic fe(II) oxidation: Impact on modern and ancient environments: Geochimica Et Cosmochimica Acta, v. 74, p. 3476-3493.

Schädler, S., Burkhardt, C., Kappler, A., 2008, Evaluation of electron microscopic sample preparation methods and imaging techniques for characterization of cell-mineral aggregates: Geomicrobiology Journal, v. 25, p. 228-239.

Schad, M., Halama, M., Bishop, B., Konhauser, K.O., Kappler, A., 2019, Temperature fluctuations in the Archean ocean as trigger for varve-like deposition of iron and silica minerals in banded iron formation: Geochimica et Cosmochimica Acta, v. 265, p. 386-412.

Sekine, Y., Shibuya, T., Postberg, F., Hsu, H., Suzuki, K., Masaki, Y., Kuwatani, T., Mori, M., Hong, P.K., Yoshizaki, M., Tachibana, Shogo., Sirono, S., 2015, High-temperature water–rock interactions and hydrothermal environments in the chondrite-like core of Enceladus: Nature Communications, 6, article number 8604.

Singer, P.C., Stumm, W., 1970, Acid mine drainage: The rate-determining step: Science, v. 167, p. 1121-1123

Stokes, G.G., 1850, On the effect of the internal friction of fluids on the motion of pendulums: Transactions of the Cambridge Philosophical Society, v. 9, p. 8.

Sutherland, B.R., Barrett, K.J., Gingras, M.K., 2015, Clay settling in fresh and salt water: Environmental Fluid Mechanics, v. 15, p. 147-160.

Thompson, K.J., Kenward, P.A., Bauer, K.W., Warchola, T., Gauger, T., Martinez, R., Simister, R.L., Michiels, C.C., LIirós, M., Reinhard, C.T., Kappler, A., Konhauser, K.O., Crowe, S.A., 2019, Photoferrotrophy, deposition of banded iron formations, and methane production in Archean oceans, Science Advances, v. 5, article number 11.

Turner, J.S., 1973, Buoyant Convection from Isolated Sources, in Buoyancy Effects in Fluid: Cambridge University Press, p. 165-206.

Wray, E.M., 1977, Stokes' law revisited: Physics Education, v. 12, p. 300-303.

Zheng, X.-Y., Beard, B.L., Reddy, T.R., Roden, E.E., Johnson, C.M., 2016, Abiologic silicon isotope fractionation between aqueous Si and Fe(III)-Si gel in simulated Archean seawater: implications for Si isotope records in Precambrian sedimentary rocks: Geochimica Et Cosmochimica Acta, v. 187, p. 102–122.

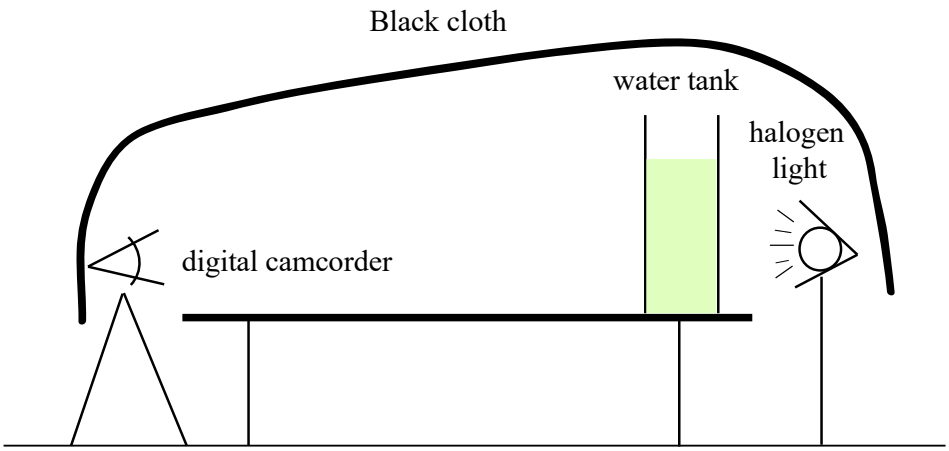

Figure 2.1. Settling experiment setup.

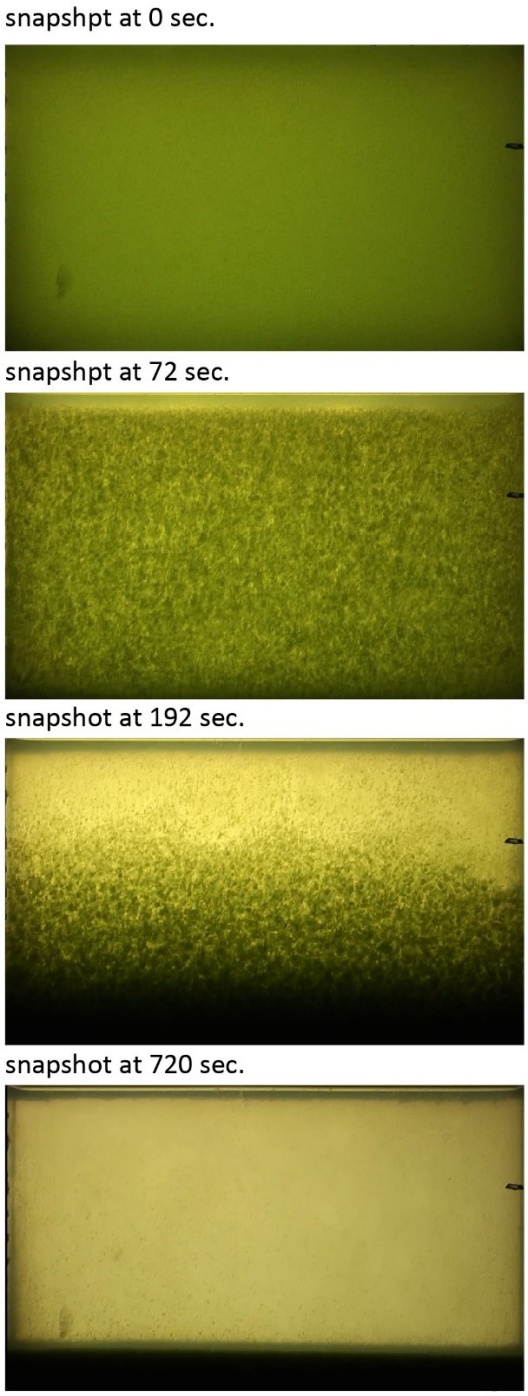

Figure 2.2. Images from a settling-front experiment with pH=11 and initial Fe(II) concentration of 1800 μM. In each image the field of view is 20 cm wide by 10 cm tall. Note the color difference between the snapshots at o sec and 720 sec, showing the co-deposition of cyanobacteria cells and ferrihydrite.

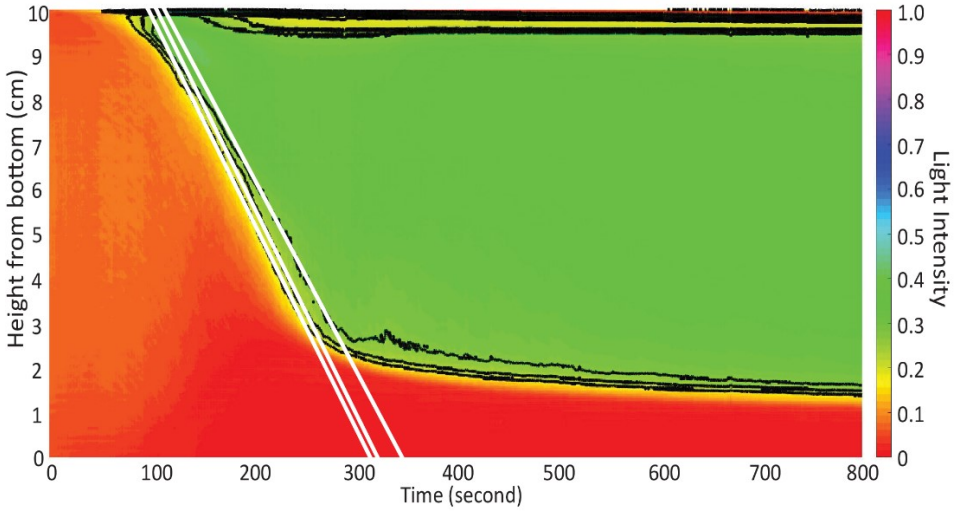

Figure 2.3. Vertical time series of horizontally averaged light intensity taken from the experiment shown in Figure 2.

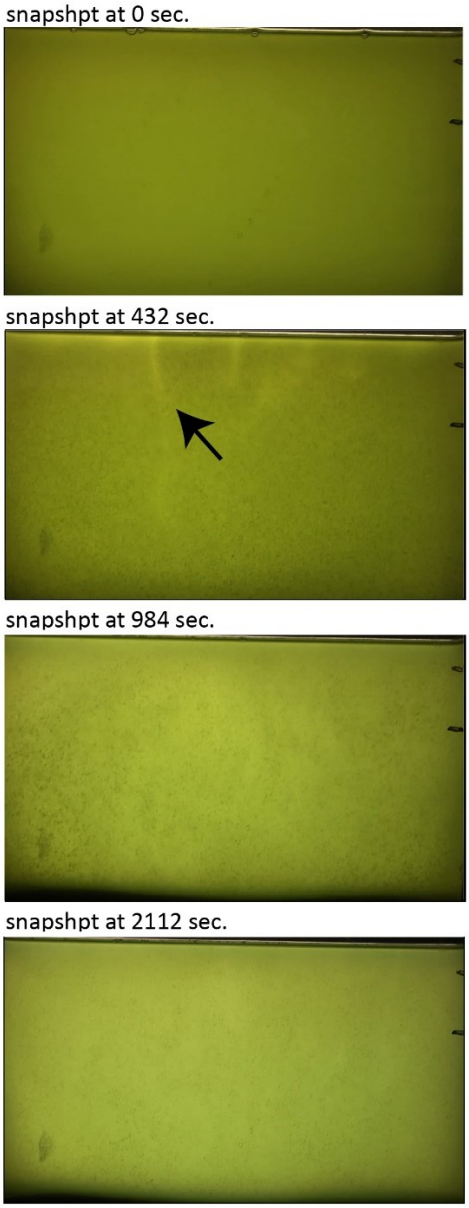

Figure 2.4. Images from a plume experiment with pH=9 and initial Fe(II) concentration of 1800 μM. In each image the field of view is 20 cm wide by 10 cm tall. The plume that was used to determine sedimentation velocity is indicated by the arrow. Note the color difference between the developed plumes and their surroundings, showing the co-deposition of cyanobacteria cells and ferrihydrite.

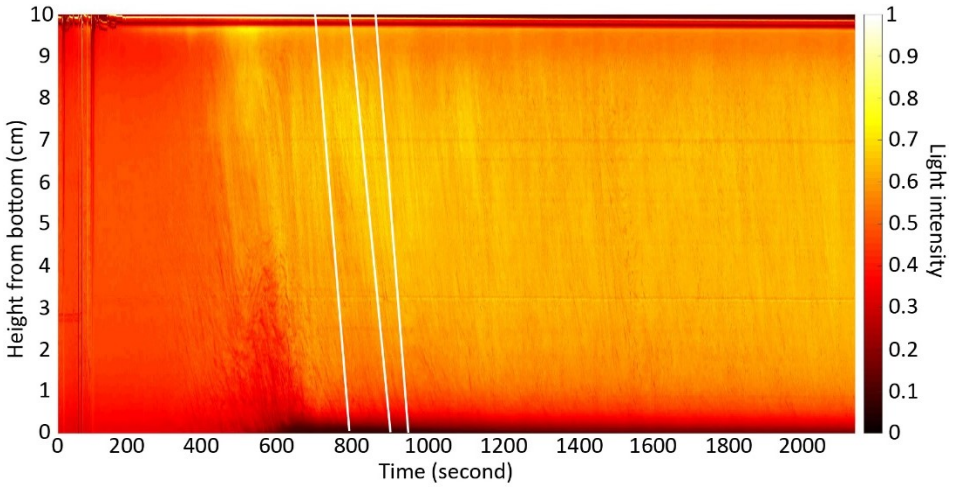

Figure 2.5. Vertical time series of a single vertical slice taken from the experiment shown in Figure 4.

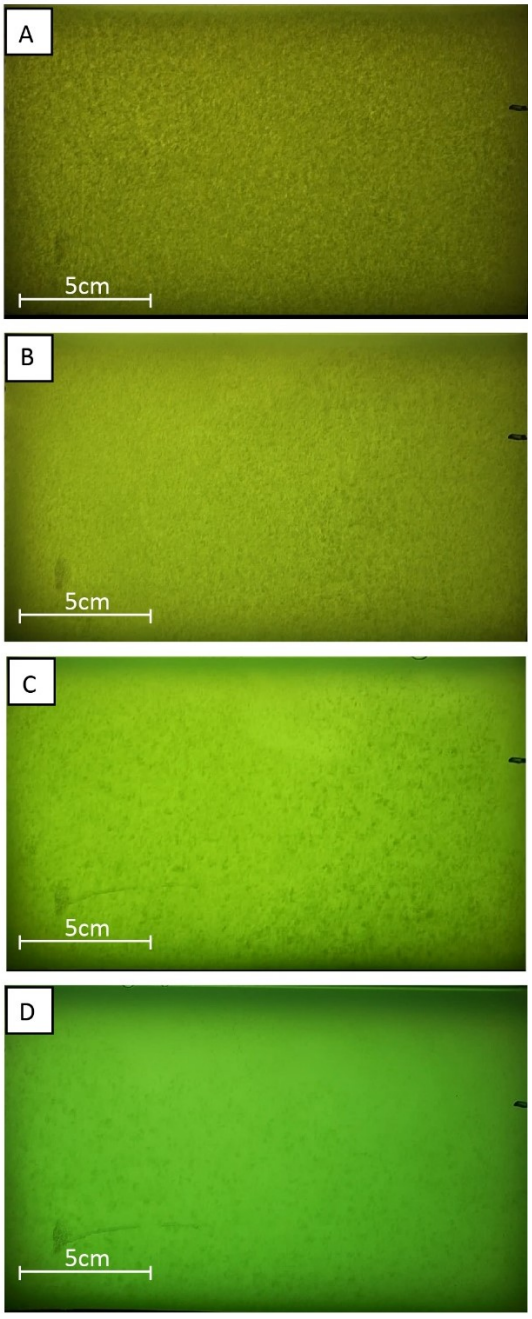

Figure 2.6. Aggregate size comparison from 4 settling-front experiments at pH = 11. (A) Fe(II) concentration = 1800 µM; (B) Fe(II) concentration = 1200 µM; (C) Fe(II) concentration = 600 µM; and (D) Fe(II) concentration = 225 µM. Inter-connected aggregates are shown in A and B. Individual aggregates are shown in C and D.

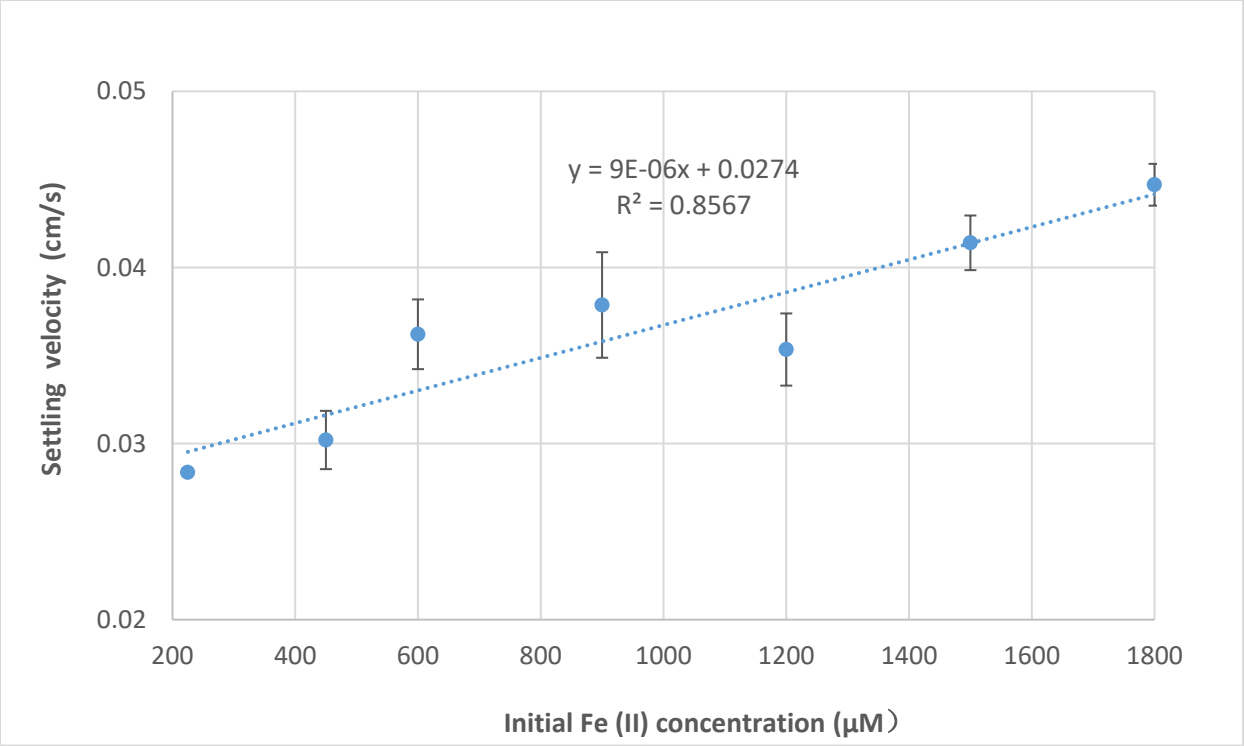

Figure 2.7. Average sedimentation velocity of concentration-front mechanism at pH 11 relative to initial Fe(II) concentration from 225 µM to 1800 µM.

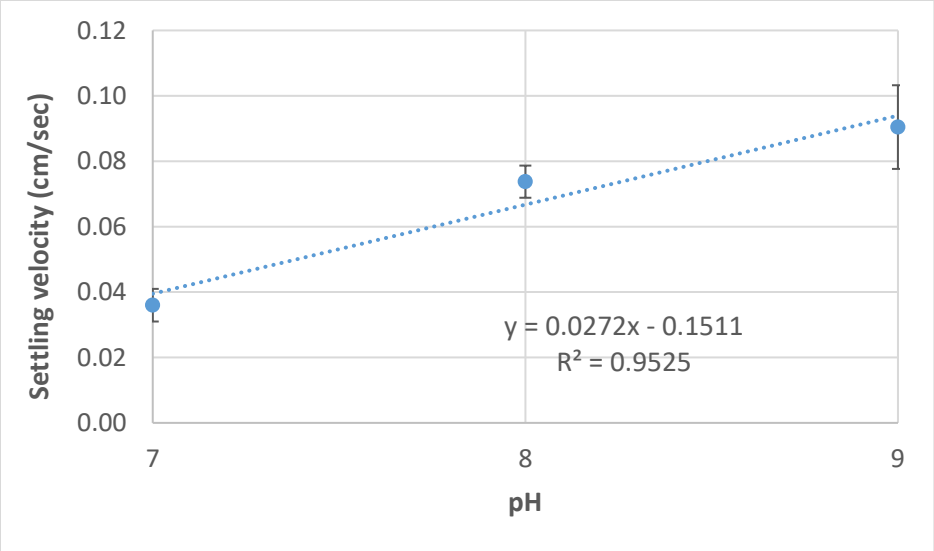

Figure 2.8. Average sedimentation velocity plume mechanism at initial Fe(II) concentration of 1800 µM relative to pH values from 7 to 9.

Table 2.1. A list of 11 experiments conducted in this paper with initial conditions, settling forms and average sedimentation velocity.

Experiment	pH	Fe (II) concentration (μM)	Settling form	Average Sedimentation velocity (cm/sec)
1	11	225	Concentration Front	0.0284 (+/- 0/0001)
2	11	450	Concentration Front	0.0302 (+/- 0.0017)
3	11	600	Concentration Front	0.0362 (+/- 0.0020)
4	11	900	Concentration Front	0.0379 (+/- 0.0030)
5	11	1200	Concentration Front	0.0353 (+/- 0.0016)
6	11	1500	Concentration Front	0.0414 (+/- 0.0016)
7	11	1800	Concentration Front	0.0447 (+/- 0.0012)
8	10	1800	Concentration Front	0.0398 (+/- 0.0016)
9	9	1800	Plumes	0.0905 (+/- 0.0128)
10	8	1800	Plumes	0.0738 (+/- 0.0049)
11	7	1800	Plumes	0.0360 (+/- 0.0050)

Chapter 3. Cyanobacteria-ferrihydrite aggregates as primary sediments to BIF and their implications for Archean-Paleoproterozoic seawater geochemistry

3.1 Introduction

Superior-type banded iron formations (BIF) are (bio)chemical sedimentary rocks that are characteristically iron-rich (~20-40% Fe) and silica-rich (~40-50% SiO_2) and were deposited over vast expanses on the continental shelves. Most such BIF were deposited throughout the late Archean and Paleoproterozoic eon (2.7-1.8 Ga). It is widely accepted that the precipitation of BIF required the activity of marine planktons for the initial oxidation of dissolved Fe(II) in seawater to flocculate Fe(III) minerals, such as ferrihydrite, $Fe(OH)_3$. Three biological oxidation mechanisms have been proposed (see Konhauser et al., 2017 for review): anoxygenic photoautotrophy, also known as photoferrotrophy (reaction 1), oxygenic photoautotrophy (reaction 2), and chemolithoautotrophy (reaction 3).

$$[1] \quad 4Fe^{2+} + HCO_3^- + 10H_2O \rightarrow 4Fe(OH)_3 + CH_2O + 7H^+$$

$$[2] \quad 2Fe^{2+} + \tfrac{1}{2}O_2 + 5H_2O \rightarrow 2Fe(OH)_3 + 4H^+$$

$$[3] \quad 6Fe^{2+} + \tfrac{1}{2}O_2 + CO_2 + 16H_2O \rightarrow CH_2O + 6Fe(OH)_3 + 12H^+$$

In all cases, it was hypothesized that microbial biomass would have settled with ferrihydrite as an iron-organic aggregate to the seafloor where the organic carbon was fermented and the oxidized using the ferric iron in ferrihydrite as the terminal electron acceptor – a process known as dissimilatory iron reduction (DIR) (Konhauser et al., 2005). This hypothesis not only explains the low content of organic carbon in IFs (<0.5 wt.%; Gole and Klein, 1981), but it also explains

negative carbon isotope values associated with the early diagenetic Fe(II)–rich carbonates (Perry et al., 1973; Walker, 1984; Baur et al., 1985; Heimann et al., 2010; Craddock and Dauphas, 2011), the small-scale heterogeneity in $\delta^{56}Fe$ values (e.g., Frost et al., 2007; Steinhofel et al., 2010; Planavsky et al., 2012), and the presence of Fe(II)-bearing minerals in BIF, such as magnetite (Fe_3O_4), siderite ($FeCO_3$) and greenalite ($(Fe)_3Si_2O_5(OH)_4$) (Li et al., 2013; Posth et al., 2013; Köhler et al., 2013; Halama et al., 2016; Robbins et al., 2019). Indeed, growth experiments with a number of different photoferrotrophic species have demonstrated various association of cells with ferrihydrite or partial encrustation of the cells (e.g., Kappler and Newman, 2004; Hegler et al., 2008; Schädler et al., 2009; Posth et al., 2010; Gauger et al., 2016; Laufer et al., 2017), with the number of cells remaining mineral-free in suspension ranging from 50% (Posth et al., 2010) to only 1% (Konhauser et al., 2005). However, this view is complicated by two recent experimental studies which demonstrated that in the presence of dissolved silica, different photoferrotroph cell surfaces repel ferric oxyhydroxides to different extents (Schad et al., 2019; Thompson et al., 2019). Therefore, in silica-rich Precambrian seawater, this repulsion would separate biomass from ferric iron and would lead to large-scale deposition of BIF lean in organic matter.

To date, although photoferrotroph-ferrihydrite aggregates have been extensively investigated, the other potentially important primary sediment to BIF - cyanobacteria-ferrihydrite aggregates - have only received very limited attentions (Thompson et al., 2019; Li et al., 2020). Conservatively speaking, cyanobacteria evolved and even flourished at onset of the Great Oxidation Event around 2.45 Ga, which overlaps in time with significant BIF deposition (Bekker et al., 2010; Konhauser et al., 2017). Therefore, it was likely that cyanobacteria played a vital role in the formation of BIF. Indeed, compared to the repulsion of Fe(III) minerals from

photoferrotrophs, Thompson et al. (2019) and Li et al. (2020) both showed strong encrustation of cyanobacteria cells on Fe (III) minerals, forming cyanobacteria-Fe(III) minerals aggregates.

The conclusion that one takes from these various Fe(II) oxidizing experiments is that presence or absence cell-ferrihydrite aggregates strongly influences the rate and extent of sedimentation of the microbial cells, i.e., the biomass. This, in turn, is significant for two reasons. First, the sedimentation of encrusted cells will bring higher amounts of organics to the seafloor than cells with weaker associations to Fe(III) minerals or mineral-free cells that remain mostly suspended in the water column (Konhauser et al., 2005). Anoxygenic phototrophs incorporate 1 mole CO_2 into biomass with the oxidation of 4 moles Fe^{2+}. If all cells (the complete biomass) would deposit together with the produced Fe(III) minerals, this would lead to a Fe(III)/C_{org} ratio of 4:1 in the sediments. As Fe(III) re-reduction coupled to biomass mineralization (e.g., DIR) requires the same 4Fe(III):1C ratio (reaction 4), this sedimentation could lead to total recycling of precipitated Fe(III).

$$[4] \quad CH_2O + 4Fe(OH)_3 \rightarrow 4Fe^{2+} + HCO_3^- + 7OH^- + 3H_2O$$

However, if minimal encrustation occurred, less biomass attached to Fe(III) minerals would have been sedimented, increasing the ratio of Fe(III)/C_{org}, thus leading to an excess of Fe(III) in the bottom sediments (Konhauser et al., 2005). The implication of excessive settled Fe(III) is that during diagenesis and metamorphism, it would transform into hematite, with little to no organic carbon; a characteristic of BIF.

Second, the sedimentation velocity of cell-Fe mineral aggregates is a crucial parameter when estimating BIF sedimentation rates. Because of density differences between organic carbon (10^{-6}-10^{-7}g cm^{-3}; this study) and ferrihydrite (3.96 g cm^{-3} depending on porosity; Posth et al., 2010),

fully encrusted cells with a high organic matter content will be lighter (have a lower density) than pure minerals or minerals only loosely associated with few cells (Posth et al., 2010). Faster sedimentation velocity inherently implies that it takes less time for aggregates to travel through the water column to the seafloor and thus more Fe minerals is deposited within a given time frame. Today, the average shelf water depth is 130 m, but sea level has shown an approximately 400 m range of variation over geological time (Tyson and Pearson, 1991). Using this upper range for times of BIF deposition – when Fe(II) was upwelled onto the shelf during transgressive events (e.g., Fralick and Pufahl, 2006), it can be estimated that it would take ferrihydrite approximately 12 days to travel through a 500 m water column (maximum depth previously inferred by Trendall, 2002 for BIF deposition) to the seafloor at a velocity of 0.05 cm sec^{-1}, from which the sediment accumulation rate was estimated to be 5 mm $year^{-1}$ (Konhauser et al., 2005). By contrast, if the sedimentation velocity were slower, less total Fe(III) would have been deposited because most ferrihydrite would have been brought back to deeper oceans by downwelling currents before they could be deposited. The consequence of such a scenario is that there would have been not enough Fe(III) minerals to form massive-scale BIF.

Previously, Li et al. (2020) published the first and only study that investigated the physical processes of ferrihydrite-cyanobacteria aggregate deposition using a novel and multidisciplinary method. To visualize the detailed sedimentation processes, they conducted most experiments with high initial pH values such as pH 11 and initial Fe(II) concentrations of 1800 µM. However, is has been estimated that Precambrian seawater pH ranged from 5.7 to 7.0 during the Archean, and increased up to 8.1 at the Proterozoic-Phanerozoic boundary (Grotzinger and Kasting, 1993; Halevy and Bachan, 2017; Krissansen-Ton et al., 2018). Moreover, the Fe(II) concentration was estimated to be from 30 µM (Holland, 1984) to 500 µM (Morris, 1993), with rare occasions of

maximum 1800 μM when the seawater was proximal to hydrothermal plumes (Edmonton et al., 1982). Dissolved silica was also enriched in seawater in the Precambrian before the emergence of silicifying microorganisms, with concentrations perhaps as high as 2.2 mM - amorphous silica solubility (Maliva et al., 1989; Siever, 1992).

To reflect a more realistic Precambrian seawater geochemistry, we empirically conducted aggregate sedimentation experiments with initial pH values ranging from 6.0 to 8.0 and a wide range of initial Fe(II) concentrations from 50 to 1800 μM in the presence of 2.2 mM dissolved silica. Specifically, under realistic Precambrian seawater geochemical conditions, we measured the sedimentation velocity of cyaonobacteria-ferrihydrite aggregates and accordingly estimated the the amount of ferric iron that conceivably could have been deposited on an annual basis during time of BIF deposition; and the association of the cell surface and mineral products to assess the amount of biomass potentially buried when cyanobacteria may have been the dominant player in BIF deposition.

3.2 Methods

3.21 Microorganisms and culturing

The cyanobacterium Synechococcus sp. PCC 7002 (referred from herein as *Synechococcus*) was first isolated from Magueyes Island, Puerto Rico (Van Baalen, 1962). This specific strain is unicellular, photoautotrophic, euryhaline, halotolerant and adapted to high dissolved Fe(II) concentration (Batterton and Van Baalen, 1971; Mloszewski et al., 2018). The wild-type strain was initially acquired from Pennsylvania State University and has been kept axenic in Dr. George Owttrim Laboratory in University of Alberta. Microbial cultures used in this project were

propagated in a growth media based on marine A+ media as designed by Stevens and Porter (1980), who supplemented $NaNO_3$ to the original A media of Stevens and Baalen (1973). EDTA, an iron chelate, was excluded from the A+ medium to eliminate any factors that may influence Fe(III) mineral formation. The final media was adjusted to pH 8.2 with HCl or Na_2CO_3 as appropriate. All cultures were incubated under 30°C and a constant light intensity of 50 μmol photons/m^2/s; and subsequently harvested for experiments when the optical density (OD_{750nm}) became greater than 0.6.

3.22 Experiment solution preparation

All experiments started with a mixture of MQ water and NaCl to a final modern ocean salinity of 0.56 M. Depending on the density of the original culture, at least 60 mL of concentrated *Synechococcus* culture was transferred into the tank using a sterile plastic pasture pipette and light absorption at OD750 nm of the homogeneous mixture was then immediately measured to achieve a final density of 0.15±0.03 after vigorous mixing. Subsequently, 0.2 M Si stock solution that was made from sodium metasilicate nonahydrate was added to reach a final concentration of 2200 μM, which was then followed by pH adjustment to target pH values using concentrated HCl and NaOH. Then, either 0.5 M of MES buffer solution to pH 6 experiment solutions for a final concentration of 5 mM or 70 μM of solid $NaHCO_3$ was added to pH 7 and pH 8 experiment solutions. Finally, experiment solution was brought up to a final volume of 1.25 L using MQ water, which was then followed by another pH adjustment. The initial pH was set at 6.2, 7.2 and 8.2 because pH dropped slightly during the course of experiment. Right before each experiment started, different amount of initially anaerobic 0.2 M ferrous chloride stock solution was added into the water tank using sterile syringes to different target final concentrations.

3.23 *Sedimentation velocity measurements for pH 6 experiments*

Although the Archean ocean pH is not well constrained, it is generally accepted that the lowest pH during Archean had a range from 5.7 to 7.0 (Grotzinger and Kasting, 1993; Halevy and Bachan, 2017; Krissansen-Ton et al., 2018). Below pH 7, *Synechococcus*-ferrihydrite aggregates deposit over a long period of time, typically days or even weeks (Li et al., 2020). Therefore, it is challenging to accurately measure the settling velocity at pH 6. Nevertheless, the change of total Fe concentration in solution over time is still achievable and can be used to test the feasibility of forming BIF at pH 6 in the Archean.

After the desired pH was stabilized, the mixture solution was then transferred to a water tank that is made of translucent acrylic plastic and has an inner dimension of 20 cm × 5.1 cm × 30 cm. Two experiments were conducted at initial Fe(II) concentrations of 50 μM and 1800 μM respectively. Immediately after addition of Fe(II) stock solution into the water tank, the mixture solution was vigorously stirred until homogenous and remained undisturbed afterwards. The first sample was extracted at the surface once the solution was calm after stirring, and subsequent samples were extracted at the same height once every 24 hours for 10 days (50 μM experiment) and 15 days (for 1800 μM experiment). An abiotic control was set up next to the experiment with identical solution composition except that there were no microbes introduced. Total Fe in solution was measured in triplicates using ferrozine assay described below to determine the amount of Fe in suspension over time and corresponding diagrams were plotted in Microsoft office Excel. A logarithmic trendline was then added on each plot with a respective equation, from which the absolute value of the maximum curvature, which is also the maximum settling rate, was calculated in $\mu M\ day^{-1}$. Assuming the sedimentation media remained a homogenous state during the settling process, we then calculated the minimum amount of time (Tmin) required for the aggregates to

settle through the 10 cm water column at the maximum rate. The sedimentation velocity was finally calculated as follows in cm sec^{-1}:

$$\text{Sedimentation velocity} = 10 \text{ cm} \div \text{Tmin}$$

3.24 Sedimentation velocity measurements for pH 7 and pH 8 experiments

We set up experiments as in Sutherland and Barrett (2015) and Li et al. (2020). The water tank used is identical to the ones described above. Black construction paper was placed at the back of the water tank from bottom to a height of 10 cm. A halogen light was placed behind the water tank for better visualization of the settling process. A Panasonic HDC-HS250 digital camcorder was used for recording. Any light interference was blocked by a black cloth that was lightly draped over the entire set-up (Figure 3.1).

The height of final solution in the water tank for each experiment was exactly 10 cm. Video recording always started right after the addition of Fe(II) solution, which was then followed by intense stirring until the solution became homogenous. The duration of each video depended on the Fe(II) concentration and pH. Each video recording was aborted when there was no aggregate settling visible to naked eyes. Every video recording of experiments was subsequently processed. Videos were trimmed down from the exact moment when settling started, followed by the fabrication of a timelapse that ran 24 times faster than the original recordings. In cases when a plume was not observed during the first recording yet most aggregates were deposited, another recording of the same media mixture started again immediately after vigorous resuspension of the deposited aggregates and ended when most aggregates were deposited at the bottom of the tank.

Final sediments at the bottom of the water tank were extracted through a sterile 10mL plastic pasture pipette at the end of each experiment to quantify total Fe content and biomass content.

Initial Fe(II) concentrations in pH 7 experiments were 1200 μM, 1500 μM and 1800 μM, and were 900 μM, 1200 μM, 1500 μM and 1800 μM in pH 8 experiments. We chose these concentrations because aggregates sedimented only via slow-dispersion mechanism below 1200 μM at pH 7 and 900 μM at pH 8. Currently, there is no accurate way to directly measure the sedimentation velocity from such sedimentation mechanism. Although the initial Fe(II) concentrations that were used in this study are higher than what would be considered bulk seawater Archean-Paleoproterozoic Fe(II) concentration between 30 μM and 500 μM (Holland, 1973; Morris 1993), it is plausible that Fe(II) sourced from a proximal hydrothermal vents could have supplied an upper range of Fe(II) concentrations around 1800 μM. More importantly, due to the fact that sedimentation velocity is directional proportional to initial Fe(II) concentrations (Li et al., 2020), the sedimentation velocity calculated from 1200 μM Fe(II) concentration at pH 7 and 900 μM Fe(II) concentration at pH 8 represent the minimum sedimentation velocity at each pH value.

Settling rate measurements were calculated as described in Li et al. (2020). Aggregates exclusively settled through a water column via the descending plume mechanism, which refers to localized convective cells created by heterogenous settling of aggregates in the solution. The descending velocity of a single plume formed in each experiment represented the maximum settling rate of the aggregates under that particular chemical condition, i.e. pH and initial Fe(II) concentration. After the corresponding timelapse was introduced to MATLAB, the software subsequently extracted a single vertical time slice per frame at the location where the plume was initially formed. MATLAB software then stacked up continuous images of light intensity versus height and eventually assembled a vertical time series. The settling rate was calculated from the

slope of three highlighted lines on the vertical time series that were delineated by high light intensity (in cm sec^{-1}). It is worth mentioning that the sedimentation velocity calculated here only accounts for descending speed of a single plume formed during the sedimentation experiment. Thus, it only represents the maximum sedimentation velocity under each condition.

To assess the effect of *Synechococcus* on sedimentation velocity of aggregates, abiotic control experiments were conducted at each initial Fe(II) concentration and pH value. The sedimentation media in the control experiments were identical to their biological counterparts except that no microorganisms were introduced. Samples of 1 mL were extracted from both sedimentation experiments and their corresponding controls at the same time during the entire settling process with 15 to 30 min increment depending on the length of each experiment. Finally, total Fe concentrations were measured using Ferrozine assay and were then plotted against time.

3.25 Biomass quantification

Quantification of biomass/cell numbers was conducted by two different methods. Optical density at 750 nm is a standard method that is used to approximate the cell density of cyanobacterial cultures by measuring the light absorption by chlorophyll *a*. In our experiments, the optical density of each culture was measured by a Beckman Coulter DU®520 UV/VIS spectrophotometer. However, quantification of cell density by measuring the optical density at 750 nm is not a viable method if the microbial culture is mixed with Fe minerals because the latter interfere with light absorption. Thus, at the end of each experiment, the cell density of settled aggregated sediments was evaluated by measuring chlorophyll *a* concentrations (Porra et al.,1989; Mloszewska et al

2018). The chlorophyll *a* concentration of the final sediment from each experiment was then converted to cell numbers for future comparisons.

To achieve an accurate correlation between OD750 nm and numerical cell density, as well as chlorophyll *a* concentration and numerical cell density, a growth curve was constructed. Six *Synechococcus* cultures were inoculated 24 hours apart from the same initial culture that had OD_{750nm} equaled to 0.15. After 48 hr of incubation of the 6^{th} culture, all six samples were taken for OD_{750nm} measurements, chlorophyll *a* concentration measurements and cell counting. Cell counting was performed on an Attune NXT acoustic focusing flow cytometer with the excitation laser at 488 nm and emission filter of 695/40 nm at the average acquisition speed of 25 µl/min for a total volume of 100µL. Both OD_{750nm} and chlorophyll *a* concentrations were plotted against cell numbers thereafter (Figures 3.2-3.3). Numerical cell densities were then calculated from the linear regression lines.

3.26 Total Fe measurements

Total Fe concentrations were measured using the Ferrozine assay throughout the experiment on a Beckman Coulter DU®520 UV/VIS spectrophotometer (Stookey, 1970; Porsch and Kappler, 2011). Ferrozine standards were made by adding ferrous ammonium sulfate hexahydrate into 1M HCl solution, ranging from 0-100 µM with a 20 µM increment. The standards were further tested for accuracy using the Agilent 8800 Triple Quadrupole ICP-MS. All standards were within 2.5 µM of discrepancy from desired values. Samples of the sedimentation media were diluted 20 to 25 times while the final sediment samples were diluted 200 to 250 times. The final results are presented in the unit of µM.

3.27 Quantification of Fe:C_{org} ratios

After the total Fe content and biomass content in the final sediment were quantified, a series of calculations were done to quantify the Fe:C_{org} ratios in the final sediment after each experiment. The calculation of C_{org} content started with conversion of chlorophyll *a* concentration to cell numbers described above, after which cell numbers were multiplied by 26.02 fg C $cell^{-1}$ to get the carbon content in the final sediments (Troussellier et al., 1997). Afterwards, carbon content was divided by 12 g mol^{-1} and subsequently converted to the final unit of µM. Lastly, Fe: C_{org} ratios were calculated from every triplicate of final sediment samples from all pH 7 and pH 8 sedimentation experiments.

3.28 Scanning electron microscopy (SEM)

Cyanobacteria-ferrihydrite aggregate samples were collected from the bottom of the water tank by sterile plastic pasture pipettes at the end of settling experiments and later put into sterile 2 mL Eppendorf tubes. After 1 hour, most aggregate sediments settled to the bottom and the top layer supernatant was expelled. Samples were then immediately stored in a 2% paraformaldehyde and 2.5% glutaraldehyde buffered fixative solution for at least 24 hours before being washed three times with 0.1 M phosphate buffer solution. Samples were then processed through a graded ethanol series followed by a graded ethanol-HMDS (Hexamethyldisilazane) series for dehydration (Bray et al., 1993). Samples were centrifuged at a slow speed of 1500 rpm for 3 min after 20 min of incubation in each solution. Finally, samples were extracted from 100% HMDS solution, gently dropped onto clean uncovered SEM stub mounts and left overnight in a fume hood until completely

dried. All samples were sputter coated with carbon and imaged on a Zeiss Sigma 300 VP-FESEM at 10 kV in the SEM lab located in the Department of Earth and Atmospheric Sciences, University of Alberta.

3.3 Results

3.31 Sedimentation velocity of pH 6 experiment

Two extended pH 6 sedimentation experiments with their corresponding abiotic control experiments were conducted to assess the viability of the minimum Archean ocean pH and to better constrain Archean ocean pH. In all 4 experiments, aggregates settled in the form of slow dispersion. There was no plume nor concentration front formed during the entirety of the experiments: this observation is consistent Li et al. (2020). Overall, the sedimentation velocity of aggregates formed at pH 6 is three magnitude lower than those at pH 7 and pH 8 (Table 1). Total Fe concentrations in solution decreased steadily from the beginning to the end of the experiments (Figures 3.4-3.5). For the sedimentation experiment and its abiotic control experiment with 50 μM initial Fe(II) concentration, the maximum sedimentation rate through a 10 cm water column was 12.02 and 23.94 μM day^{-1}, respectively, which was then converted to sedimentation velocities of 0.000024 cm s^{-1} and 0.000051 cm s^{-1}, respectively. The two logarithmic trendlines fitted well with total Fe concentration change over time; both with R^2 values close to 0.9 (Figure 3.4). Surprisingly, the sedimentation velocity measured for experiments with 1800 μM initial Fe(II) concentration is slower than those with 50 μM. The sedimentation experiment had a velocity of 0.000021 cm s^{-1} and its corresponding abiotic control experiment had a velocity of 0.000016 cm s^{-1}. The maximum sedimentation rate through a 10 cm water column of both experiments are 338.1 μM day^{-1} and

238.4 μM day^{-1}, respectively. The logarithmic trendline correlated with total Fe concentration change over time very well with both R^2 values greater than 0.93 (Figure 3.5).

3.32 Sedimentation velocity of pH 7 and pH 8 experiment

The sedimentation velocities calculated for experiments at pH 7 and pH 8 are shown in Table 2. In all 7 experiments, cell-mineral aggregates settled exclusively via the plume mechanism. This observation is consistent with the previous study where identical aggregates only settled in the form of plumes between pH 7 and pH 9 (Li et al., 2020).

Sedimentation velocities of the three pH 7 experiments were visibly slower than pH 8 experiments, ranging from 0.034 (+/-0.010) cm s^{-1} to 0.036 (+/-0.004) cm s^{-1}. They took more than 180 min for the most aggregates to be deposited. The sedimentation media remained stagnant in the first 90 min. Similar to pH 8 experiments, a single plume formed first that subsequently initiated the dynamic fluid motion. Immediately afterwards, multiple plumes formed and the entire body of sedimentation media started moving across the water tank. Aggregates were slowly growing in size but smaller than those formed at the end of pH 8 experiments. The size of aggregates that can be visually differentiated as they were up to 0.1 cm in diameter. The remaining sedimentation media has a light green color at the end of experiments but appeared to be clouded because there were many small aggregates remained in suspension (Figure 3.7).

The average sedimentation velocity varied drastically from 0.056 (+/-0.008) cm s^{-1} to 0.074 (+/-0.005) cm s^{-1} for the pH 8 experiments. Experiments took up to 120 min for most aggregates to be deposited. During the first 45 min to 1 hour in each experiment, aggregate settling was minimum because it took time for soluble Fe(II) that was introduced into the sedimentation media

to be gradually oxidized by O_2 to form the ferric iron aggregates. The first plume usually appeared after a significant amount of small aggregates formed *in situ*, which was evident from the color transition of the sedimentation media from initially vibrant green to a dark green (Figure 3.6). The initiation of the first plume caused active agitation of previously stagnant sedimentation media. The descending and subsequent ascending fluid motion from the first plume lead to multiple localized density contrast and therefore the formation of multiple plumes. This series of chain-reaction like motions also caused initially fine-grained individual aggregates to slowly bundle up and eventually coalesce to reach particle sizes of 0.1 to 0.3 cm in diameter. Towards the end of each experiment, these large aggregates started to settle individually while more plumes formed and dissipated. Finally, a layer of loosely packed aggregates deposited at the bottom of the water tank. The remaining sedimentation media became semi-transparent and light green with only a few visible and suspended aggregates.

Abiotic control experiments show two effects of *Synechococcus* on the sedimentation velocity. For all three abiotic control experiments at pH 7, the change of total Fe concentration in solution was faster in the abiotic control experiments compared to corresponding sedimentation experiments (Figures 3.8-3.10). Two of four pH 8 experiments, with initial Fe(II) concentration to be 1800 μM and 900 μM, showed the same effect (Figures 3.11-3.12). However, the other two pH 8 abiotic control experiments with Fe(II) concentrations of 1200 μM and 1500 μM showed no effect of *Synechococcus* on sedimentation rate as the change of total Fe concentration in solution over time followed a similar trend as the corresponding sedimentation experiment with *Synechococcus* cultures (Figures 3.13-3.14) .

3.33 Fe:C_{org} ratios of final sediments

The ratios of Fe to organic carbon were calculated from every pH 7 and pH 8 experiment. We did not measure the $Fe:C_{org}$ ratios for pH 6 experiments because the chlorophyll *a* content of *Synechococcus* cells in the final sediments of pH 6 experiments might have deteriorated over the course of week-long experiments and thus could not be used to accurately estimate the cell densities (Table 3). Total Fe content in the final sediment varied from 13478.26 (+/- 1583.88) μM to 21159.42 (+/- 1889.97) μM amongst the 7 sedimentation experiments. The total organic carbon content in the final sediments ranged from 58.86 (+/- 15.54) μM to 259.88 (+/- 3.86) μM. Finally, $Fe:C_{org}$ ratio ranged from 68.27 (+/- 10.65) to 269.32 (+/- 51.44).

3.4 Discussion

3.41 Co-deposition of Synechococcus cells with Fe minerals

As discussed above, work with photoferrotrophs have shown that in the presence of dissolved silica, there is minimal cell-mineral aggregate formation (Schad et al., 2019; Thompson et al., 2019). As a consequence, there should have been very little organic carbon in the primary sediment to BIF if photoferrotrophs were the sole oxidizer of Fe(II). However, in this study, we found compelling evidence of strong encrustation of *Synechococcus* cells with Fe minerals, in the presence of dissolved Si. First, the apparent visual comparison between the beginning of the sedimentation experiment with a vibrant green color of *Synechococcus* cells and the semi-transparent light green color of the final supernatant after each experiment finished is the direct representation of cells co-deposited with ferrihydrite during sedimentation (Figures 3.6-3.7).

Second, the SEM images of the final sediment confirmed that *Synechococcus* cells not only co-deposited with Fe minerals, but some were entrained and protected within the cell-mineral

aggregate structures (Figure 3.16). The implication of shielded organic carbon is that some biomass would have been protected from heterotrophic microorganisms such as methanogens and fermentators, and thus was preserved at a later stage in BIF formation (Konhauser et al., 2005).

Third, the chlorophyll *a* extraction performed in this study further showed that *Synechococcus* cells actively encrusted onto Fe minerals and were subsequently deposited. More importantly, cell density was concentrated during sedimentation process and resulted in an elevated biomass content in the final sediment. Indeed, the elevated biomass that deposited with Fe minerals would have provided a steady source of organic carbons for microorganisms that are capable of DIR and methanogenesis that resided in the subsurface seafloor; and eventually formed the unique mineralogical assemblages that we see in BIF today.

3.42 Fe:C_{org} ratios and excess Fe(III)

The theoretical Fe:C_{org} ratio in BIF was derived from a series of chemical and biological reactions (Equation 1, 2 and 3; Konhauser et al., 2005). Regardless of either cyanobacteria or photoferrotrophs being the major oxidizer of Fe(II), the ratio remains at 4:1. However, in an ocean open to an oxygenated atmosphere, excess oxygen would have been available to react with dissolved Fe(II), thus increasing the Fe:C ratio in excess of 4:1. In terms of Earth's history, this coincides with the Great Oxidation Event that began ca. 2.45 Ga (Konhauser et al., 2011); atmospheric O_2 levels continue to rise until around 2.0 Ga - the Lomagundi event (Mänd et al., 2020), after which they subsequently decline to levels <1% of present atmospheric levels (Planavsky et al., 2014).

In this study, all of the sedimentation experiments were open to atmosphere and thus oxygen was not the limiting factor. With similar initial cell densities ($OD750_{nm}$ ~ 0.15), the result of $Fe:C_{org}$ ratios from pH 7 experiments were between 68.27 (+/- 10.65) and 98.88 (+/- 13.90), 17 to 25 times higher than the theoretical ratio and directly proportional to the initial Fe(II) concentration with a R^2 value to be 0.99. Assuming this correlation holds true through a wide range of Fe(II) concentrations, then the $Fe:C_{org}$ ratio would be from 7.9 with 30 μM of Fe(II) to 31.8 with 500 μM of Fe(II), again higher than the theoretical ratio. The ratio of $Fe:C_{org}$ being greater than 4 implies that there was an excess of Fe(III) in the primary sediments after Fe(III) being re-reduced by DIR. As a result, the remaining Fe(III) was eventually transformed into hematite during later diagenesis and metamorphism and became part of BIF mineral assemblage.

3.43 The effects of Synechococcus on the sedimentation velocity

We conducted abiotic control experiments for every pH 6, 7 and 8 sedimentation experiment to examine the effect of *Synechococcus* cells on sedimentation velocity. Amongst all 9 experiments, 6 (1 at pH 6, 3 at pH 7 and 2 at pH 8) showed that *Synechococcus* had a negative effect on the sedimentation velocity, meaning that *Synechococcus* cells slowed the sedimentation process of the ferrihydrite. The reason is that the encrustation of cells onto Fe minerals, although leading to an increased volume of the aggregates, nonetheless significantly decreased the density of the aggregates. Thus, overall, we observed increased buoyancy of the aggregates that eventually caused slower sedimentation. Two of the 3 remaining experiments showed no effects of *Synechococcus* on the sedimentation (Figure 3.13 and Figure 3.14). This is probably due to coincident early formation of a large aggregate that caused the first plume to start descending

earlier than the rest of the experiment. Once the stagnant sedimentation media was agitated by the first plume, aggregates grew larger and thus deposited faster than usual.

3.44 Sedimentation velocity and BIF formation

The sedimentation velocity of pH 8 experiments ranged from 0.056 (+/-0.005) cm sec^{-1} with 900 μM Fe(II) to 0.074 (+/-0.005) cm sec^{-1} with 1800 μM Fe(II), and positively correlates with initial Fe(II) concentrations (Figure 3.15) This is consistent with the earlier findings of Li et al. (2020) who similarly observed that sedimentation velocity is directly proportional to the initial Fe(II) concentrations at more alkaline pH conditions. However, the pH 7 experiments do not display this trend strongly, implying that either this correlation is only applicable to pH greater than 7, or we have reached the detection limit of this method such that the results from different initial Fe(II) concentrations were close.

Sedimentation velocity of pH 7 experiments clustered around 0.035 cm sec^{-1}, ranging from 0.034 (+/-0.010) cm sec^{-1} to 0.036 (+/- 0.004) cm sec^{-1}. If the pH in the Archean and Proterozoic was around 7, then 0.036 cm sec^{-1} would represent the maximum settling velocity of cell-ferrihydrite aggregates. Recall that the sedimentation velocity in experiments that settled via plume mechanism only accounted for the descending rate of a single plume, which means that only a small fraction of aggregates settled at this velocity, while the remaining aggregates settled at an even slower rate. Assuming that cyanobacteria-ferrihydrite aggregates formed in the first 100 m water column above the photoferrotrophs, and deposited through an average depth of 500 m (Trendall, 2002), the minimum time it would have taken is 16.08 days, more than 7 days longer than what Konhauser et al. (2005) have estimated on photoferrotroph-ferrihydrite aggregates. A

slower sedimentation velocity inherently implies that less cyanobacteria-ferrihydrite aggregates would have been deposited per unit time. The 16.08 days is also longer than the water residence time in many modern coastal settings (Gu et al., 2012; Kenov et al., 2012; Defne and Ganju, 2015), which indicates that a small portion of aggregates formed would have been brought back to deeper ocean. As a result, the Fe(III) minerals in the aggregates would subsequently been recycled and the organic carbon (i.e. the cyanobacteria cells) oxidized.

We also calculated how much unconsolidated aggregates would have been deposited every year. We took the amount of total Fe lost during a unit time from each of the three pH 7 experiments and converted it using the molar mass and density of porous ferrihydrite aggregates (107 g mol^{-1}, Schad et al., 2019; 2.0 g cm^{-3}, Posth et al., 2010). The result ranged from 0.128 mm $year^{-1}$ from 1800 μM Fe(II) experiment to 0.072 mm $year^{-1}$ from 1200 μM Fe(II) experiment. Our results are in agreement with previously estimated BIF sedimentation rate of 0.033mm $year^{-1}$ based on U-Pb ages of zircons from a mudrock formation in the Joffre Member from Brockman iron formation, where it was estimated that a total of 166 m of BIF was deposited between the age of 24596 +/-3Ma to 2454+/-3 Ma, and an unconsolidated sedimentation rate of 0.66 mm $year^{-1}$ using a compaction ratio of 95% (Pickard, 2002; Konhauser et al., 2005).

3.45 Archean and Paleoproterozoic ocean pH

One aspect to our experiments that we never intended to pursue, but fortuitously have data to do so is the pH of the Archean-Paleoproterozoic oceans when BIF were being deposited. To date, paleo-seawater pH is still poorly constrained and of great controversy. A significant early attempt to ascertain Archean pH was Grotzinger and Kasting (1993) who modeled the Precambrian

seawater composition and concluded that the allowable pH of Archean and Paleoproterozoic seawater should have been between 5.7 to 8.1. Since then, more recent studies on this matter used sophisticated elemental cycling models such as carbon cycles (Krissansen-Totton et al., 2018) or some major components of seawater such as Na, K, Mg, Ca, and Fe (Halevy and Bachan, 2017). In the case of the carbon models, Krissansen-Totton et al. (2018) incorporated temperature and pH-dependant seafloor weathering in their models and showed that the Precambrian seawater pH evolved from 6.6 at the Archean-Hadean boundary to 7.0 at the Archean-Proterozoic boundary and eventually to 7.9 at the Proterozoic-Phanerozoic boundary. By contrast, Halevy and Bcahan (2017) used multiple major seawater components in their models to show that seawater pH changed from early Archean value of 6.5 to late Proterozoic value of 7.5 Collectively, the various studies constrain Archean to Paleoproterozoic ocean pH between 5.7-8.1.

We used here a different approach to constrain Archean seawater pH. Li et al. (2020) measured the sedimentation velocity of ferrihydrite in seawater-like conditions at extremely high dissolved Fe(II) concentrations (1800 uM) and demonstrated a positive correlation with seawater pH. Using a similar approach, but over a wider pH and Fe(II) concentration range, we corroborate those earlier findings. For instance, at pH 6 the sedimentation velocity was extremely slow, ranging from 0.000016 to 0.000051 cm sec^{-1}. Assuming aggregates travel through a water column at a steady velocity, the time it would take for Fe aggregates to settle through a 150 m water column to the bottom of a continental shelf would be from 3404 to 10851 days; or from 11347 to 36169 days for a 500 m water column during maximum sea level rise. Importantly, the seawater residence time in modern coastal settings such as Barnegat Bay in New Jersey, Changjiang effluent plume in China, and Mondego Estuary in Portugal ranged from 1 or 2 days to maximum 50 days only under rare circumstances (Gu et al., 2012; Kenov et al., 2012; Defne and Ganju, 2015). It is

generally accepted that Fe(II) in early oceans were sourced from hydrothermal vents and then brought up to continental shelf by upwelling currents (Holland, 1973; Posth et al., 2013). With a minimum sedimentation time of 3404 days from our pH 6 experiments over a wide range of initial Fe(II) concentrations, with or without microorganisms involved, there would not be enough time to deposit the precursor ferrihydrite that initially comprised BIF sediment. Instead, most ferrihydrite would have been brought back to deeper ocean without being oxidized. Furthermore, if we calculate the sedimentation rate as in Konhauser et al. (2005) and Kappler et al. (2005) based on changes in total Fe concentrations in solution over time, the sedimentation rate is 0.000048 mm $year^{-1}$ for 50 μM Fe(II) experiment and 0.0011mm $year^{-1}$ for 1800 μM Fe(II) experiment, both of which are orders of magnitudes slower than previously estimated BIF sedimentation rate of 0.033mm $year^{-1}$ based on U-Pb ages of zircons from a mudrock formation in Brockman iron formation, and an unconsolidated sedimentation rate of 0.66 mm $year^{-1}$ using a compaction ratio of 95% (Pickard, 2002). Thus, with confidence, we propose that it was unlikely BIF were formed in oceans with only pH 6 due to the extremely slow sedimentation velocity, which could have not been sufficient to deposit massive iron formations such as Dales Gorge Group.

3.5 Conclusion

The sedimentation velocity of cell-mineral aggregates is a fundamental parameter to understand the formation of BIF, and local and global scale biogeochemical cycles of essential elements. However, it has never been precisely measured in the past. Here in this work, we present a highly multidisciplinary approach to measure the sedimentation velocity of *Synechococcus*-ferrihydrite aggregates, aiming to examine the formation, sedimentation velocity, and key features of such aggregates that formed *in situ* under a wide range of chemical conditions. Based on extensive

experiments that were conducted, we conclude that: the (1) maximum sedimentation velocity of *Synechococcus*-ferrihydrite aggregates that formed at pH 6 is 0.000024 cm sec^{-1}; and it was unlikely that BIF formed at pH 6 due to the extremely low sedimentation velocity; (2) more reasonable sedimentation velocity was in pH 7 experiments ranging from 0.034 (+/-0.010) cm s^{-1} to 0.036 (+/-0.004) cm s^{-1} and pH 7 was more likely to be the Archean and Paleoproterozoic ocean pH; (3) minimum Fe:C_{org} ratio when there was free oxygen in ancient oceans was close to 8:1, which resulted in an excess of Fe(III) in the primary sediments that was eventually transformed to hematite; and (4) *Synechococcus* cells strongly encrusted on Fe minerals and co-deposited with it, but were likely to be consumed later by microorganisms that were capable of DIR and fermentation.

3.6 References

Batterton, J.C. and Van Baalen, C., 1971. Growth responses of blue-green algae to sodium chloride concentration. Archiv für Mikrobiologie, 76(2), pp.151-165.

Bray, D.F., Bagu, J. and Koegler, P., 1993. Comparison of hexamethyldisilazane (HMDS), Peldri II, and critical-point drying methods for scanning electron microscopy of biological specimens. Microscopy research and technique, 26(6), pp.489-495.

Chan, C.S., Emerson, D. and Luther III, G.W., 2016. The role of microaerophilic Fe-oxidizing micro-organisms in producing banded iron formations. Geobiology, 14(5), pp.509-528.

Craddock, P.R. and Dauphas, N., 2011. Iron and carbon isotope evidence for microbial iron respiration throughout the Archean. Earth and Planetary Science Letters, 303(1-2), pp.121-132.

Croal, L.R., Johnson, C.M., Beard, B.L. and Newman, D.K., 2004. Iron isotope fractionation by Fe (II)-oxidizing photoautotrophic bacteria. Geochimica et cosmochimica acta, 68(6), pp.1227-1242.

Crowe, S.A., Jones, C., Katsev, S., Magen, C., O'Neill, A.H., Sturm, A., Canfield, D.E., Haffner, G.D., Mucci, A., Sundby, B. and Fowle, D.A., 2008. Photoferrotrophs thrive in an Archean Ocean analogue. Proceedings of the National Academy of Sciences, 105(41), pp.15938-15943.

Czaja, A.D., Johnson, C.M., Beard, B.L., Roden, E.E., Li, W. and Moorbath, S., 2013. Biological Fe oxidation controlled deposition of banded iron formation in the ca. 3770 Ma Isua Supracrustal Belt (West Greenland). Earth and Planetary Science Letters, 363, pp.192-203.

Defne, Z. and Ganju, N.K., 2015. Quantifying the residence time and flushing characteristics of a shallow, back-barrier estuary: Application of hydrodynamic and particle tracking models. Estuaries and Coasts, 38(5), pp.1719-1734.

Edmond, J.M., Von Damm, K.L., McDuff, R.E. and Measures, C.I., 1982. Chemistry of hot springs on the East Pacific Rise and their effluent dispersal. Nature, 297(5863), pp.187-191.

Ehrenreich, A. and Widdel, F., 1994. Anaerobic oxidation of ferrous iron by purple bacteria, a new type of phototrophic metabolism. Applied and environmental microbiology, 60(12), pp.4517-4526.

Fralick, P. and Pufahl, P.K., 2006. Iron formation in Neoarchean deltaic successions and the microbially mediated deposition of transgressive systems tracts. Journal of Sedimentary Research, 76(9), pp.1057-1066.

Frost, C.D., von Blanckenburg, F., Schoenberg, R., Frost, B.R. and Swapp, S.M., 2007. Preservation of Fe isotope heterogeneities during diagenesis and metamorphism of banded iron formation. Contributions to Mineralogy and Petrology, 153(2), p.211.

Garrels, R.M., Perry, E.A. and Mackenzie, F.T., 1973. Genesis of Precambrian iron-formations and the development of atmospheric oxygen. Economic Geology, 68(7), pp.1173-1179.

Gauger, T., Byrne, J.M., Konhauser, K.O., Obst, M., Crowe, S. and Kappler, A., 2016. Influence of organics and silica on Fe (II) oxidation rates and cell–mineral aggregate formation by the green-sulfur Fe (II)-oxidizing bacterium *Chlorobium ferrooxidans* KoFox–Implications for Fe (II) oxidation in ancient oceans. Earth and Planetary Science Letters, 443, pp.81-89.

Gole, M.J. and Klein, C., 1981. Banded iron-formations through much of Precambrian time. The Journal of Geology, 89(2), pp.169-183.

Grotzinger, J.P. and Kasting, J.F., 1993. New constraints on Precambrian ocean composition. The Journal of Geology, 101(2), pp.235-243.

Gu, H., Moore, W.S., Zhang, L., Du, J. and Zhang, J., 2012. Using radium isotopes to estimate the residence time and the contribution of submarine groundwater discharge (SGD) in the Changjiang effluent plume, East China Sea. Continental Shelf Research, 35, pp.95-107.

Halama, K.E., Konhauser, K.O., Kappler, A., 2016. Using modern ferruginous habitats to interpret Precambrian banded iron formation deposition. International Journal of Astrobiology, 15 (3), pp. 205-217

Halevy, I. and Bachan, A., 2017. The geologic history of seawater pH. Science, 355(6329), pp.1069-1071.

Hartman H (1984) The evolution of photosynthesis and microbial mats: A speculation on the banded iron formations. In: Cohen Y, Castenholz RW, Halvorson HO (eds) Microbial Mats: Stromatolites . Alan Liss Inc., New York, pp 449–453

Hegler, F., Posth, N.R., Jiang, J. and Kappler, A., 2008. Physiology of phototrophic iron (II)-oxidizing bacteria: implications for modern and ancient environments. FEMS Microbiology Ecology, 66(2), pp.250-260.

Heimann, A., Johnson, C.M., Beard, B.L., Valley, J.W., Roden, E.E., Spicuzza, M.J. and Beukes, N.J., 2010. Fe, C, and O isotope compositions of banded iron formation carbonates demonstrate

a major role for dissimilatory iron reduction in~ 2.5 Ga marine environments. Earth and Planetary Science Letters, 294(1-2), pp.8-18.

Heising, S., Richter, L., Ludwig, W. and Schink, B., 1999. Chlorobium ferrooxidans sp. nov., a phototrophic green sulfur bacterium that oxidizes ferrous iron in coculture with a "Geospirillum" sp. strain. Archives of Microbiology, 172(2), pp.116-124.

Holland, H.D., 1973, The oceans; A possible source of iron in iron-formations: Economic Geology, v.68, p. 1169-1172.

Holm, N.G., 1989. The 13C12C ratios of siderite and organic matter of a modern metalliferous hydrothermal sediment and their implications for banded iron formations. Chemical Geology, 77(1), pp.41-45.

Isley, A.E., 1995. Hydrothermal plumes and the delivery of iron to banded iron formation. The Journal of Geology, 103(2), pp.169-185.

Jiao, N., Yang, Y., Hong, N., Ma, Y., Harada, S., Koshikawa, H. and Watanabe, M., 2005. Dynamics of autotrophic picoplankton and heterotrophic bacteria in the East China Sea. Continental Shelf Research, 25(10), pp.1265-1279.

Johnson, C.M., Roden, E.E., Welch, S.A. and Beard, B.L., 2005. Experimental constraints on Fe isotope fractionation during magnetite and Fe carbonate formation coupled to dissimilatory hydrous ferric oxide reduction. Geochimica et Cosmochimica Acta, 69(4), pp.963-993.

Kappler, A., Pasquero, C., Konhauser, K.O. and Newman, D.K., 2005. Deposition of banded iron formations by anoxygenic phototrophic Fe (II)-oxidizing bacteria. Geology, 33(11), pp.865-868.

Kasting, J.F., Holland, H.D. and Kump, L.R., 1992. Atmospheric evolution: the rise of oxygen. The Proterozoic Biosphere: A Multidisciplinary Study, pp.1185-1188.

Kenov, I.A., Garcia, A.C. and Neves, R., 2012. Residence time of water in the Mondego estuary (Portugal). Estuarine, Coastal and Shelf Science, 106, pp.13-22.

Köhler, I., Konhauser, K.O., Papineau, D., Bekker, A. and Kappler, A., 2013. Biological carbon precursor to diagenetic siderite with spherical structures in iron formations. Nature Communications, 4(1), pp.1-7.

Konhauser, K.O., Hamade, T., Raiswell, R., Morris, R.C., Ferris, F.G., Southam, G. and Canfield, D.E., 2002. Could bacteria have formed the Precambrian banded iron formations?. Geology, 30(12), pp.1079-1082.

Konhauser, K.O., Newman, D.K. and Kappler, A., 2005. The potential significance of microbial Fe (III) reduction during deposition of Precambrian banded iron formations. Geobiology, 3(3), pp.167-177.

Konhauser, K.O., Planavsky, N.J., Hardisty, D.S., Robbins, L.J., Warchola, T.J., Haugaard, R., Lalonde, S.V., Partin, C.A., Oonk, P.B.H., Tsikos, H. and Lyons, T.W., 2017. Iron formations: A global record of Neoarchaean to Palaeoproterozoic environmental history. Earth-Science Reviews, 172, pp.140-177.

Krissansen-Totton, J., Arney, G.N. and Catling, D.C., 2018. Constraining the climate and ocean pH of the early Earth with a geological carbon cycle model. Proceedings of the National Academy of Sciences, 115(16), pp.4105-4110.

Laufer, K., Niemeyer, A., Nikeleit, V., Halama, M., Byrne, J.M. and Kappler, A., 2017. Physiological characterization of a halotolerant anoxygenic phototrophic Fe (II)-oxidizing green-sulfur bacterium isolated from a marine sediment. FEMS Microbiology Ecology, 93(5).

Li, W., Czaja, A.D., Van Kranendonk, M.J., Beard, B.L., Roden, E.E. and Johnson, C.M., 2013. An anoxic, Fe (II)-rich, U-poor ocean 3.46 billion years ago. Geochimica et Cosmochimica Acta, 120, pp.65-79.

Li, Y., Sutherland, B.R., Gingras, M.K., Owttrim, G.W., Konhauser K.O., 2020. A novel approach to investigate the deposition of (bio)chemical sediments: The sedimentation velocity of cyanobacteria-ferrihydrite aggregates. Journal of Sedimentary Research, In review.

Maliva, R.G., Knoll, A.H. and Siever, R., 1989. Secular change in chert distribution; a reflection of evolving biological participation in the silica cycle. Palaios, 4(6), pp.519-532.

Mänd, K., Lalonde, S.V., Robbins, L.J., Thoby, M., Paiste, K., Kreitsmann, T., Paiste, P., Reinhard, C.T., Romashkin, A.E., Planavsky, N.J. and Kirsimäe, K., 2020. Palaeoproterozoic oxygenated oceans following the Lomagundi–Jatuli Event. Nature Geoscience, 13(4), pp.302-306.

Mloszewska, A.M., Cole, D.B., Planavsky, N.J., Kappler, A., Whitford, D.S., Owttrim, G.W., Konhauser, K.O., 2018, UV radiation limited the expansion of cyanobacteria in early marine photic environments: Nature Communication, 9, article number 3088

Morris, R.C., 1993, Genetic modelling for banded iron-formation of the hamersley group, pilbara craton, western Australia: Precambrian Research, v. 60, p. 243-286.

Nealson, K.H. and Myers, C.R., 1990. Iron reduction by bacteria: a potential role in the genesis of banded iron formations. American Journal of Science, 290, pp.35-45.

Olson, S.L., Reinhard, C.T. and Lyons, T.W., 2016. Cyanobacterial diazotrophy and Earth's delayed oxygenation. Frontiers in microbiology, 7, p.1526.

Pecoits, E., Smith, M.L., Catling, D.C., Philippot, P., Kappler, A., and Konhauser, K.O., 2015, Atmospheric hydrogen peroxide and Eoarchean iron formations: Geobiology, v. 13, p. 1–14, https://doi.org/10.1111/ gbi.12116.

Perry, E.C., Tan, F.C. and Morey, G.B., 1973. Geology and stable isotope geochemistry of the Biwabik Iron Formation, northern Minnesota. Economic Geology, 68(7), pp.1110-1125.

Pickard, A.L., Barley, M.E. and Krapež, B., 2004. Deep-marine depositional setting of banded iron formation: sedimentological evidence from interbedded clastic sedimentary rocks in the early Palaeoproterozoic Dales Gorge Member of Western Australia. Sedimentary Geology, 170(1-2), pp.37-62.

Porsch, K. and Kappler, A., 2011. FeII oxidation by molecular O2 during HCl extraction. *Environmental Chemistry*, *8*(2), pp.190-197.

Posth, N.R., Huelin, S., Konhauser, K.O. and Kappler, A., 2010. Size, density and composition of cell–mineral aggregates formed during anoxygenic phototrophic Fe (II) oxidation: impact on modern and ancient environments. Geochimica et Cosmochimica Acta, 74(12), pp.3476-3493.

Posth, N.R., Konhauser, K.O. and Kappler, A., 2013. Microbiological processes in banded iron formation deposition. Sedimentology, 60(7), pp.1733-1754.

Posth, N.R., Canfield, D.E. and Kappler, A., 2014. Biogenic Fe (III) minerals: from formation to diagenesis and preservation in the rock record. Earth-Science Reviews, 135, pp.103-121.

Poulain, A.J. and Newman, D.K., 2009. Rhodobacter capsulatus catalyzes light-dependent Fe (II) oxidation under anaerobic conditions as a potential detoxification mechanism. Applied and environmental microbiology, 75(21), pp.6639-6646.

Planavsky, N., Rouxel, O.J., Bekker, A., Hofmann, A., Little, C.T. and Lyons, T.W., 2012. Iron isotope composition of some Archean and Proterozoic iron formations. Geochimica et Cosmochimica Acta, 80, pp.158-169.

Planavsky, N.J., Reinhard, C.T., Wang, X., Thomson, D., McGoldrick, P., Rainbird, R.H., Johnson, T., Fischer, W.W. and Lyons, T.W., 2014. Low Mid-Proterozoic atmospheric oxygen levels and the delayed rise of animals. science, 346(6209), pp.635-638.

Schädler, S., Burkhardt, C., Hegler, F., Straub, K.L., Miot, J., Benzerara, K. and Kappler, A., 2009. Formation of cell-iron-mineral aggregates by phototrophic and nitrate-reducing anaerobic Fe (II)-oxidizing bacteria. Geomicrobiology Journal, 26(2), pp.93-103.

Siever, R., 1992. The silica cycle in the Precambrian. Geochimica et Cosmochimica Acta, 56(8), pp.3265-3272.

Steinhoefel, G., von Blanckenburg, F., Horn, I., Konhauser, K.O., Beukes, N.J. and Gutzmer, J., 2010. Deciphering formation processes of banded iron formations from the Transvaal and the Hamersley successions by combined Si and Fe isotope analysis using UV femtosecond laser ablation. Geochimica et Cosmochimica Acta, 74(9), pp.2677-2696.

Stevens, S.E. and Van Baalen, C., 1973. Characteristics of nitrate reduction in a mutant of the blue-green alga Agmenellum quadruplicatum. Plant physiology, 51(2), pp.350-356.

Stevens, S.E. and Porter, R.D., 1980. Transformation in Agmenellum quadruplicatum. Proceedings of the National Academy of Sciences, 77(10), pp.6052-6056.

Stolper, D.A., Revsbech, N.P. and Canfield, D.E., 2010. Aerobic growth at nanomolar oxygen concentrations. Proceedings of the National Academy of Sciences, 107(44), pp.18755-18760.

Stookey, L.L., 1970. Ferrozine---a new spectrophotometric reagent for iron. Analytical chemistry, 42(7), pp.779-781.

Sutherland, B.R., Barrett, K.J. and Gingras, M.K., 2015. Clay settling in fresh and salt water. Environmental Fluid Mechanics, 15(1), pp.147-160.

Trendall, A.F., 2002. The significance of iron-formation in the Precambrian stratigraphic record. Precambrian sedimentary environments: A modern approach to ancient depositional systems, pp.33-66.

Troussellier, M., Bouvy, M., Courties, C. and Dupuy, C., 1997. Variation of carbon content among bacterial species under starvation condition. Aquatic Microbial Ecology, 13(1), pp.113-119.

Tyson, R.V. and Pearson, T.H., 1991. Modern and ancient continental shelf anoxia: an overview. Geological Society, London, Special Publications, 58(1), pp.1-24.

Van Baalen, C.H.A.S.E., 1962. Studies on marine blue-green algae. Botanica Marina, 4(1-2), pp.129-139.

Walker, J.C., 1984. Suboxic diagenesis in banded iron formations. Nature, 309(5966), pp.340-342.

Widdel, F., Schnell, S., Heising, S., Ehrenreich, A., Assmus, B. and Schink, B., 1993. Ferrous iron oxidation by anoxygenic phototrophic bacteria. Nature, 362(6423), pp.834-836.

Wu, W., Swanner, E.D., Hao, L., Zeitvogel, F., Obst, M., Pan, Y. and Kappler, A., 2014. Characterization of the physiology and cell–mineral interactions of the marine anoxygenic phototrophic Fe (II) oxidizer Rhodovulum iodosum–implications for Precambrian Fe (II) oxidation. FEMS Microbiology Ecology, 88(3), pp.503-515.

Yamaguchi, K.E., Johnson, C.M., Beard, B.L. and Ohmoto, H., 2005. Biogeochemical cycling of iron in the Archean–Paleoproterozoic Earth: constraints from iron isotope variations in sedimentary rocks from the Kaapvaal and Pilbara Cratons. Chemical Geology, 218(1-2), pp.135-169.

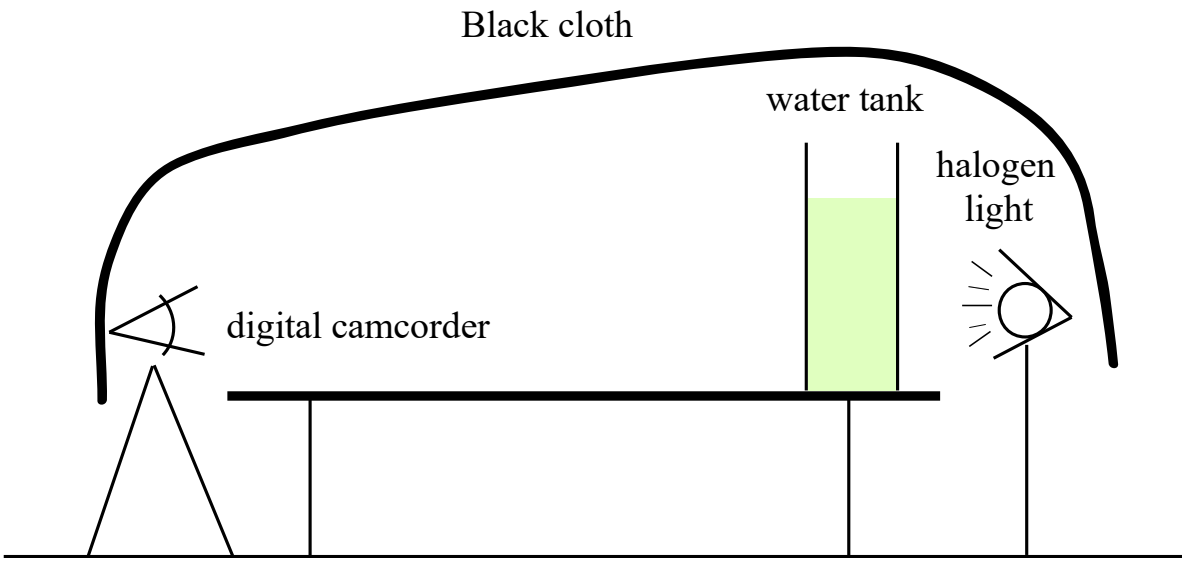

Figure 3.1. Sedimentation experiment setup.

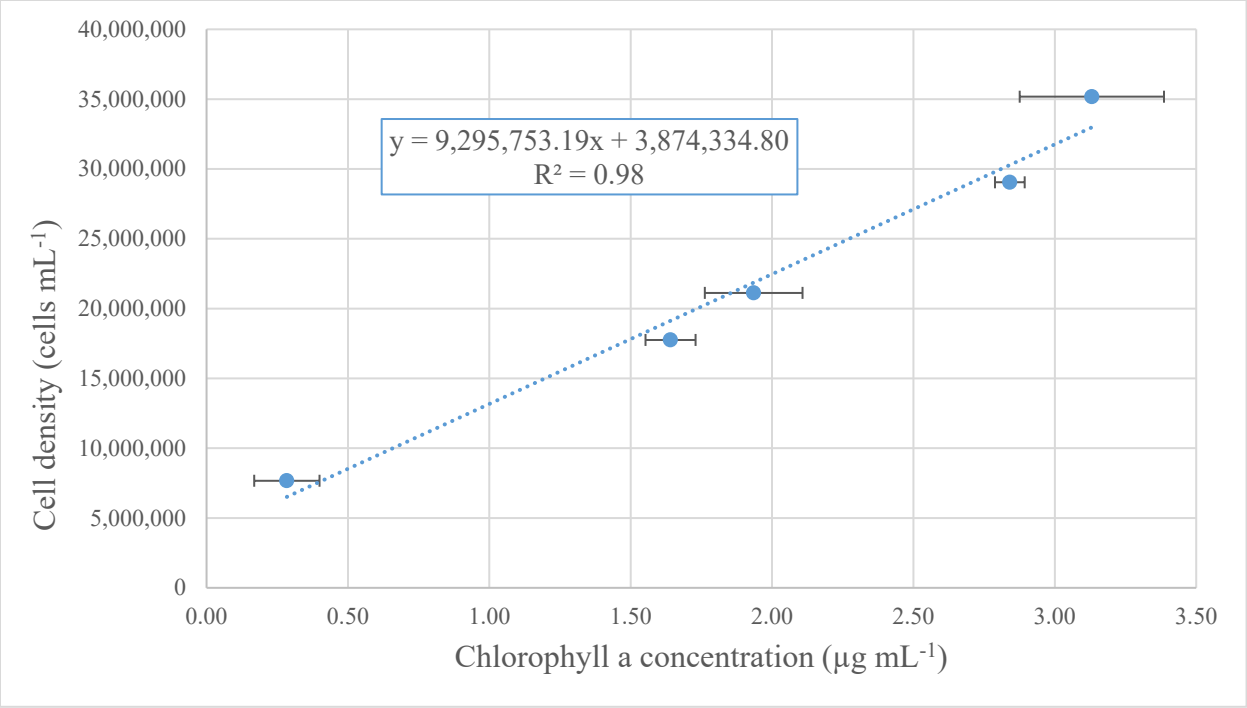

Figure 3.2. The correlation between cell density and chlorophyll a concentration for cyanobacterium *Synechococcus* sp. PCC 7002.

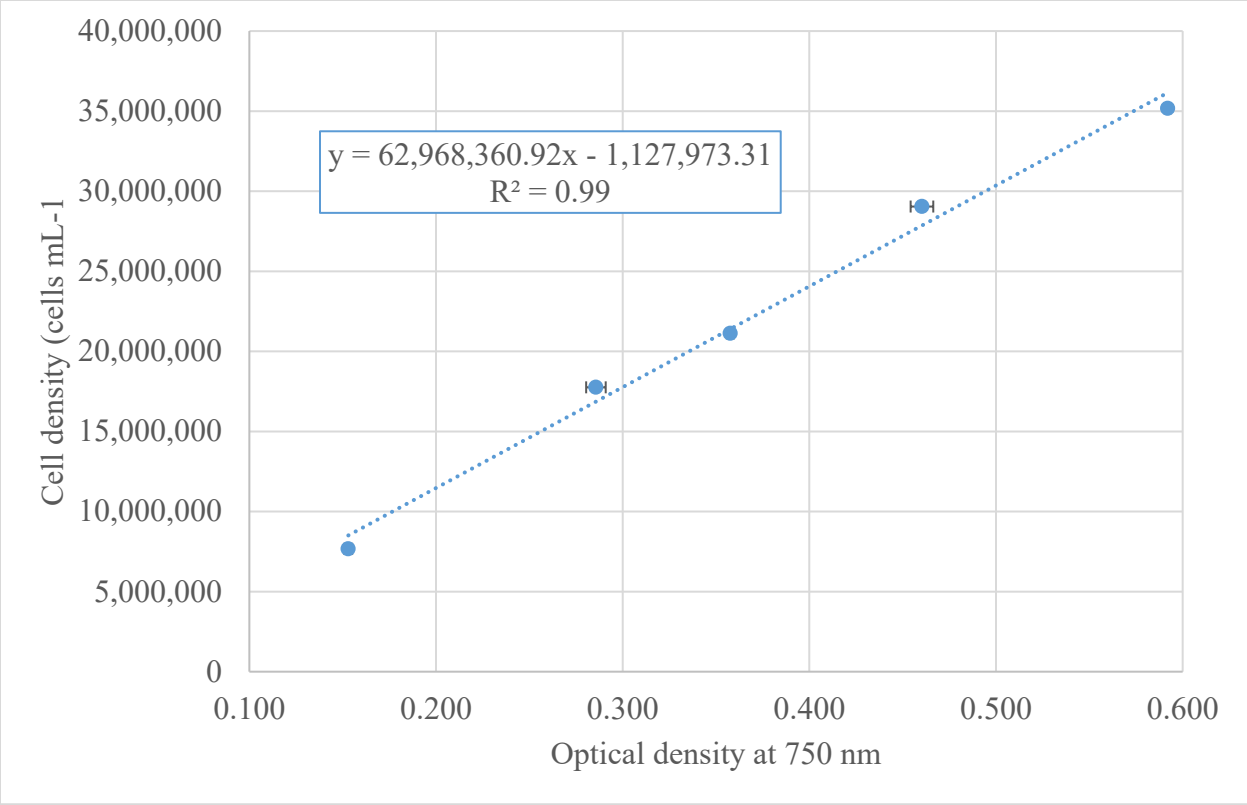

Figure 3.3. The correlation between cell density and optical density at 7500 nm for cyanobacterium *Synechococcus* sp. PCC 7002.

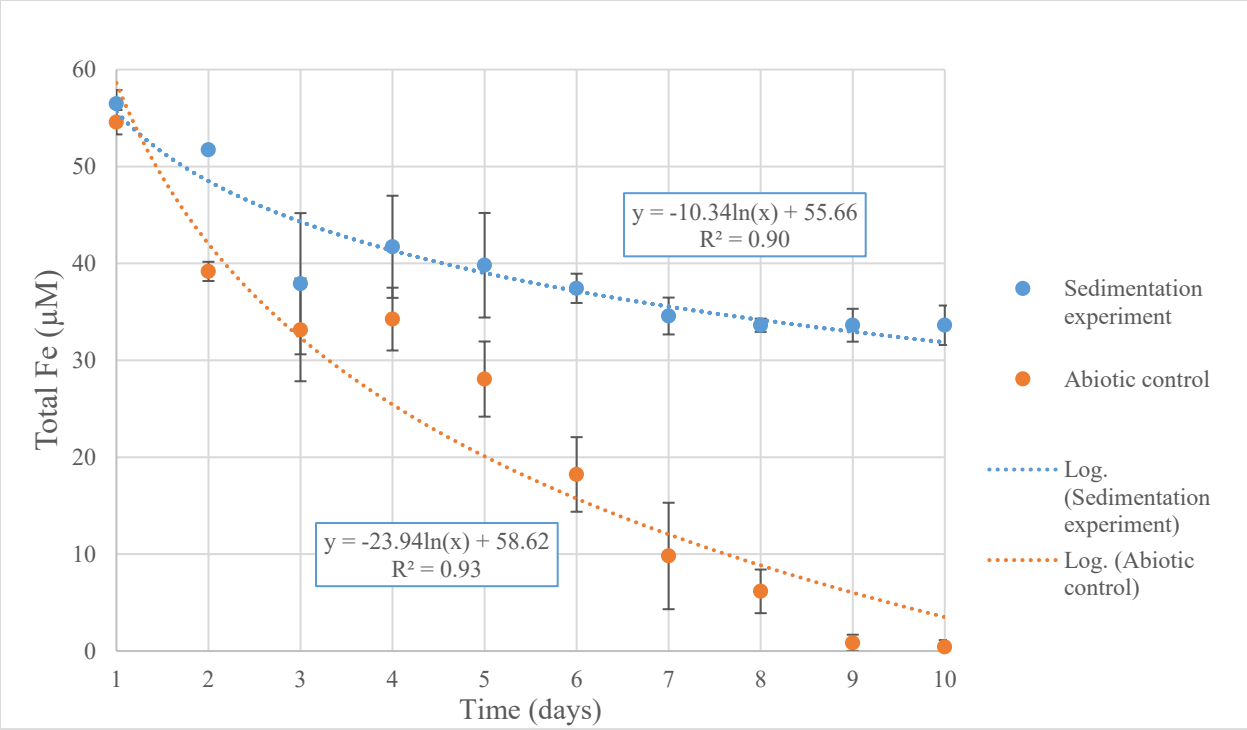

Figure 3.4. Change of total Fe concentration in solution over time in pH 6 sedimentation experiment with 50 µM initial Fe(II) concentration.

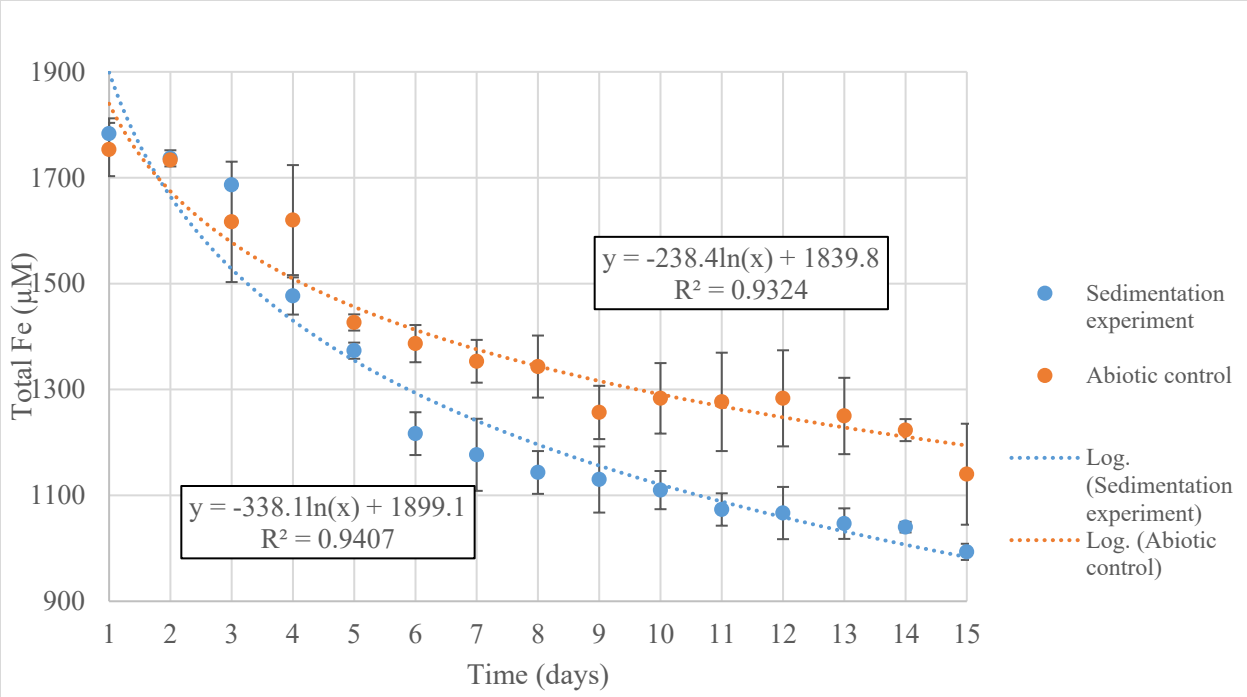

Figure 3.5. Change of total Fe concentration in solution over time in pH 6 sedimentation experiment with 1800 µM initial Fe(II) concentration.

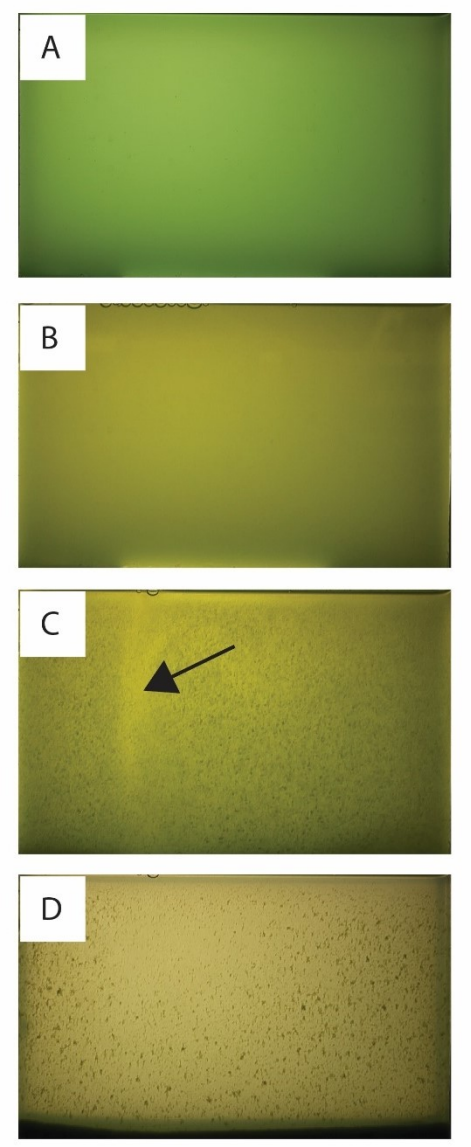

Figure 3.6. Snapshots of the sedimentation process of a pH 8 experiment with 1500 μM Fe(II) concentration. A) the start of experiment before the addition of Fe(II), the vibrant green color from cyanobacteria cells; B) immediately after the addition of Fe(II) solution and stirred to homogenous; C) The first plume formed during sedimentation process; D) The end of experiment. The height of each shot is 10 cm.

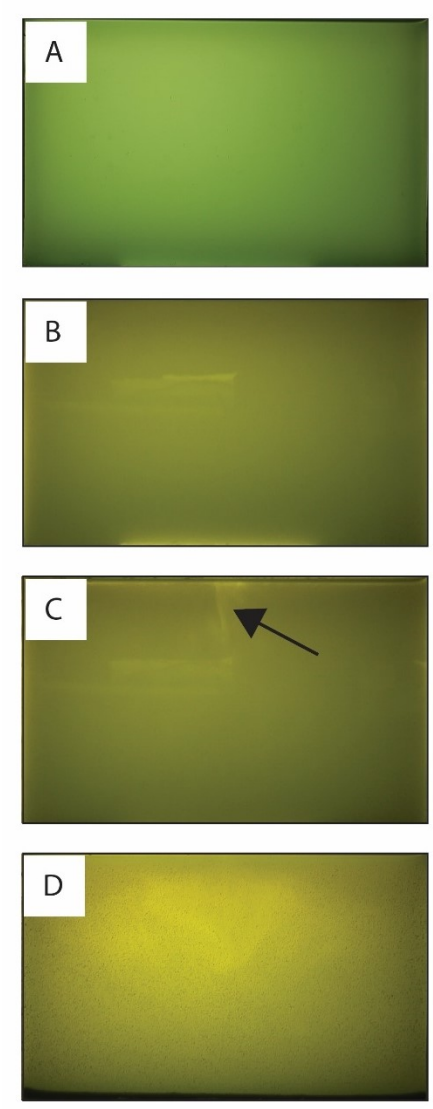

Figure 3.7. Snapshots of the sedimentation process of a pH 7 experiment with 1500 μM Fe(II) concentration. A) the start of experiment before the addition of Fe(II), the vibrant green color from cyanobacteria cells; B) immediately after the addition of Fe(II) solution and stirred to homogenous; C) The first plume formed during sedimentation process; D) The end of experiment. The height of each shot is 10 cm.

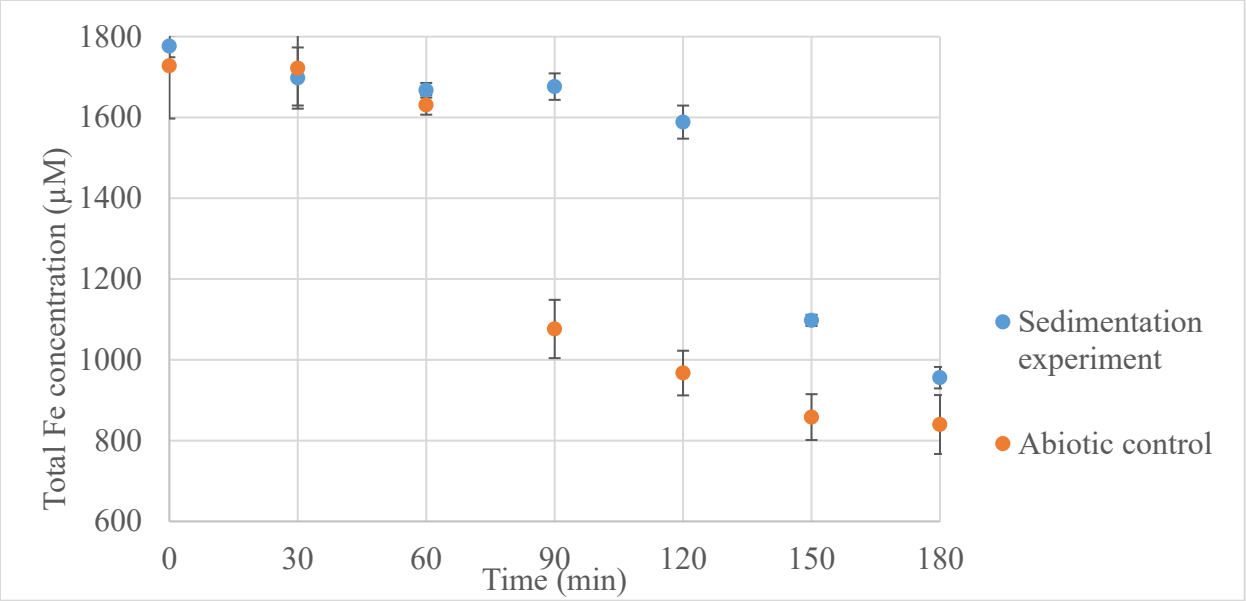

Figure 3.8. Change of total Fe concentration in solution over time from pH 7 experiment with 1800 µM Fe(II)

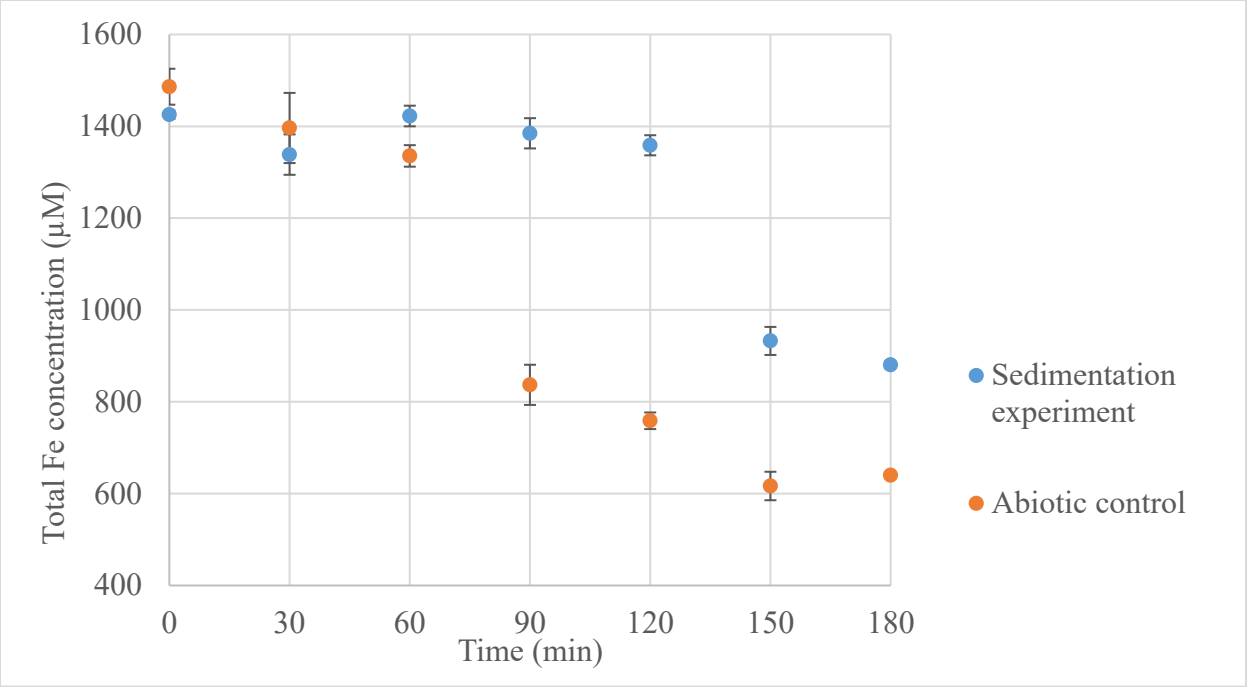

Figure 3.9. Change of total Fe concentration in solution over time from pH 7 experiment with 1500 µM Fe(II)

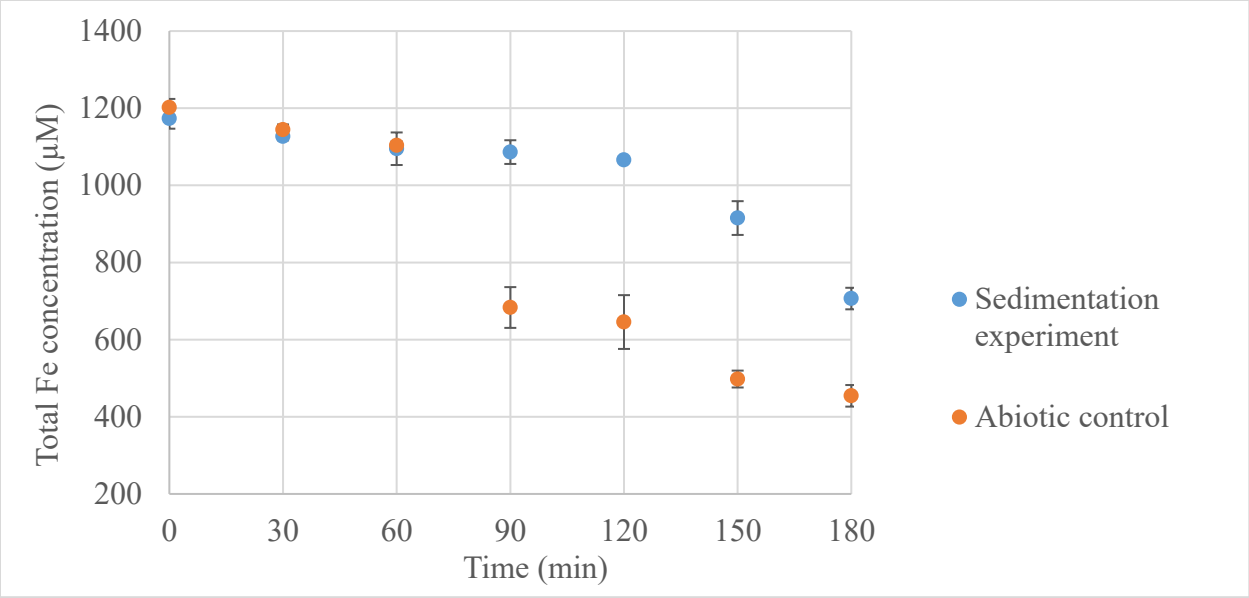

Figure 3.10. Change of total Fe concentration in solution over time from pH 7 experiment with 1200 µM Fe(II)

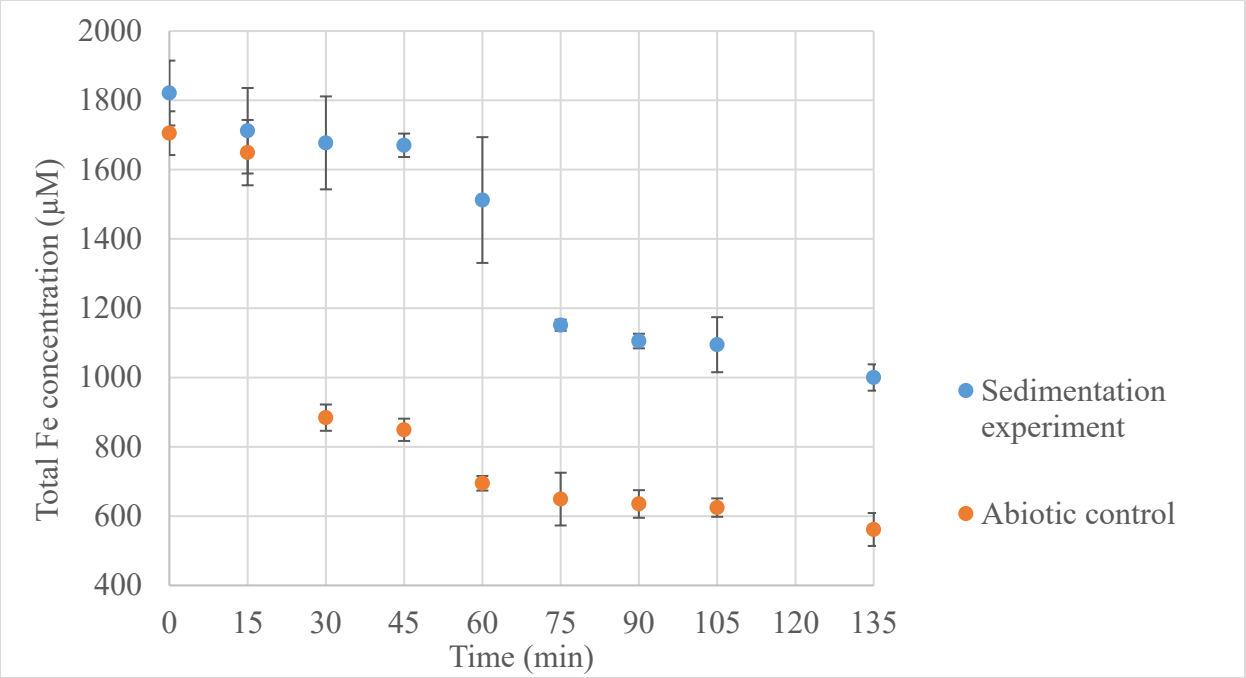

Figure 3.11. Change of total Fe concentration in solution over time from pH 8 experiment with 1800 µM Fe(II)

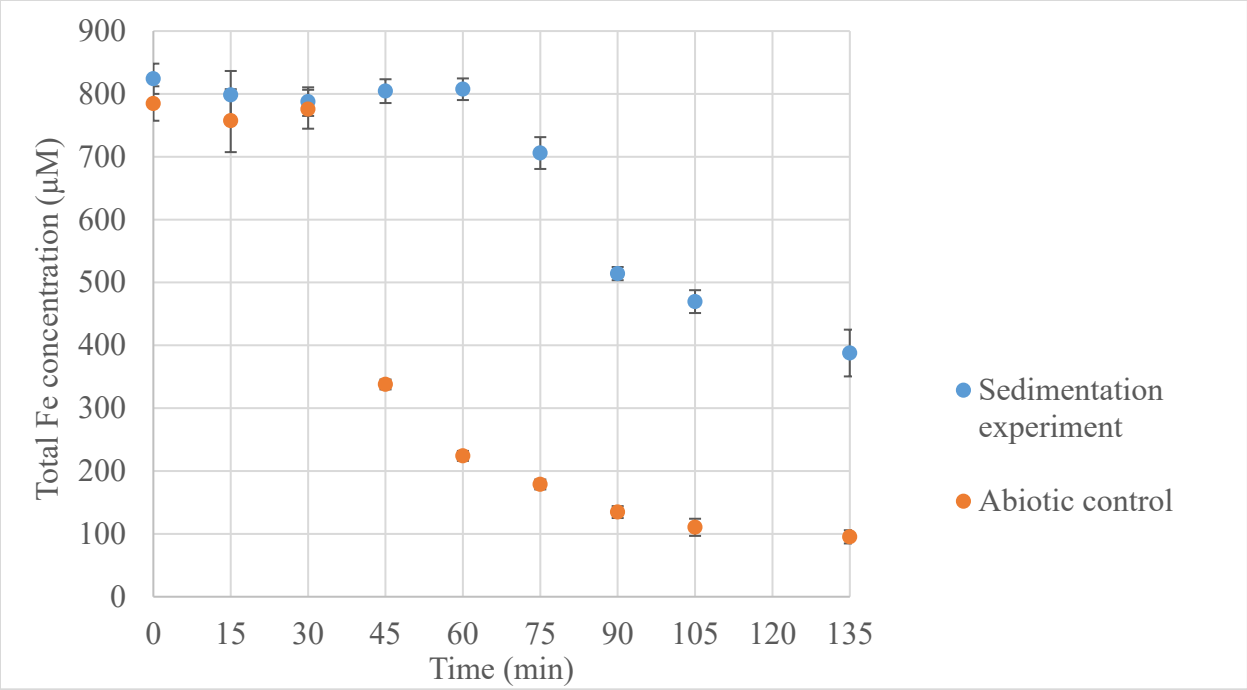

Figure 3.12. Change of total Fe concentration in solution over time from pH 8 experiment with 900 µM Fe(II)

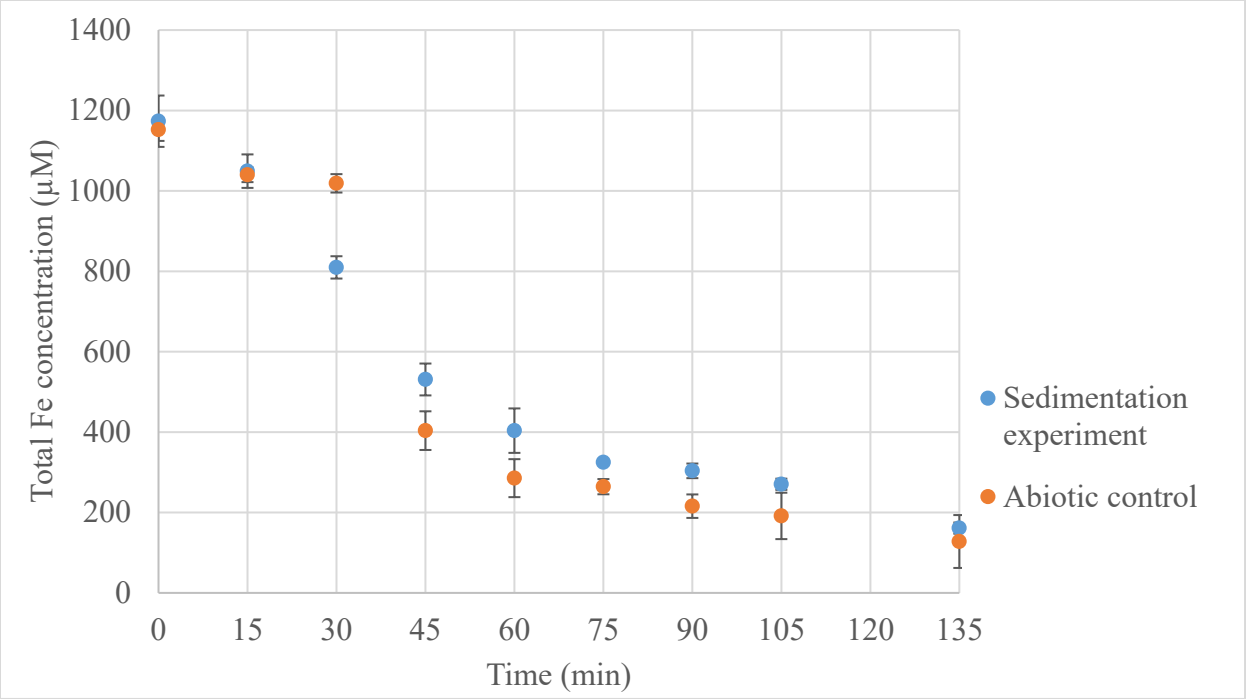

Figure 3.13. Change of total Fe concentration in solution over time from pH 8 experiment with 1200 µM Fe(II)

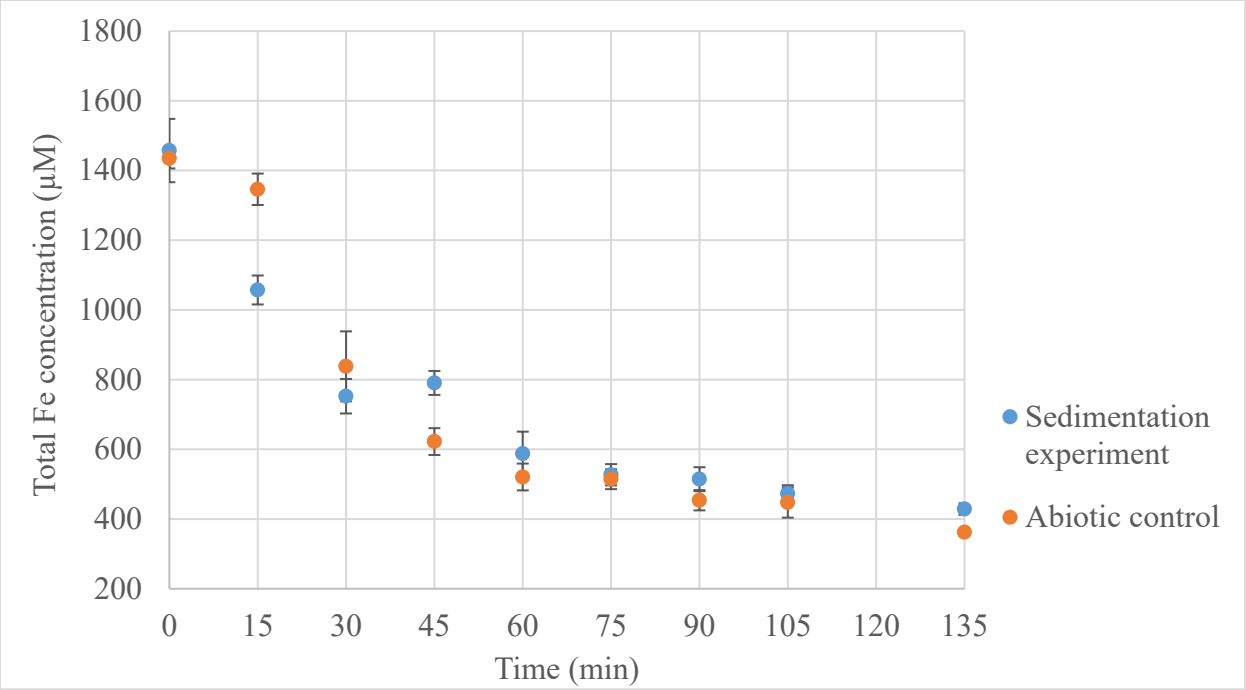

Figure 3.14. Change of total Fe concentration in solution over time from pH 8 experiment with 1500 µM Fe(II)

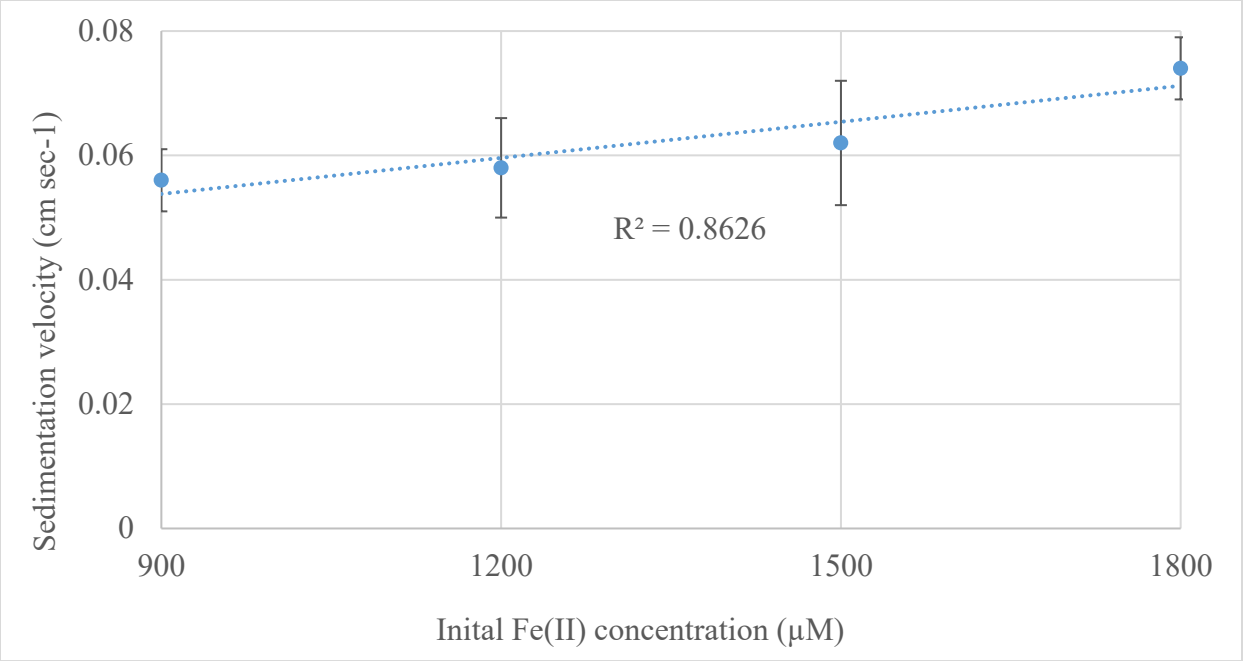

Figure 3.15. The correlation between sedimentation velocity and initial Fe(II) concentrations at pH 8.

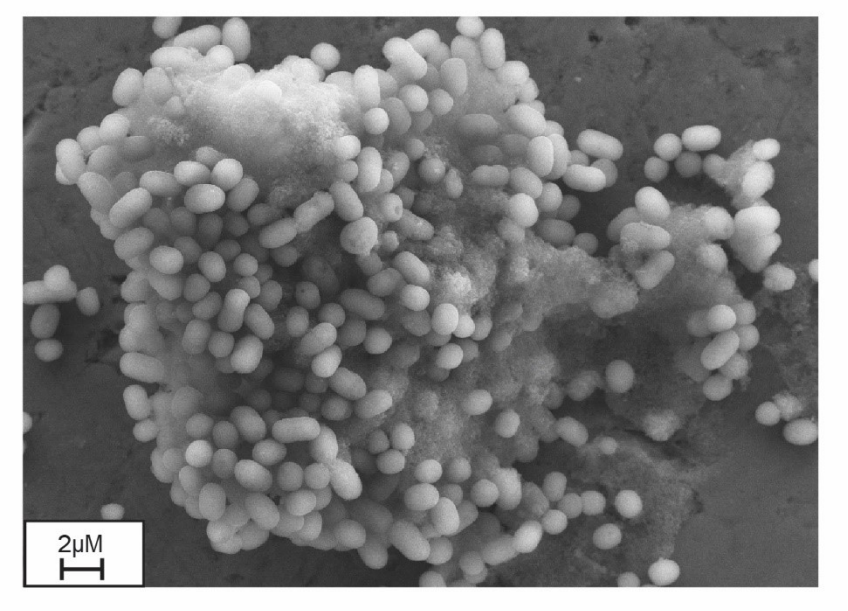

Figure 3.16. A SEM micrograph of the *Synechococcus*-ferrihydrite aggregates, displaying strong encrustation of cells onto Fe minerals.

Table 3.1. Sedimentation velocity of pH 6 experiments.

Experiment	Initial pH	Fe(II) concentration (μM)	Maximum sedimentation rate through a 10 cm water column (μM/day)	Average Sedimentation Velocity (cm sec^{-1})
1	6	58	12.02	0.000024
2	6	53 (abiotic control)	23.94	0.000051
3	6	1783	338.1	0.000021
4	6	1753 (abiotic control)	238.4	0.000016

Table 3.2. Sedimentation velocity of pH 7 and pH 8 experiments.

Experiment	Initial pH	Fe(II) concentration (μM)	Average Sedimentation Velocity (cm sec^{-1})
1	7	1200	0.035 (+/- 0.003)
2	7	1500	0.034 (+/-0.010)
3	7	1800	0.036 (+/- 0.004)
4	8	900	0.056 (+/-0.005)
5	8	1200	0.058 (+/-0.008)
6	8	1500	0.062 (+/-0.010)
7	8	1800	0.074 (+/-0.005)

Table 3.3 The Fe:C_{org} ratios from pH 7 and pH 8 experiments.

Experiment (pH; Initial Fe(II))	Total Fe in final sediment	Totol organic Carbon in final sediments	Fe:C_{org} ratio
pH7; 1200 µM	13478.26 (+/- 1583.88) µM	200.61 (+/- 30.65) µM	68.27 (+/- 10.65)
pH 7; 1500 µM	21159.42 (+/- 1889.97) µM	259.88 (+/- 3.86) µM	81.43 (+/- 1.20)
pH 7; 1800 µM	19122.73 (+/- 2114.00) µM	196.21 (+/- 29.92) µM	98.88 (+/- 13.90)
pH 8; 900 µM	15421.21 (+/- 1469.62) µM	58.86 (+/- 15.54) µM	269.32 (+/- 51.44)
pH 8; 1200 µM	15612.12 (+/- 1110.93) µM	150.96 (+/- 17.71) µM	104.44 (+/- 13.00)
pH 8; 1500 µM	15714.29 (+/- 1081.70) µM	160.57 (+/- 3.47) µM	97.90 (+/- 2.09)
pH 8; 1800 µM	20429.82 (+/- 770.98) µM	219.03 (+/- 19.46) µM	93.71 (+/- 7.93)

Chapter 4. Conclusions and Future work

4.1 Sedimentation velocity of *Synechococcus*-ferrihydrite aggregates and the formation of BIF

The sedimentation velocity of cell-mineral aggregates is a fundamental parameter to understand the formation of BIF, and local and global scale biogeochemical cycles of essential elements. However, it has never been precisely measured in the past. Here, I present a highly multidisciplinary approach to measure the sedimentation velocity of *Synechococcus*-ferrihydrite aggregates, aiming to examine the formation, sedimentation velocity, and key features of such aggregates that formed *in situ* under a wide range of chemical conditions. Based on the extensive experiments conducted, I conclude that: (1) The maximum sedimentation velocity of *Synechococcus*-ferrihydrite aggregates that formed at pH 6 is 0.000024 cm sec^{-1}; and it was unlikely that BIF formed at pH 6 due to the extremely low sedimentation velocity that cannot fulfil to form BIF on a massive scale; (2) The more reasonable sedimentation velocity was in pH 7 experiments ranging from 0.034 (+/-0.010) cm s^{-1} to 0.036 (+/-0.004) cm s^{-1} and pH 7 was more likely to be the Archean and Paleoproterozoic ocean pH; (3) the minimum Fe:C_{org} ratio was when there was free oxygen in ancient oceans was close to 8:1, which resulted in an excess of Fe(III) in the primary sediments that was eventually transformed to hematite; and (4) *Synechococcus* cells strongly encrusted on Fe minerals and co-deposited with it, but were likely to be consumed later by microorganisms that were capable of DIR and fermentation.

4.2 Future work

1) During sedimentation experiments that were conducted in chapter 2 and chapter 3, we found that the sedimentation velocity is also related to the configuration of the vessel, which indicates that in real life, the sedimentation velocity of chemical sediments is also affected by the shape and size of the sedimentary basin, even with the same pH and initial Fe(II) concentrations. The deep-and-narrow type of sedimentary basins intuitively have smaller cross-sectional area than those that are wide and shallow. Therefore, horizontally, the aggregate density is higher in basins that are narrower and deeper. Moreover, the greater the height of the basin, aggregates travel for longer distance and thus gradually become bigger and heavier than those that travel for shorter distance. As a result, we hypothesize that with the same initial Fe(II) concentration and pH, the sedimentation velocity of chemical sediments such as cell-mineral aggregates settle faster in deep and narrow basins such as modern black sea than in those that are wider and shallower. This hypothesis can be tested through similar sedimentation experiments that were conducted in this study. Instead of using water tanks of identical dimensions, different waters tanks with different width: height ratios should be used to represent different modern sedimentary basin dimensions.

2) In chapter 3, we used 95% as the sediment compaction ratio from Pickard (2002) and Konhauser et al. (2005). However, different sediments should have different compaction ratios. Indeed, the porous nature of ferric hydroxide-*Synechococcus* aggregates suggests that ferric hydroxide-*Synechococcus* aggregates should have a different compaction ratio than clastic sediments such as clays. The compaction ratio of cell-mineral aggregates plays an important role when calculating the sediment accumulation rate of Fe. Thus, it is of necessity to precisely measure the sediment compaction ratio of ferric hydroxide-*Synechococcus* aggregates to better constrain the sediment accumulation rate and eventually Fe budgets and cycling in ancient oceans.

3) The oxidation rate of Fe (II) by photoferrotrophs has been well studied (Kappler et al., 2005). Kappler et al. (2005) concluded that anoxygenic photoferrotrophic bacteria have the capability of oxidizing all Fe(II) in Archean oceans even with the presence of cyanobacteria. Yet, there is no studies to our knowledge that address the specific oxidation rate of Fe(II) by abundant cyanobacteria species such as *Synechococcus* species and *Prochlorococcus* species in the context of Archean seawater chemistry. Although the timing of Cyanobacteria emergence on Earth is controversial and varies drastically from different studies (refs), most agreed that by 2.45 Ga the time of the Great Oxidation Event - that cyanobacteria flourished in the surface waters of ancient oceans (Bekker et al., 2010; Konhauser et al., 2017). Thus, the role that cyanobacteria played in the formation of BIF should not be neglected or excluded. To further our understanding of what roles cyanobacteria played in the formation of BIF and to what extend, more fundamental studies should be conducted in the future, including the oxidation rate of Fe(II) by major cyanobacteria species.

4.3 References

Blank, C.E., 2004. Evolutionary timing of the origins of mesophilic sulphate reduction and oxygenic photosynthesis: a phylogenomic dating approach. Geobiology, 2(1), pp.1-20.

Kappler, A., Pasquero, C., Konhauser, K.O. and Newman, D.K., 2005. Deposition of banded iron formations by anoxygenic phototrophic Fe (II)-oxidizing bacteria. Geology, 33(11), pp.865-868.

Konhauser, K.O., Newman, D.K. and Kappler, A., 2005. The potential significance of microbial Fe (III) reduction during deposition of Precambrian banded iron formations. Geobiology, 3(3), pp.167-177.

Pickard, A.L., Barley, M.E. and Krapež, B., 2004. Deep-marine depositional setting of banded iron formation: sedimentological evidence from interbedded clastic sedimentary rocks in the early Palaeoproterozoic Dales Gorge Member of Western Australia. Sedimentary Geology, 170(1-2), pp.37-62.

Rasmussen, B., Fletcher, I.R., Brocks, J.J. and Kilburn, M.R., 2008. Reassessing the first appearance of eukaryotes and cyanobacteria. Nature, 455(7216), pp.1101-1104.

References

Arnold, H.D., 1911, LXXIV. Limitations imposed by slip and inertia terms upon Stokes' law for the motion of spheres through liquids, The London, Edinburgh, and Dublin Philosophical Magazine and Journal of Science, v. 22, p. 755-775.

Batterton, J.C. and Van Baalen, C., 1971. Growth responses of blue-green algae to sodium chloride concentration. Archiv für Mikrobiologie, 76(2), pp.151-165.

Bekker, A., Slack, J.F., Planavsky, N., Krapez, B., Hofmann, A., Konhauser, K.O. and Rouxel, O.J., 2010. Iron formation: the sedimentary product of a complex interplay among mantle, tectonic, oceanic, and biospheric processes. Economic Geology, 105(3), pp.467-508.

Blank, C.E., 2004. Evolutionary timing of the origins of mesophilic sulphate reduction and oxygenic photosynthesis: a phylogenomic dating approach. Geobiology, 2(1), pp.1-20.

Bolhar, R., Kamber, B.S., Moorbath, S., Fedo, C.M. and Whitehouse, M.J., 2004. Characterisation of early Archaean chemical sediments by trace element signatures. Earth and Planetary Science Letters, 222(1), pp.43-60.James, H.L., 1954. Sedimentary facies of iron-formation. Economic Geology, 49(3), pp.235-293.

Bray, D.F., Bagu, J. and Koegler, P., 1993. Comparison of hexamethyldisilazane (HMDS), Peldri II, and critical-point drying methods for scanning electron microscopy of biological specimens. Microscopy research and technique, 26(6), pp.489-495.

Bruland, K.W. and Lohan, M.C., 2004. Em Treatise on Geochemistry–The Oceans and Marine Geochemistry v. 6.

Canfield, D.E. and Kappler, A., 2014. Biogenic Fe (III) minerals: from formation to diagenesis and preservation in the rock record. Earth-Science Reviews, 135, pp.103-121.

Chan, C.S., Emerson, D. and Luther III, G.W., 2016. The role of microaerophilic Fe-oxidizing micro-organisms in producing banded iron formations. Geobiology, 14(5), pp.509-528.

Cloud, P., 1973. Paleoecological significance of the banded iron-formation. Economic Geology, 68(7), pp.1135-1143.

Craddock, P.R. and Dauphas, N., 2011. Iron and carbon isotope evidence for microbial iron respiration throughout the Archean. Earth and Planetary Science Letters, 303(1-2), pp.121-132.

Croal, L.R., Johnson, C.M., Beard, B.L. and Newman, D.K., 2004. Iron isotope fractionation by Fe (II)-oxidizing photoautotrophic bacteria. Geochimica et cosmochimica acta, 68(6), pp.1227-1242.

Crowe, S.A., Jones, C., Katsev, S., Magen, C., O'Neill, A.H., Sturm, A., Canfield, D.E., Haffner, G.D., Mucci, A., Sundby, B. and Fowle, D.A., 2008. Photoferrotrophs thrive in an Archean Ocean analogue. Proceedings of the National Academy of Sciences, 105(41), pp.15938-15943.

Czaja, A.D., Johnson, C.M., Beard, B.L., Roden, E.E., Li, W. and Moorbath, S., 2013. Biological Fe oxidation controlled deposition of banded iron formation in the ca. 3770 Ma Isua Supracrustal Belt (West Greenland). Earth and Planetary Science Letters, 363, pp.192-203.

Defne, Z. and Ganju, N.K., 2015. Quantifying the residence time and flushing characteristics of a shallow, back-barrier estuary: Application of hydrodynamic and particle tracking models. Estuaries and Coasts, 38(5), pp.1719-1734.

Dzombak, D.A., Morel, F.M.M., 1990, Surface Complexation Modeling: Hydrous Ferric Oxide: John Wiley & Sons.

Edmond, J.M., Von Damm, K.L., McDuff, R.E., Measures, C. I., 1982, Chemistry of hot springs on the east pacific rise and their effluent dispersal: Nature, v. 297, p. 187-191.

Ehrenreich, A. and Widdel, F., 1994. Anaerobic oxidation of ferrous iron by purple bacteria, a new type of phototrophic metabolism. Applied and environmental microbiology, 60(12), pp.4517-4526.

Fralick, P. and Pufahl, P.K., 2006. Iron formation in Neoarchean deltaic successions and the microbially mediated deposition of transgressive systems tracts. Journal of Sedimentary Research, 76(9), pp.1057-1066.

Froelich, P.N., Blanc, V., Mortlock, R.A., Chillrud, S.N., Dunstan, W., Udomkit, A. and Peng, T.H., 1992. River fluxes of dissolved silica to the ocean were higher during glacials: Ge/Si in diatoms, rivers, and oceans. Paleoceanography, 7(6), pp.739-767.

Frost, C.D., von Blanckenburg, F., Schoenberg, R., Frost, B.R. and Swapp, S.M., 2007. Preservation of Fe isotope heterogeneities during diagenesis and metamorphism of banded iron formation. Contributions to Mineralogy and Petrology, 153(2), p.211.

Halama, K.E., Konhauser, K.O., Kappler, A., 2016. Using modern ferruginous habitats to interpret Precambrian banded iron formation deposition. International Journal of Astrobiology, 15 (3), pp. 205-217

Garrels, R.M., Perry, E.A. and Mackenzie, F.T., 1973. Genesis of Precambrian iron-formations and the development of atmospheric oxygen. Economic Geology, 68(7), pp.1173-1179.

Gauger, T., Byrne, J.M., Konhauser, K.O., Obst, M., Crowe, S. and Kappler, A., 2016. Influence of organics and silica on Fe (II) oxidation rates and cell–mineral aggregate formation by the green-sulfur Fe (II)-oxidizing bacterium Chlorobium ferrooxidans KoFox–Implications for Fe (II) oxidation in ancient oceans. Earth and Planetary Science Letters, 443, pp.81-89.

Gole, M.J., Klein, C., 1981, Banded iron-formations through much of precambrian time: Journal of Geology, v. 89, p. 169-183.

Grotzinger, J.P. and Kasting, J.F., 1993. New constraints on Precambrian ocean composition. The Journal of Geology, 101(2), pp.235-243.

Gu, H., Moore, W.S., Zhang, L., Du, J. and Zhang, J., 2012. Using radium isotopes to estimate the residence time and the contribution of submarine groundwater discharge (SGD) in the Changjiang effluent plume, East China Sea. Continental Shelf Research, 35, pp.95-107.

Halama, K.E., Konhauser, K.O., Kappler, A., 2016. Using modern ferruginous habitats to interpret Precambrian banded iron formation deposition. International Journal of Astrobiology, 15 (3), pp. 205-217

Halevy, I. and Bachan, A., 2017. The geologic history of seawater pH. Science, 355(6329), pp.1069-1071.Mortlock, R.A., Froelich, P.N., Feely, R.A., Massoth ,G.J., Butterfield, D.A., Lutpon, J.E., 1993. Silica and germanium in Pacific Ocean hydrothermal vents and plumes.Earth and Planetary Science Letters 119:365-378.

Hartman H (1984) The evolution of photosynthesis and microbial mats: A speculation on the banded iron formations. In: Cohen Y, Castenholz RW, Halvorson HO (eds) Microbial Mats: Stromatolites . Alan Liss Inc., New York, pp 449–453.

Hegler, F., Posth, N.R., Jiang, J. and Kappler, A., 2008. Physiology of phototrophic iron (II)-oxidizing bacteria: implications for modern and ancient environments. FEMS Microbiology Ecology, 66(2), pp.250-260.

Heimann, A., Johnson, C.M., Beard, B.L., Valley, J.W., Roden, E.E., Spicuzza, M.J. and Beukes, N.J., 2010. Fe, C, and O isotope compositions of banded iron formation carbonates demonstrate a major role for dissimilatory iron reduction in~ 2.5 Ga marine environments. Earth and Planetary Science Letters, 294(1-2), pp.8-18.

Heising, S., Richter, L., Ludwig, W. and Schink, B., 1999. Chlorobium ferrooxidans sp. nov., a phototrophic green sulfur bacterium that oxidizes ferrous iron in coculture with a "Geospirillum" sp. strain. Archives of Microbiology, 172(2), pp.116-124.

Holland, H.D., 1984. The chemical evolution of the atmosphere and oceans. Princeton University Press.Jiao, N., Yang, Y., Hong, N., Ma, Y., Harada, S., Koshikawa, H. and Watanabe, M., 2005. Dynamics of autotrophic picoplankton and heterotrophic bacteria in the East China Sea. Continental Shelf Research, 25(10), pp.1265-1279.

Holm, N.G., 1989. The 13C12C ratios of siderite and organic matter of a modern metalliferous hydrothermal sediment and their implications for banded iron formations. Chemical Geology, 77(1), pp.41-45.

Isley, A.E., 1995. Hydrothermal plumes and the delivery of iron to banded iron formation. The Journal of Geology, 103(2), pp.169-185.

Jiao, N., Yang, Y., Hong, N., Ma, Y., Harada, S., Koshikawa, H. and Watanabe, M., 2005. Dynamics of autotrophic picoplankton and heterotrophic bacteria in the East China Sea. Continental Shelf Research, 25(10), pp.1265-1279.

Johnson, C.M., Roden, E.E., Welch, S.A. and Beard, B.L., 2005. Experimental constraints on Fe isotope fractionation during magnetite and Fe carbonate formation coupled to dissimilatory hydrous ferric oxide reduction. Geochimica et Cosmochimica Acta, 69(4), pp.963-993.

Kappler, A. and Newman, D.K., 2004. Formation of Fe (III)-minerals by Fe (II)-oxidizing photoautotrophic bacteria. Geochimica et Cosmochimica Acta, 68(6), pp.1217-1226.

Kappler, A., Pasquero, C., Konhauser, K.O. and Newman, D.K., 2005. Deposition of banded iron formations by anoxygenic phototrophic Fe (II)-oxidizing bacteria. Geology, 33(11), pp.865-868.

Kasting, J.F., Holland, H.D. and Kump, L.R., 1992. Atmospheric evolution: the rise of oxygen. The Proterozoic Biosphere: A Multidisciplinary Study, pp.1185-1188.

Kenov, I.A., Garcia, A.C. and Neves, R., 2012. Residence time of water in the Mondego estuary (Portugal). Estuarine, Coastal and Shelf Science, 106, pp.13-22.

Köhler, I., Konhauser, K.O., Papineau, D., Bekker, A. and Kappler, A., 2013. Biological carbon precursor to diagenetic siderite with spherical structures in iron formations. Nature Communications, 4(1), pp.1-7.

Konhauser, K.O., Hamade, T., Raiswell, R., Morris, R.C., Ferris, F.G., Southam, G. and Canfield, D.E., 2002. Could bacteria have formed the Precambrian banded iron formations?. Geology, 30(12), pp.1079-1082.

Konhauser, K.O., Newman, D.K. and Kappler, A., 2005. The potential significance of microbial Fe (III) reduction during deposition of Precambrian banded iron formations. Geobiology, 3(3), pp.167-177.Posth, N.R.,

Konhauser, K.O., Amskold, L., Lalonde, S.V., Posth, N.R., Kappler, A. and Anbar, A., 2007. Decoupling photochemical Fe (II) oxidation from shallow-water BIF deposition. Earth and Planetary Science Letters, 258(1-2), pp.87-100.

Konhauser, K.O., Planavsky, N.J., Hardisty, D.S., Robbins, L.J., Warchola, T.J., Haugaard, R., Lalone, S.V., Partin, C.A., Onnk, P.B.H., Tsikos, H., Lyons, T.W., Bekker, A., Johnson, C.M., 2017, Iron formations: A global record of Neoarchaean to Palaeoproterozoic environmental history: Earth-Science Review, v. 172, p. 140-177.

Konhauser, K.O., Planavsky, N.J., Hardisty, D.S., Robbins, L.J., Warchola, T.J., Haugaard, R., Lalonde, S.V., Partin, C.A., Oonk, P.B.H., Tsikos, H. and Lyons, T.W., 2017. Iron formations: A global record of Neoarchaean to Palaeoproterozoic environmental history. Earth-Science Reviews, 172, pp.140-177.

Konhauser, K.O., Robbins, L.J., Alessi, D.S., Flynn, S.L., Gingras, M.K., Martinez, R.E., Kappler, A., Swanner, E.D., Li, Y-L., Crowe, S.A., Planavsky, N.J., Reinhard, C.T., Lalonde, S.V., 2018, Phytoplankton contributions to the trace-element composition of precambrian banded iron formations: GSA Bulletin, v. 130, p. 941-951.

Krissansen-Totton, J., Arney, G.N. and Catling, D.C., 2018. Constraining the climate and ocean pH of the early Earth with a geological carbon cycle model. Proceedings of the National Academy of Sciences, 115(16), pp.4105-4110.Widdel, F., Schnell, S.,

Kump, L.R., Seyfried, W.E., 2005, Hydrothermal fe fluxes during the precambrian: Effect of low oceanic sulfate concentrations and low hydrostatic pressure on the composition of black smokers: Earth and Planetary Science Letters, v. 235, p. 654-662.

Laufer, K., Niemeyer, A., Nikeleit, V., Halama, M., Byrne, J.M. and Kappler, A., 2017. Physiological characterization of a halotolerant anoxygenic phototrophic Fe (II)-oxidizing green-sulfur bacterium isolated from a marine sediment. FEMS Microbiology Ecology, 93(5).

Li, W., Czaja, A.D., Van Kranendonk, M.J., Beard, B.L., Roden, E.E. and Johnson, C.M., 2013. An anoxic, Fe (II)-rich, U-poor ocean 3.46 billion years ago. Geochimica et Cosmochimica Acta, 120, pp.65-79.

Li, Y-L., Konhauser, K.O., Kappler, A., and Hao, X-L., 2013, Experimental low-grade alteration of biogenic magnetite indicates microbial involvement in generation of banded iron formations: Earth and Planetary Science Letters, v. 361, p. 229-237.

Li, Y., Sutherland, B.R., Gingras, M.K., Owttrim, G.W., Konhauser K.O., 2020. A novel approach to investigate the deposition of (bio)chemical sediments: The sedimentation velocity of cyanobacteria-ferrihydrite aggregates. Journal of Sedimentary Research, In review.

Maliva, R.G., Knoll, A.H. and Siever, R., 1989. Secular change in chert distribution; a reflection of evolving biological participation in the silica cycle. Palaios, 4(6), pp.519-532.

Mänd, K., Lalonde, S.V., Robbins, L.J., Thoby, M., Paiste, K., Kreitsmann, T., Paiste, P., Reinhard, C.T., Romashkin, A.E., Planavsky, N.J. and Kirsimäe, K., 2020. Palaeoproterozoic oxygenated oceans following the Lomagundi–Jatuli Event. Nature Geoscience, 13(4), pp.302-306.

Millero., F., 2001, Speciation of metals in natural waters: Geochemical Transactions, v. 2, p. 57-65.

Mloszewska, A.M., Cole, D.B., Planavsky, N.J., Kappler, A., Whitford, D.S., Owttrim, G.W., Konhauser, K.O., 2018, UV radiation limited the expansion of cyanobacteria in early marine photic environments: Nature Communication, 9, article number 3088

Morris, R.C., 1993, Genetic modelling for banded iron-formation of the hamersley group, pilbara craton, western Australia: Precambrian Research, v. 60, p. 243-286.

Nealson, K.H. and Myers, C.R., 1990. Iron reduction by bacteria: a potential role in the genesis of banded iron formations. American Journal of Science, 290, pp.35-45.

Olson, S.L., Reinhard, C.T. and Lyons, T.W., 2016. Cyanobacterial diazotrophy and Earth's delayed oxygenation. Frontiers in microbiology, 7, p.1526.

Pecoits, E., Smith, M.L., Catling, D.C., Philippot, P., Kappler, A., and Konhauser, K.O., 2015, Atmospheric hydrogen peroxide and Eoarchean iron formations: Geobiology, v. 13, p. 1–14, https://doi.org/10.1111/ gbi.12116.

Perry, E.C., Tan, F.C. and Morey, G.B., 1973. Geology and stable isotope geochemistry of the Biwabik Iron Formation, northern Minnesota. Economic Geology, 68(7), pp.1110-1125.

Phoenix, V.R., Adams, D.G., Konhauser, K.O., 2000, Cyanobacterial viability during hydrothermal biomineralization: Chemical Geology, v. 169, p. 329-338.

Pickard, A.L., Barley, M.E. and Krapež, B., 2004. Deep-marine depositional setting of banded iron formation: sedimentological evidence from interbedded clastic sedimentary rocks in the early Palaeoproterozoic Dales Gorge Member of Western Australia. Sedimentary Geology, 170(1-2), pp.37-62.

Playter, T., Konhauser, K.O., Owttrim, G.W., Hodgson, C., Warchola, T., Mloszewska, A.M., Sutherland, B.R., Bekker, A., Zonneveld, J.-P., Pemberton, S.G., Gingras, M., 2017, Microbe-clay interactions as a mechanism for the preservation of organic matter and trace metal biosignatures in black shales: Chemical Geology, v. 459, p. 75-90.

Porsch, K. and Kappler, A., 2011. FeII oxidation by molecular O2 during HCl extraction. *Environmental Chemistry*, *8*(2), pp.190-197.

Posth, N.R., Huelin, S., Konhauser, K.O. and Kappler, A., 2010. Size, density and composition of cell–mineral aggregates formed during anoxygenic phototrophic Fe (II) oxidation: impact on modern and ancient environments. Geochimica et Cosmochimica Acta, 74(12), pp.3476-3493.

Posth, N.R., Konhauser, K.O. and Kappler, A., 2013. Microbiological processes in banded iron formation deposition. Sedimentology, 60(7), pp.1733-1754.

Posth, N.R., Canfield, D.E. and Kappler, A., 2014. Biogenic Fe (III) minerals: from formation to diagenesis and preservation in the rock record. Earth-Science Reviews, 135, pp.103-121.

Poulain, A.J. and Newman, D.K., 2009. Rhodobacter capsulatus catalyzes light-dependent Fe (II) oxidation under anaerobic conditions as a potential detoxification mechanism. Applied and environmental microbiology, 75(21), pp.6639-6646.

Planavsky, N., Rouxel, O.J., Bekker, A., Hofmann, A., Little, C.T. and Lyons, T.W., 2012. Iron isotope composition of some Archean and Proterozoic iron formations. Geochimica et Cosmochimica Acta, 80, pp.158-169.

Planavsky, N.J., Reinhard, C.T., Wang, X., Thomson, D., McGoldrick, P., Rainbird, R.H., Johnson, T., Fischer, W.W. and Lyons, T.W., 2014. Low Mid-Proterozoic atmospheric oxygen levels and the delayed rise of animals. science, 346(6209), pp.635-638.

Rasmussen, B., Fletcher, I.R., Brocks, J.J. and Kilburn, M.R., 2008. Reassessing the first appearance of eukaryotes and cyanobacteria. Nature, 455(7216), pp.1101-1104.

Schädler, S., Burkhardt, C., Kappler, A., 2008, Evaluation of electron microscopic sample preparation methods and imaging techniques for characterization of cell-mineral aggregates: Geomicrobiology Journal, v. 25, p. 228-239.

Schad, M., Halama, M., Bishop, B., Konhauser, K.O., Kappler, A., 2019, Temperature fluctuations in the Archean ocean as trigger for varve-like deposition of iron and silica minerals in banded iron formation: Geochimica et Cosmochimica Acta, v. 265, p. 386-412.

Sekine, Y., Shibuya, T., Postberg, F., Hsu, H., Suzuki, K., Masaki, Y., Kuwatani, T., Mori, M., Hong, P.K., Yoshizaki, M., Tachibana, Shogo., Sirono, S., 2015, High-temperature water–rock interactions and hydrothermal environments in the chondrite-like core of Enceladus: Nature Communications, 6, article number 8604.

Singer, P.C., Stumm, W., 1970, Acid mine drainage: The rate-determining step: Science, v. 167, p. 1121-1123

Siever, R., 1992. The silica cycle in the Precambrian. Geochimica et Cosmochimica Acta, 56(8), pp.3265-3272.

Steinhoefel, G., von Blanckenburg, F., Horn, I., Konhauser, K.O., Beukes, N.J. and Gutzmer, J., 2010. Deciphering formation processes of banded iron formations from the Transvaal and the

Hamersley successions by combined Si and Fe isotope analysis using UV femtosecond laser ablation. Geochimica et Cosmochimica Acta, 74(9), pp.2677-2696.

Stevens, S.E. and Van Baalen, C., 1973. Characteristics of nitrate reduction in a mutant of the blue-green alga Agmenellum quadruplicatum. Plant physiology, 51(2), pp.350-356.

Stevens, S.E. and Porter, R.D., 1980. Transformation in Agmenellum quadruplicatum. Proceedings of the National Academy of Sciences, 77(10), pp.6052-6056.

Stokes, G.G., 1850, On the effect of the internal friction of fluids on the motion of pendulums: Transactions of the Cambridge Philosophical Society, v. 9, p. 8.

Stolper, D.A., Revsbech, N.P. and Canfield, D.E., 2010. Aerobic growth at nanomolar oxygen concentrations. Proceedings of the National Academy of Sciences, 107(44), pp.18755-18760.

Stookey, L.L., 1970. Ferrozine---a new spectrophotometric reagent for iron. Analytical chemistry, 42(7), pp.779-781.

Sutherland, B.R., Barrett, K.J., Gingras, M.K., 2015, Clay settling in fresh and salt water: Environmental Fluid Mechanics, v. 15, p. 147-160.

Thompson, K.J., Kenward, P.A., Bauer, K.W., Warchola, T., Gauger, T., Martinez, R., Simister, R.L., Michiels, C.C., LIirós, M., Reinhard, C.T., Kappler, A., Konhauser, K.O., Crowe, S.A., 2019, Photoferrotrophy, deposition of banded iron formations, and methane production in Archean oceans, Science Advances, v. 5, article number 11.

Trendall, A.F., 2002. The significance of iron-formation in the Precambrian stratigraphic record. Precambrian sedimentary environments: A modern approach to ancient depositional systems, pp.33-66.

Troussellier, M., Bouvy, M., Courties, C. and Dupuy, C., 1997. Variation of carbon content among bacterial species under starvation condition. Aquatic Microbial Ecology, 13(1), pp.113-119.

Turner, J.S., 1973, Buoyant Convection from Isolated Sources, in Buoyancy Effects in Fluid: Cambridge University Press, p. 165-206.

Tyson, R.V. and Pearson, T.H., 1991. Modern and ancient continental shelf anoxia: an overview. Geological Society, London, Special Publications, 58(1), pp.1-24.

Van Baalen, C.H.A.S.E., 1962. Studies on marine blue-green algae. Botanica Marina, 4(1-2), pp.129-139.

Widdel, F., Schnell, S., Heising, S., Ehrenreich, A., Assmus, B. and Schink, B., 1993. Ferrous iron oxidation by anoxygenic phototrophic bacteria. Nature, 362(6423), pp.834-836.

Wray, E.M., 1977, Stokes' law revisited: Physics Education, v. 12, p. 300-303.

Wu, W., Swanner, E.D., Hao, L., Zeitvogel, F., Obst, M., Pan, Y. and Kappler, A., 2014. Characterization of the physiology and cell–mineral interactions of the marine anoxygenic phototrophic Fe (II) oxidizer Rhodovulum iodosum–implications for Precambrian Fe (II) oxidation. FEMS Microbiology Ecology, 88(3), pp.503-515.

Yamaguchi, K.E., Johnson, C.M., Beard, B.L. and Ohmoto, H., 2005. Biogeochemical cycling of iron in the Archean–Paleoproterozoic Earth: constraints from iron isotope variations in sedimentary rocks from the Kaapvaal and Pilbara Cratons. Chemical Geology, 218(1-2), pp.135-169.

Zheng, X.-Y., Beard, B.L., Reddy, T.R., Roden, E.E., Johnson, C.M., 2016, Abiologic silicon isotope fractionation between aqueous Si and Fe(III)-Si gel in simulated Archean seawater:

implications for Si isotope records in Precambrian sedimentary rocks: Geochimica Et Cosmochimica Acta, v. 187, p. 102–122.

Appendix A. Supplementary material for Chapter 2.

Table A1. Spreadsheet of sedimentation velocity calculation.

pH	initial Fe(II) (μM)	X1 (sec)	Y1(cm)	X2(sec)	Y2(cm)	w cm/s	mean w	stdev w
11	1800	151.00	7.55	248.00	3.09	0.0460	0.0447	0.0012
11		148.00	8.01	259.00	3.09	0.0443		
11		168.00	7.73	273.00	3.13	0.0437		
11	1500	116.00	8.44	241.00	3.31	0.0410	0.0414	0.0016
11		129.00	8.78	260.00	3.16	0.0429		
11		140.00	8.85	289.00	2.91	0.0399		
11	1200	159.00	9.09	308.00	3.99	0.0342	0.0353	0.0020
11		220.00	8.02	247.00	7.00	0.0377		
11		280.00	7.17	387.00	3.52	0.0341		
11	900	241.00	8.12	358.00	4.09	0.0344	0.0379	0.0030
11		287.00	7.80	374.00	4.39	0.0392		
11		315.00	7.80	418.00	3.68	0.0400		
11	600	337.00	8.63	444.00	5.27	0.0315	0.0362	0.0020
11		410.00	8.39	562.00	3.04	0.0352		
11		496.00	8.10	563.00	5.30	0.0419		
11	450	351.00	6.00	382.00	5.01	0.0321	0.0302	0.0017
11		422.00	6.50	540.00	3.01	0.0296		
11		468.00	7.01	572.00	4.00	0.0289		
11	225	339.00	6.79	470.00	3.08	0.0283	0.0284	0.0001
11		429.00	6.20	545.00	2.90	0.0284		
11		469.00	7.24	585.00	3.95	0.0283		
10	1800	174.00	7.88	320.00	2.00	0.0402	0.0398	0.0016
10		193.00	8.16	356.00	1.96	0.0380		
10		241.00	7.94	394.00	1.64	0.0412		
9	1800	613.00	8.56	635.00	6.48	0.0945	0.0904	0.0128
9		906.00	8.16	935.00	5.95	0.0761		
9		428.00	7.96	456.00	5.14	0.1008		
8	1800	934.00	7.54	976.00	4.63	0.0694	0.0738	0.0049
8		1061.00	8.27	1094.00	5.87	0.0727		
8		941.00	7.90	971.00	5.53	0.0791		
7	1800	4054.00	8.00	4148.00	5.00	0.0319	0.0360	0.0050
7		5619.00	7.83	5668.00	5.79	0.0416		
7		7217.00	5.85	7300.00	2.98	0.0345		

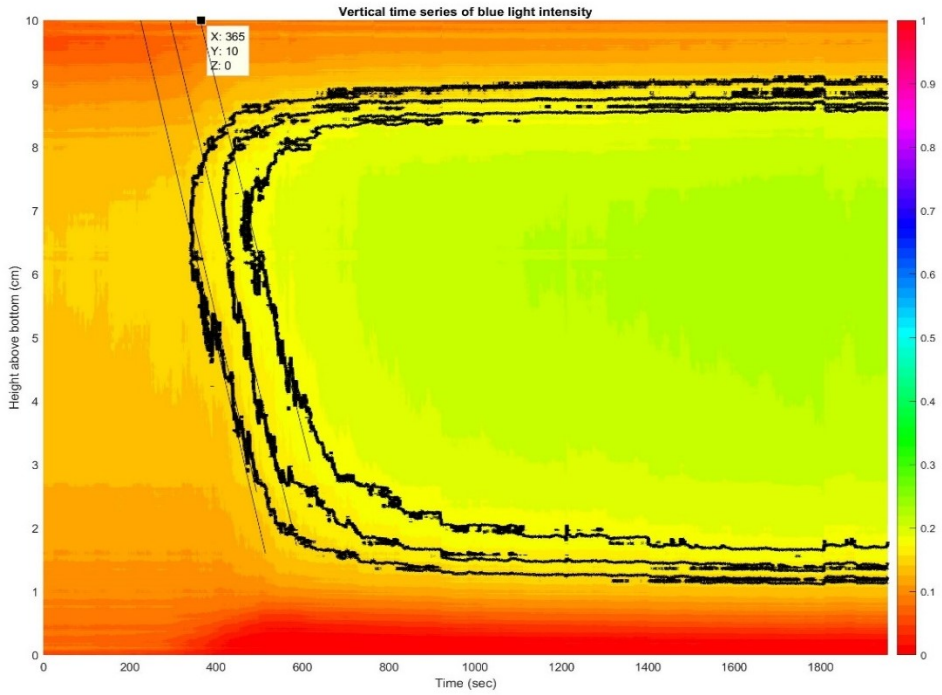

Figure A1. Vertical time series. Experiment: pH 11 and 225 µM initial Fe(II)

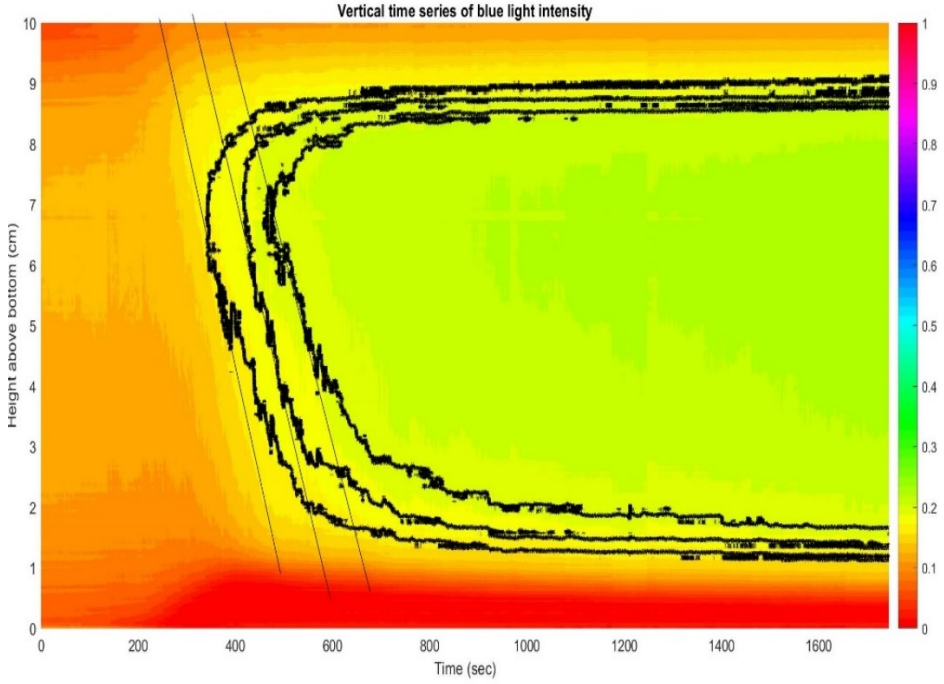

Figure A2. Vertical time series. Experiment: pH 11 and 450 µM initial Fe(II)

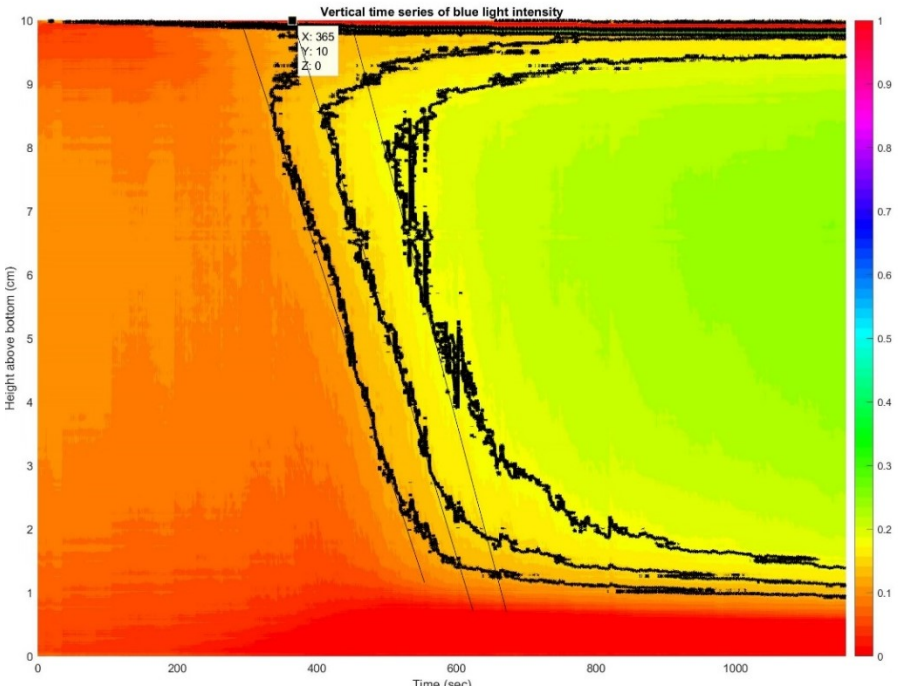

Figure A3. Vertical time series. Experiment: pH 11 and 600 µM initial Fe(II)

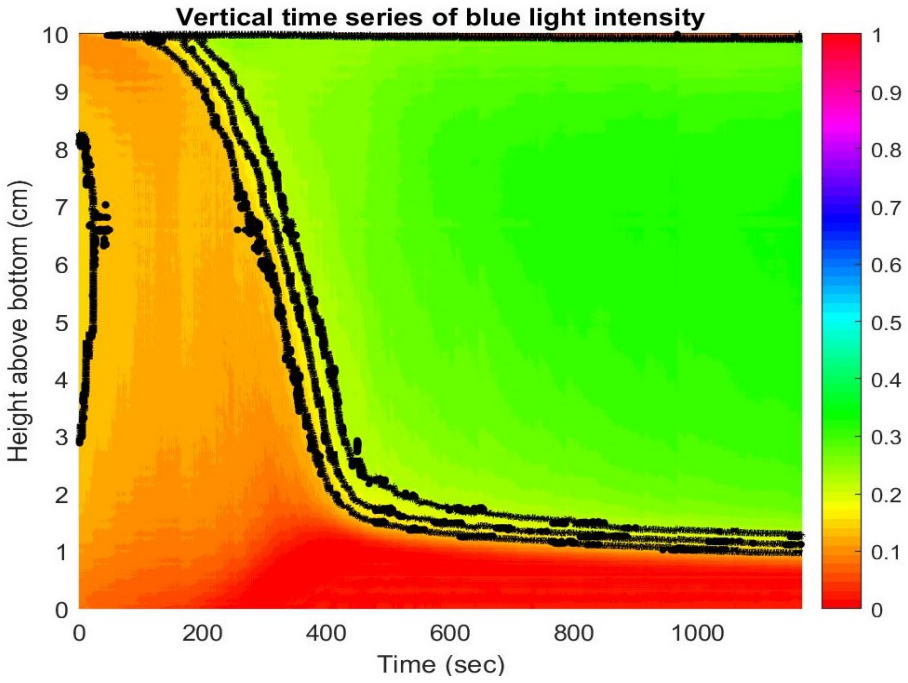

Figure A4. Vertical time series. Experiment: pH 11 and 900 µM initial Fe(II)

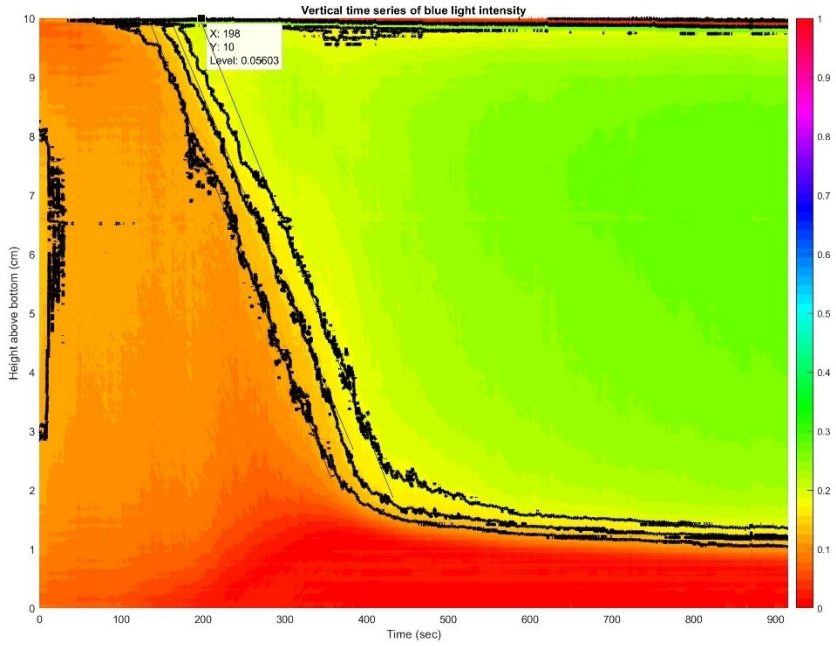

Figure A5. Vertical time series. Experiment: pH 11 and 1200 µM initial Fe(II)

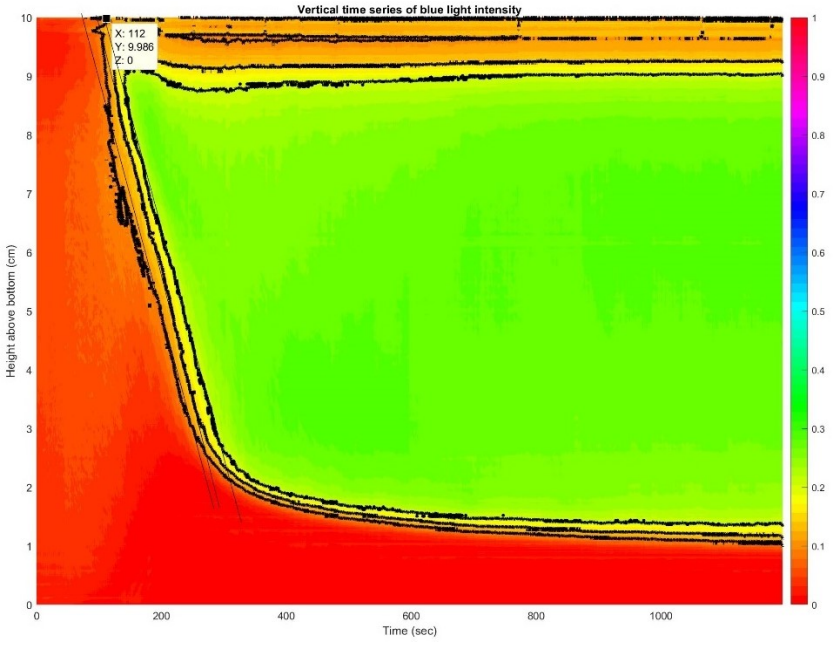

Figure A6. Vertical time series. Experiment: pH 11 and 1500 µM initial Fe(II)

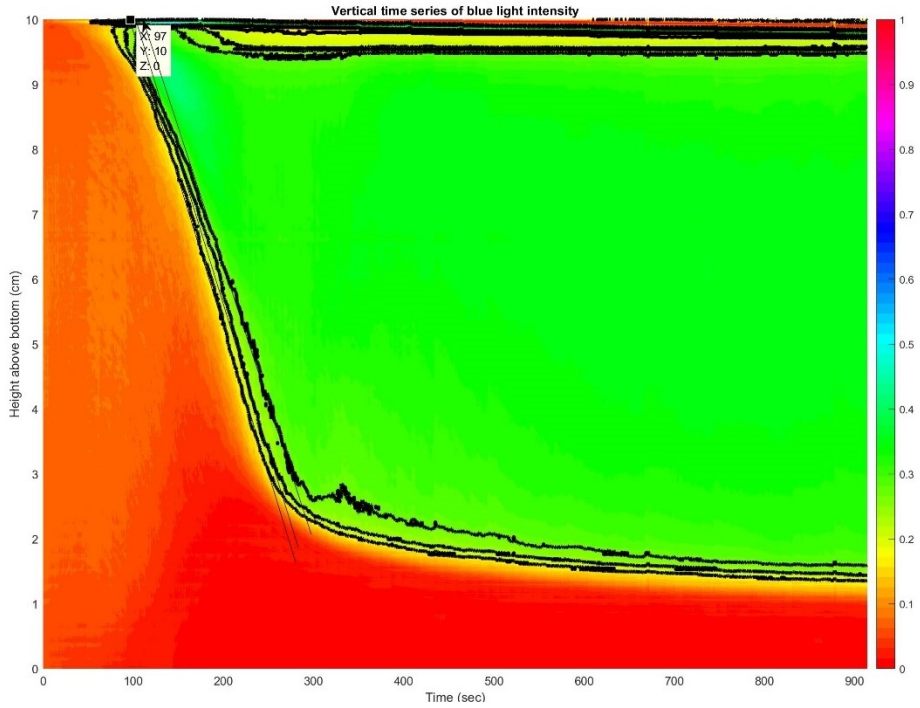

Figure A7. Vertical time series. Experiment: pH 11 and 1800 µM initial Fe(II)

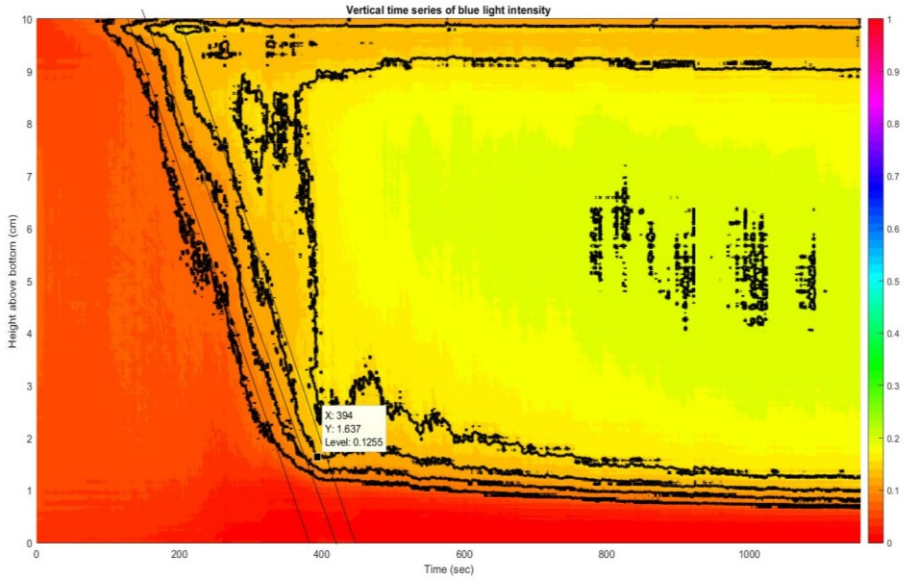

Figure A8. Vertical time series. Experiment: pH 10 and 1800 µM initial Fe(II)

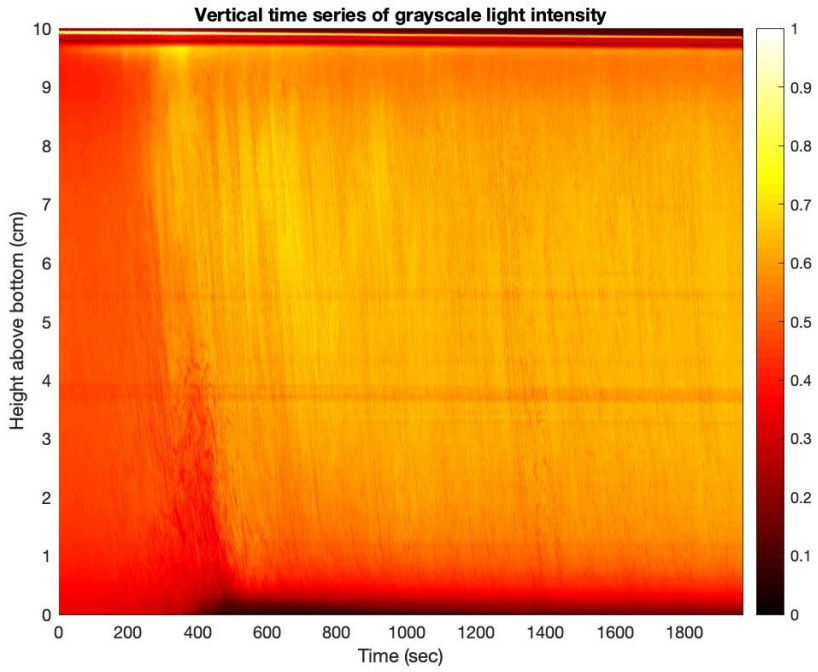

Figure A9. Vertical time series. Experiment: pH 9 and 1800 µM initial Fe(II)

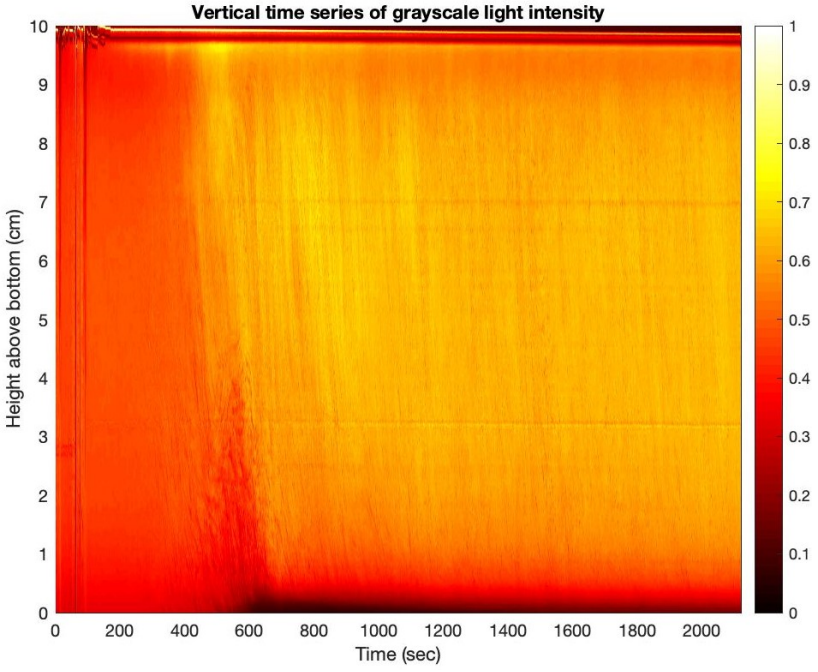

Figure A10. Vertical time series. Experiment: pH 8 and 1800 µM initial Fe(II)

Appendix B. Supplementary material for Chapter 3.

Table B1. Sedimentation velocity calculation.

pH	initial Fe(II) (µM)	X1 (sec)	Y1(cm)	X2(sec)	Y2(cm)	w cm/s	mean w	stdev w
7	1800	4054.00	8.00	4148.00	5.00	0.0319	0.0360	0.0050
7		5619.00	7.83	5668.00	5.79	0.0416		
7		7217.00	5.85	7300.00	2.98	0.0345		
7	1500	2106.00	7.11	2162.00	4.65	0.0440	0.0345	0.0098
7		2358.00	8.35	2434.00	5.68	0.0351		
7		2677.00	9.02	2754.00	7.14	0.0243		
7	1200	2229.00	7.81	2273.00	6.43	0.0315	0.0351	0.0034
7		2996.00	7.77	3042.00	6.00	0.0384		
7		2140.00	7.55	2079.00	5.40	0.0353		
8	1800	934.00	7.54	976.00	4.63	0.0694	0.0738	0.0049
8		1061.00	8.27	1094.00	5.87	0.0727		
8		941.00	7.90	971.00	5.53	0.0791		
8	1500	1174.00	8.22	1187.00	7.28	0.0721	0.0619	0.0100
8		913.00	8.00	936.00	6.59	0.0614		
8		1625.00	6.05	1677.00	3.34	0.0521		
8	1200	2956.00	7.66	2988.00	5.51	0.0674	0.0577	0.0085
8		3329.00	6.97	3358.00	5.40	0.0541		
8		3321.00	7.20	3354.00	5.49	0.0517		
8	900	2431.00	8.89	2455.00	7.53	0.0564	0.0558	0.0047
8		1896.00	9.20	1951.00	5.90	0.0601		
8		3028.00	7.16	3065.00	5.28	0.0508		

Table B2. Total Fe changes over time. pH 7, and 1800 μM Fe(II)

Sample Number	Total Fe 1	Total Fe 2	Total Fe 3	Average	STDV
A0	1776.36	1803.64	1749.09	1776.36	27.27
A2	1758.18	1721.82	1612.73	1697.58	75.70
A4	1685.45	1667.27	1649.09	1667.27	18.18
A6	1685.45	1703.64	1640.00	1676.36	32.78
A8	1549.09	1630.91	1585.45	1588.48	40.99
A9	1112.73	1094.55	1085.45	1097.58	13.89
A10	984.78	932.61	950.00	955.80	26.57
afs (final sediments)	21259.09	19077.27	17031.82	19122.73	2114.00
Abiotic Control					
C0	1676.36	1630.91	1876.36	1727.88	130.58
C2	1803.64	1740.00	1621.82	1721.82	92.26
C4	1612.73	1658.18	1621.82	1630.91	24.05
C6	994.55	1130.91	1103.64	1076.36	72.16
C8	940.00	930.91	1030.91	967.27	55.30
C9	876.36	903.64	794.55	858.18	56.77
C10	923.91	793.48	802.17	839.86	72.93

Table B3. Total Fe changes over time. pH 7, and 1500 μM Fe(II)

Sample Number	Total Fe 1	Total Fe 2	Total Fe 3	Average	STDV
A0	1436.96	1428.26	1410.87	1425.36	9.32
A2	1315.22	1393.48	1306.52	1338.41	43.99
A4	1402.17	1454.35	1410.87	1422.46	22.51
A6	1341.30	1376.09	1436.96	1384.78	32.92
A8	1289.13	1384.78	1402.17	1358.70	21.88
A9	941.30	897.83	958.70	932.61	30.54
A10	854.35	897.83	889.13	880.43	8.70
afs (final sediment)	21847.83	19021.74	22608.70	21159.42	1804.45
Abiotic Control					
C0	1489.13	1523.91	1445.65	1486.23	39.14
C2	1463.04	1289.13	1436.96	1396.38	76.38
C4	1410.87	1289.13	1306.52	1335.51	23.43
C6	819.57	802.17	889.13	836.96	43.77
C8	697.83	793.48	784.78	758.70	18.10
C9	636.96	576.09	636.96	616.67	30.99
C10	636.96	636.96	645.65	639.86	4.43

Table B4. Total Fe changes over time. pH 7, and 1200 μM Fe(II)

Sample Number	Total Fe 1	Total Fe 2	Total Fe 3	Average	STDV
A0	1184.78	1193.48	1141.30	1173.19	26.30
A2	1158.70	1115.22	1106.52	1126.81	10.18
A4	1150.00	1028.26	1106.52	1094.93	42.24
A6	1071.74	1123.91	1063.04	1086.23	30.72
A8	1054.35	1071.74	1071.74	1065.94	3.35
A9	932.61	950.00	863.04	915.22	43.77
A10	671.74	750.00	697.83	706.52	27.95
afs (final sediment)	12934.78	15326.09	12173.91	13478.26	1583.88
Abiotic Control					
C0	1141.30	1245.65	1219.57	1202.17	21.88
C2	1158.70	1123.91	1150.00	1144.20	13.70
C4	1071.74	1123.91	1115.22	1103.62	10.18
C6	654.35	645.65	750.00	683.33	52.84
C8	628.26	723.91	584.78	645.65	69.75
C9	567.39	454.35	471.74	497.83	21.88
C10	393.48	463.04	506.52	454.35	27.95

Table B5. Total Fe changes over time. pH 8, and 1800 μM Fe(II)

Sample Number	Total Fe 1	Total Fe 2	Total Fe 3	Average	STDV
A0	1747.37	1926.32	1789.47	1821.05	93.56
A1	1852.63	1621.05	1663.16	1712.28	123.36
A2	1610.53	1831.58	1589.47	1677.19	134.12
A3	1694.74	1684.21	1631.58	1670.18	33.84
A4	1547.37	1315.79	1673.68	1512.28	181.51
A5	1147.37	1168.42	1136.84	1150.88	16.08
A6	1126.32	1084.21	1105.26	1105.26	21.05
A7	1178.95	1084.21	1021.05	1094.74	79.47
A8	1031.58	1010.53	957.89	1000.00	37.95
C0	1705.26	1642.11	1768.42	1705.26	63.16
C1	1757.89	1589.47	1600.00	1649.12	94.35
C2	915.79	894.74	842.11	884.21	37.95
C3	842.11	821.05	884.21	849.12	32.16
C4	694.74	715.79	673.68	694.74	21.05
C5	736.84	610.53	600.00	649.12	76.15
C6	652.63	589.47	663.16	635.09	39.85
C7	600.00	621.05	652.63	624.56	26.49
C8	515.79	610.53	557.89	561.40	47.47

Table B6. Total Fe changes over time. pH 8, and 1500 μM Fe(II)

Sample Number	Total Fe 1	Total Fe 2	Total Fe 3	Average	STDV
A0	1542.86	1361.90	1466.67	1457.14	90.85
A1	1038.10	1104.76	1028.57	1057.14	41.51
A2	695.24	780.95	780.95	752.38	49.49
A3	780.95	761.90	828.57	790.48	34.34
A4	571.43	657.14	533.33	587.30	63.41
A5	504.76	561.90	514.29	526.98	30.61
A6	552.38	485.71	504.76	514.29	34.34
A7	476.19	447.62	495.24	473.02	23.97
A8	409.52	438.10	438.10	428.57	16.50
Afs(final sediment)	14476.19	16476.19	16190.48	15714.29	1081.70
Abiotic control					
C0	1428.57	1409.52	1466.67	1434.92	29.10
C1	1361.90	1380.95	1295.24	1346.03	45.01
C2	942.86	742.86	828.57	838.10	100.34
C3	580.95	628.57	657.14	622.22	38.49
C4	514.29	561.90	485.71	520.63	38.49
C5	542.86	514.29	485.71	514.29	28.57
C6	447.62	428.57	485.71	453.97	29.10
C7	438.10	495.24	409.52	447.62	43.64
C8	361.90	352.38	371.43	361.90	9.52

Table B7. Total Fe changes over time. pH 8, and 1200 μM Fe(II)

Sample Number	Total Fe 1	Total Fe 2	Total Fe 3	Average	STDV
A0	1240.00	1167.27	1112.73	1173.33	63.85
A1	1058.18	1085.45	1003.64	1049.09	41.66
A2	785.45	840.00	803.64	809.70	27.77
A3	503.64	512.73	576.36	530.91	39.63
A4	440.00	340.00	430.91	403.64	55.30
A5	321.82	330.91	321.82	324.85	5.25
A6	285.45	303.64	321.82	303.64	18.18
A7	285.45	258.18	267.27	270.30	13.89
A8	176.36	149.09	158.18	161.21	13.89
Afs(final sediment)	15854.55	14400.00	16581.82	15612.12	1110.93
Abiotic control					
C0	1176.36	1121.82	1158.18	1152.12	27.77
C1	1058.18	1040.00	1021.82	1040.00	18.18
C2	994.55	1021.82	1040.00	1018.79	22.88
C3	458.18	367.27	385.45	403.64	48.10
C4	312.73	312.73	230.91	285.45	47.24
C5	285.45	258.18	249.09	264.24	18.92
C6	194.55	203.64	249.09	215.76	29.22
C7	158.18	258.18	158.18	191.52	57.74
C8	85.45	94.55	203.64	127.88	65.77

Table B8. Total Fe changes over time. pH 8, and 900 μM Fe(II)

Sample Number	Total Fe 1	Total Fe 2	Total Fe 3	Average	STDV
A0	833.18	796.82	842.27	824.09	24.05
A1	778.64	842.27	774.09	798.33	38.12
A2	810.45	765.00	787.73	787.73	22.73
A3	783.18	819.55	810.45	804.39	18.92
A4	819.55	787.73	815.00	807.42	17.21
A5	710.45	678.64	728.64	705.91	25.31
A6	525.91	505.91	510.45	514.09	10.48
A7	469.55	451.36	487.73	469.55	18.18
A8	346.82	396.82	419.55	387.73	37.21
Afs(final sediment)	15663.64	13845.45	16754.55	15421.21	1469.62
Abiotic control					
C0	810.45	787.73	755.91	784.70	27.40
C1	705.91	760.45	805.91	757.42	50.07
C2	751.36	810.45	765.00	775.61	30.94
C3	333.18	346.82	333.18	337.73	7.87
C4	219.55	233.18	219.55	224.09	7.87
C5	183.18	169.55	183.18	178.64	7.87
C6	142.27	137.73	124.09	134.70	9.46
C7	124.09	96.82	110.45	110.45	13.64
C8	101.36	101.36	83.18	95.30	10.50